LAB-ON-A-CHIP for individual cell response to light stimulation

A three-layer MEMS device

Roel Stortelder

Master thesis in partial fulfillment of
the master Biomedical Engineering
and the master Electrical Engineering

中国科学院
苏州生物医学工程技术研究所
SUZHOU INSTITUTE OF BIOMEDICAL ENGINEERING AND
TECHNOLOGY CHINESE ACADEMY OF SCIENCES

TU Delft

LAB-ON-A-CHIP FOR INDIVIDUAL CELL RESPONSE TO LIGHT STIMULATION

A THREE-LAYER MEMS DEVICE

by

Roel Stortelder

in partial fulfillment of the requirements for the degrees of

Master of Science
in Electrical Engineering

and

Master of Science
in Biomedical Engineering

at the Delft University of Technology,
to be defended publicly on June 17, 2019 at 9:00 AM.

Student number:	4144244	
Supervisor:	Prof.dr. G. Q. Zhang,	Delft University of Technology
Thesis committee:	Prof.dr. J. F. Dong,	Suzhou Institute of Biomedical Engineering and Technology
	Dr.ing. H. W. van Zeijl,	Delft University of Technology
	Dr.ir. D. H. Plettenburg,	Delft University of Technology

This thesis is confidential and cannot be made public until June 17, 2019.

TU Delft Delft University of Technology

ABSTRACT

Analyzing the different signaling pathways of cells is key in understanding the basic functions of the cells in all organic systems from algae to humans. Not only do they help solve our questions on how organisms function, they also allow for new cures to be explored. A large variety of these signaling pathways can be influenced by light and can, for example, stimulate or inhibit cell growth. This research thesis introduces a new lab-on-a-chip MEMS device to help with the cell signaling exploration with a focus on optical cell stimulation. From a culture of HeLa cells, the chip is able to separate individual cells into different chambers by means of microfluidics. These microfluidic channels are processed using SU-8 and place each cell above an LED. In total, each chip houses ten LEDs with four different wavelengths ranging from 450 to 850 nm. Each of these LEDs is individually addressable through an Arduino MEGA with a Matlab user interface. After an introduction into cell signaling, the thesis describes how the chip is build up from two silicon wafers and one glass wafer, and explores novel assembly methods like SU-8 wafer bonding and the use of apertures.

PREFACE

This thesis is written for the fulfilment of the two master degrees Electrical Engineering (EE) and Biomedical Engineering (BME) in the form of a double degree. In order to make a clear distinction between the two subjects, some chapter titles are given a 'BME' or 'EE' prefix corresponding with their subject. The results and conclusions are formed from the complete project and do therefore not have a master degree assigned to them.

At the Suzhou Institute of Biomedical Engineering and Technology (SIBET) under the supervision of prof.dr. J.F. Dong the response of cells to different wavelengths and intensities of LED light is studied. The current research is focused on Candida Albicans (C. Albicans) treatment and cellular signaling. As a collaboration with prof.dr. G.Q. Zhang of the Delft University of Technology a proposal was done for a lab-on-a-chip that could aid the research into light-induced cellular signaling. This master research project is described in this thesis and helped me understand the theory and practice biomedical and micro-electronic problems.

I want to express my gratitude to prof.dr. G.Q. Zhang and prof.dr. J.F. Dong for providing me with the ability and financial support to do the research project in Suzhou, China, and the manufacturing in the Else Kooi Laboratory (EKL) in the Netherlands. Special thanks goes out to dr.ing. H.W. van Zeijl for his close supervision and support for the cleanroom processing. Furthermore, I would like to thank MSc. T.F. Wang for his support in the cell laboratories and his help with the Chinese language. Another thanks goes to all other staff members and students of EKL and SIBET who contributed to the completion of this project.

Roel Stortelder
Delft, June 2019

CONTENTS

List of Figures

List of Tables

1

INTRODUCTION

Not long after the invention of the laser, Endre Mester from the Semmelweis University used the first version of low-level light therapy (LLLT) on mice with cancer [1]. His study showed that with the use of a 694nm laser the cancer did not develop and the hair at the treated location grew back much faster compared to the control group. This discovery led the way for further research into the effect of light on the (human) cell biology.

Although there has been a substantial amount of research on light stimulation and the resulting effects, the exact mechanisms triggering the response are still unknown. Especially the response of a single cell to different wavelengths of light can give an insight to the mechanisms responsible for the healing effect of light stimulation.

The research goal of this project is to design and fabricate a lab-on-a-chip for the optical stimulation of cells with a transparent cover for the use with the microscopes available at SIBET.

This thesis describes the development of a single device able to separate individual HeLa cells and expose them with 450nm, 660nm, 780nm, and 850nm wavelength light at different intensities. The device is processed at the cleanroom 100 of the Else Kooi Laboratory at the Delft University of Technology and is composed of a combination of two silicon wafers and one glass wafer. The microstructures that form the microfluidics are composed of a layer of SU-8 sandwiched between the silicon and glass wafers.

Chapter 2 gives an introduction to cell signaling and explains the importance of the research on this subject. Chapter 3 shows how these cellular signals can be measured through confocal microscopy and gives experimental results for the imaging of reactive oxygen species. An introduction to the involvement of MEMS in cell research is given with device examples from the literature in Chapter 4. The materials used in MEMS devices for biomedical applications are discussed in Chapter 5 together with some example processes which could improve the biocompatibility of non-biocompatible materials. Chapter 6 describes the final design of the device with a description of the processing steps and particle flow simulations. The results are shown in Chapter 7 and the conclusion and future recommendations of this thesis are given in Chapter 8 and 9.

2

BME: CELL SIGNALING

All organisms consisting of more than one cell use both intracellular and extracellular signaling to manage a broad spectrum of biological processes. This includes not only the transmission of neurotransmitters between the synapses of two connected neurons, but also signaling for organogenesis, responses to tissue damage, and many other processes [2]. The signals can be formed from a large variety of biological chemicals including, but not limited to, hormones and cytokines, as well as ions and neurotransmitters. These signal molecules are received by receptor proteins on the cell membrane or, in some cases, are directly diffused through the membrane. Good examples of cellular signaling that are involved in nearly every aspect of cellular life are calcium signaling, the Ras-Raf-MEK-ERK pathway, and reactive oxygen species (ROS) signaling.

2.1. CALCIUM SIGNALING

2.1.1. PROTEINS

A large part of the function of a cell membrane is controlled by proteins connected to or embedded in the phospholipid bilayer [2]. These membrane proteins are used for a vast variety of functions including, among others, signal transmission between the intracellular and extracellular, molecule or ion transport, cell adhesion, and transferase [3].

Membrane transport proteins, also known as protein channels, move small molecules and/or ions through the phospholipid bilayer. These proteins are classified as integral transmembrane proteins, meaning they stay attached to the membrane permanently, only to release when it breaks, and span across the membrane. Depending on the protein this transport can be passive through facilitated diffusion without any energy consumption and is mostly used for transport of charged ions and polar molecules. Another option is active diffusion that requires energy in the form of adenosine triphosphate (ATP) or an electrochemical gradient. Active transport of molecules and ions allows the proteins to counter normal diffusion and, for example, create a potential difference across the membrane as is used in the action potential signal of neurons.

Cell surface receptor proteins are also integral membrane proteins which span across the membrane, but do not transport molecules or ions. These receptors are used for signal transfers between the cell and extracellular molecules. These molecules can be anything from nutrients to hormones, but also proteins on the surface of other cells. While the previous two examples are permanently connected to a membrane, this is not the case for all proteins contributing to signaling pathways. Some examples of such proteins are phospholipases, protein-kinase C (PKC), phosphoinositide 3-kinase (PI3K), KRAS and Munc.

2.1.2. CALCIUM AS A CONTROLLER AND SIGNAL

The function and/or location of proteins is determined by the charge and shape of the biomolecule. For part of these proteins, this shape and charge is changed by binding to the Ca^{2+} [4]. The ability of calcium ions to alter the shape and charge of a protein is a vital part of cellular signaling [5].

In resting conditions, the Ca^{2+} concentration in the cytoplasm is maintained around 100 nM, which is typically 20.000-fold lower than the concentrations in the extracellular fluid [5]. A lot of energy is used to

move Ca^{2+} from the cytosol through the membrane to the extracellular fluid, the endoplasmic reticulum, and mitochondria. ATPase pumps are the workhorses in calcium signaling. These pumps come in the form of sacroendoplasmic reticular calcium ATPases (SERCA), which pump calcium into the endoplasmic reticulum, and plasma membrane calcium ATPases (PMCA), which pump calcium out of the cell. In the case of SERCA pumps two calcium ions are moved through the membrane per ATP, while PMCA pumps require one ATP per single calcium ion. Other methods of moving calcium in and out of the cytoplasm involve exchange channels. Sodium calcium exchangers (NCX) transport one calcium ion in exchange for three sodium ions, and sodium calcium potassium exchangers (NCKX) exchange one calcium ion and one potassium ion for four sodium ions. Figure 2.1 gives an overview of some calcium pumps and other calcium-sensitive proteins.

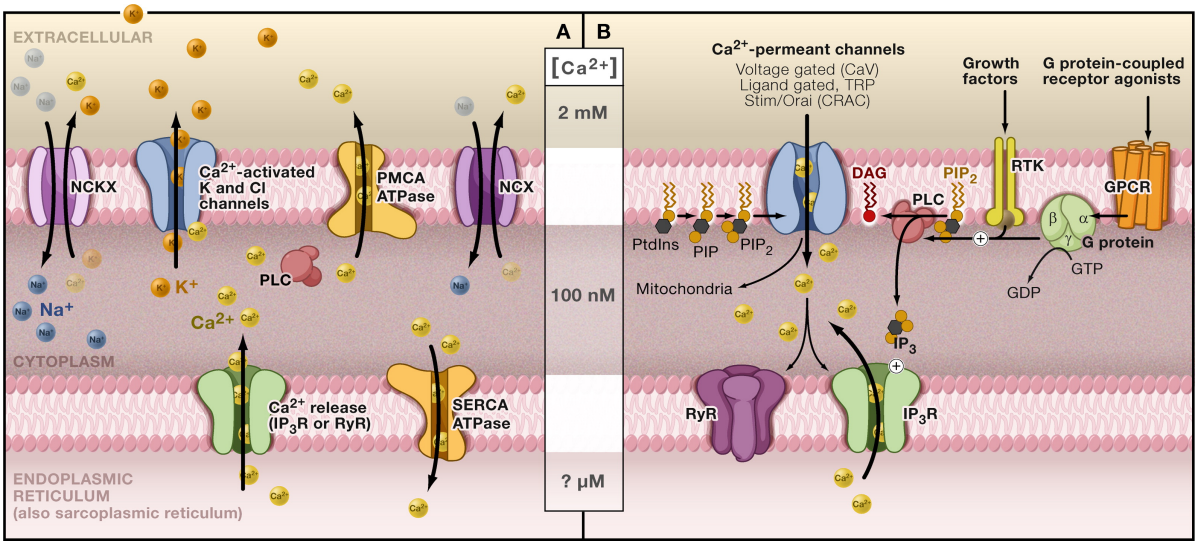

Figure 2.1: (A) The mechanism of calcium pumps in cellular membranes controlling the Ca^{2+} concentrations inside the cell. (B) Example of Ca^{2+} signaling. Opening Ca^{2+}-permeant channels causes a chain reaction, activating multiple proteins on the cell membrane and endoplasmic reticulum. Image reproduced from Cell (2007) *131*, 1047-1058. Copyright 2007 Elsevier Inc. [5].

By releasing internal Ca^{2+} buffers or by channeling Ca^{2+} through the passive protein channels in the membrane, the calcium concentration in the cytoplasm can be increased. With the release of these calcium ions into the cytoplasm, concentration levels can spike up to 1000 nM. This can change the membrane potential, but also affects the thousands of calcium-sensitive proteins that could be present in the cell. Other processes include cell proliferation, secretion, metabolism, steroid synthesis, and many more processes vital to the normal function of a cell [6]. An overview of the Ca^{2+} signalling toolkit is given in Figure 2.2.

2.2. RAS-RAF-MEK-ERK PATHWAY

Despite much more specific compared to calcium signaling, the Ras-Raf-MEK-ERK pathway is a vital chain of proteins responsible for the regulation of cell growth, division, and death [7]. In short the signal pathway transports information from receptors responding to, for example, growth factors and hormones to the cell core. As a result of the response from the receptors Ras guanosine triphosphate (GTP)-levels are increased, resulting in kinase activation. Ras-GTP induces Raf translocation which, through several phosphorylation events, moves through mitogen-activated protein kinase extracellular regulated kinase (MAPK/ERK or MEK) and extracellular regulated kinase (ERK). This in turn phospholyrates cytoskeletal proteins and transcription factors leading to gene transcription.

Due to the importance of the Ras-Raf-MEK-ERK pathway in cell growth and gene transcription, it forms a vulnerability for cancerous mutations [8]. In 15% of the cancers found in humans, BRaf is mutated to an oncogenic form, meaning or cell division [9]. The Ras-Raf-MEK-ERK pathway is therefore an important signaling pathway for research on the cure of cancer.

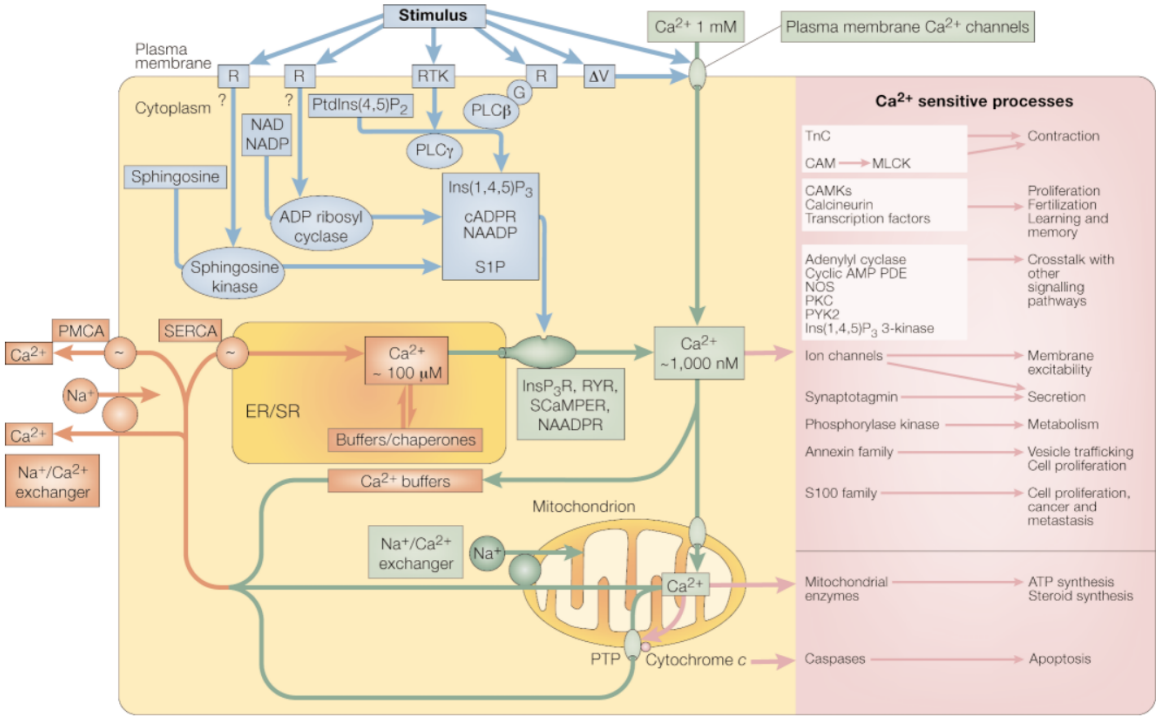

Figure 2.2: The extensive calcium signalling toolkit explaining signalling pathways and calcium-sensitive processes. Image reproduced from Nature Reviews Molecular Cell Biology (2000) *1*, 11-21. Copyright 2000 Macmillan Magazines Ltd. [6].

2.3. ROS SIGNALING

Reactive oxygen species (ROS) are a byproduct of the metabolism of oxygen and, even though they are toxic to cells in high concentrations, play an important role in cell function and signaling [10]. Due to the fact that cells are able to rapidly produce, convert, or eject ROS, the chemicals are highly effective as signal transmitters. High local production speeds and high global detoxification speeds can also lead to very local ROS signalling within a cell, resulting in the possibility of subcellular signaling. Most of the ROS are sourced from superoxide, an ion produced from the oxygen molecule through reduction, in the mitochondria [11] and are so-called endogene ROS, meaning they are produced inside the cell. These ROS are mainly produced by NADPH oxidase complexes present in the cell membrane, endoplasmic reticulum, and, as previously stated, the mitochondria [12].

The large variety of ROS (superoxide, hydrogen peroxide, hydroxyl radical, etc.) make it a very versatile signaling agent. As ROS play a key part in metabolism, being produced in the mitochondria as a byproduct of ATP, it is a very good indicator of cellular metabolism, especially since it can be easily attached to fluorescent dyes like Life Technologies' CellROX [13]. With these fluorescent dyes the present of high ROX concentrations can be viewed using a confocal microscope on a subcellular level.

2.4. THE INFLUENCE OF LIGHT

The understanding of cell signaling has taught us a lot about evolution and cell biology in general, but it also enables us to directly watch cellular responses to external factors. As previously mentioned, cellular signals are influenced by a vast amount of different factors like temperature, chemical concentrations, and light, which creates the opportunity to better understand the effect of medicine or other therapies. In this study we focus on the cellular response to light therapy, and, more specifically, the effect of light on cellular signaling.

2.4.1. LIGHT THERAPY

Light therapy, or phototherapy, is a well known form of non-invasive therapy and can be applied using a variety of different light sources from light-emitting diodes (LED) to lasers or even solar light. These sources can, of course, emit different intensities and wavelengths of light or, in case of for example the sun, emit a broad

spectrum of light. Besides the natural tanning from the sun, with different sources and wavelengths, different medical conditions are targeted: a 595 nm pulsed dye laser (PDL) improves hypertrophic scars [14], 635 nm lasers are used for fat layer reduction (or low-level laser therapy-assisted liposuction) [15], a 904 nm pulsed laser reduces pain from chronic joint disorders [16], 430 to 1450 nm light sources are used in treatment of acne vulgaris [17], 500 to 1100 nm light sources reduce hair loss [18], 808 to 905 nm lasers are used to reduce lymphedema after breast cancer [19], and many other combinations of medical conditions and light wavelengths. These treatments are, however, very non-specific with limited results. This is where optogenetics comes in: a light treatment with specific well-known results.

2.4.2. OPTOGENETICS

A more invasive form of light therapy is optogenetics, where genetically modified cells have light-specific reactions. These cells express light-sensitive opsins like ion channels and pumps, which are activated or deactivated by specific light wavelengths, intensities and even pulse-frequencies. While channelrhodopsin-2 (ChR2) is the most commonly used protein, some other well known activating and inhibitory opsins can be summarized as follows [20]:

Activating opsins:

- ChR2
  - Starting point of light-gated nonspecific transmembrane cation channels.
  - Activated with blue light (460nm).
  - Activation results in depolarization of the cell.
- ChETA and ChEF/ChIEF
  - Modified version of ChR2 for very fast response and high neural firing rates.
  - Activated with blue light.
  - Millisecond scale response times.
- ChR2(C128S/D156A)
  - Modified version of ChR2 resulting in a bi-stable opsin.
  - Activated with blue light, deactivated with yellow light.
  - Millisecond scale response times.
- VChR1
  - Red-shifted activation (535 nm).
  - Low photocurrent in mammalian systems.
  - Residual sensitivity to blue light.
- C1V1
  - Modified version of VChR1.
  - Red-shifted activation (539 nm).
  - Improved photocurrent.
  - Long deactivation kinetics compared to ChR2.
  - Residual sensitivity to blue light.
- ReaChR
  - Red-shifted activation (590-630 nm).
  - Higher photocurrents and improved deactivation kinetics compared to VChR1 and C1V1.
  - High wavelength response enables activation through the skull.
  - Residual sensitivity to blue light.

- Chrimson
  - Red-shifted activation (505 nm).
  - No residual sensitivity to blue light.
- Chronos
  - Blue light- and green light-activation.
  - Very high light-sensitivity.
  - Fast activation and deactivation kinetics.
  - Can be used together with Chrimson because of very high sensitivity and multi-color activation.

Inhibitory opsins:

- NpHR
  - Light-activated chloride pump resulting in hyperpolarization.
  - Activated with green to yellow light (525-650 nm).
  - Poor surface membrane localization.
- eNpHR3.0
  - Modified version of NpHR.
  - Activated with green, yellow or red light (peak sensitivity at 590 nm).
  - Improved surface membrane localization.
  - Improved photocurrents.
- Arch, Mac, ArchT, and eBR
  - Light-activated proton pumps resulting in hyperpolarization.
  - Red-shifted activation (520-550 nm).
  - Improved recovery times compared to chloride pumps.
  - High photocurrents.
- iC1C2
  - Light-activated inhibitory chloride channel based on C1C2.
  - Blue-shifted activation.
  - Improved kinetics over other inhibitory opsins.
- SwiChR
  - A bi-stable version of iC1C2.
  - Blue-shifted activation, red-shifted deactivation (632 nm).
  - Improved kinetics over other inhibitory opsins.

Cells expressing light-sensitive opsins are of particular interest for neural therapies and treatments. With the ability to control cellular polarity, light sensitive opsins are able to induce action potentials or reduce the chance of one happening naturally, thus giving one control over neural signaling. This control proved useful in a number of conditions including Parkinson's disease [21], but even shows potential as a less invasive alternative to the traditional pacemaker [22] [23].

3

BME: CONFOCAL MICROSCOPY AND CELL RESPONSE

There are numerous methods to control and observe cellular signaling like using electrical probes or opto-acoustics, but confocal microscopy is the most frequently used and results in images with subcellular structures clearly visible. As was explained in the previous chapter, fluorescent dyes can be attached to specific chemicals used in cell signaling like ROS. With this dye present in the extracellular and intracellular fluids, when ROS is released from the mitochondria or other cellular mechanisms, the dye will attach itself to these ROS. Using a filtered light source like a laser or LED, the fluorescent dye can be stimulated with a dye-specific wavelength, which will be converted to a different dye-specific wavelength measurable with camera. This chapter explains the basic functions of a confocal microscope and experimental results on HeLa cells using an ROS-specific dye.

3.1. CONFOCAL MICROSCOPY

Just like a regular microscope, a confocal microscope consists of a set of lenses, mirrors, a light source and camera. However, the way a confocal microscope is built up is completely different. The light from the light source is not a broad spectrum of light, but instead a very narrow bandwidth of a specific wavelength is used that matches the chemicals in the to be imaged sample. This light is reflected off a dichroic mirror and focused by the objective lenses. When it hits the sample, the fluorescent dye converts the light to a different wavelength, which bounces back into the same objective lenses. The dichroic mirror does not reflect this new wavelength and transmits it through to the camera behind. Using pin holes at the lightsource and camera, the system is able to capture images of the sample at a specific focal point. When imaging transparent objects like a cell, this image of only the focal point results in a horizontal slice of the cell. As all other reflections from areas outside the focal point are stopped by the pinhole, the contrast is enhanced and details become more visible. Figure 3.1 shows a schematic drawing of the principle behind a confocal microscope [24]. Three dimensional (3D) images can be created by combining multiple images of the same sample at different focal points.

As the transmission and reflection of the dichroic mirror is not perfect and light is lost outside the focal plane, a high-power laser is often used for the excitation. In order to increase both the power and field of view, the laser is scanned across the sample to cover a larger area with a higher power. This is also known as Laser Scanning Microscopy (LSM).

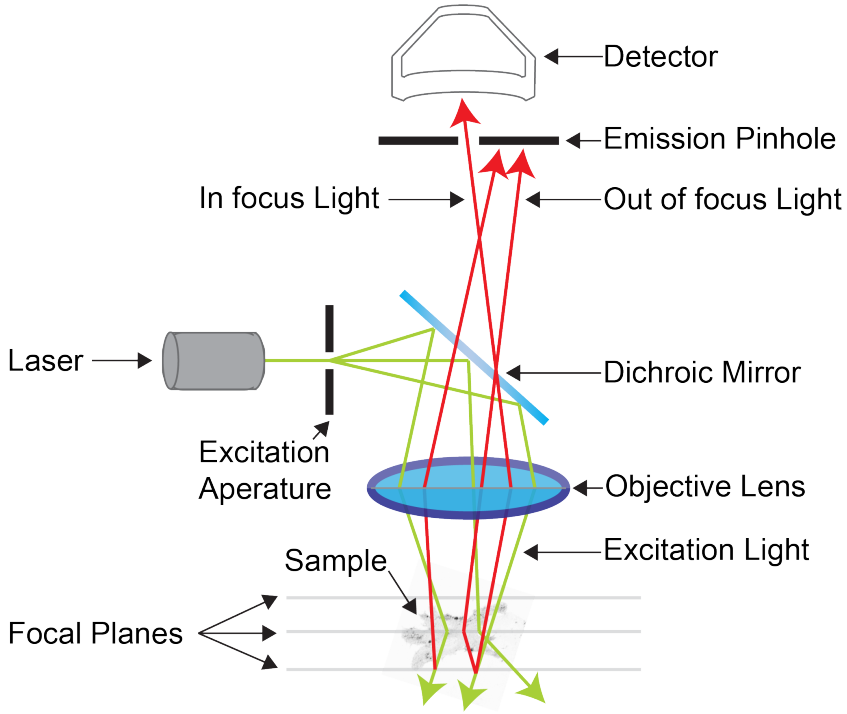

Figure 3.1: A schematic overview of a confocal microscope. The light source could be of any type, but a laser is preferred due to its high power. The green arrow depict the excitation light, the red arrow the emission light. Image reproduced from the Institute for Molecular Bioscience website. Copyright 2019 The University of Queensland [24].

3.2. CELLULAR ROS-RESPONSE TO LIGHT STIMULATION

As was explained in the previous chapter, a numerous amount of cellular mechanisms are influenced by light. In humans light is not only a trigger for retinal receptors and vitamin D production, it also has an effect on cell signaling. Like explained before, ROS is one of the major players when it comes to light-induced signalling, cell growth, and necrosis [25]. As ROS concentrations can be manipulated with light stimulation and can easily be made visible using a fluorescent dye, this signaling pathway is used as a basis for experiments with our to be designed lab-on-a-chip.

3.2.1. HELA CELL LINE

For initial experiments of the ROS response to light stimulation a healthy, reliable, and well-known cell line is required in order to simplify the culturing, testing, and validation. The HeLa cell line is the perfect candidate for this purpose. HeLa is one of the most commonly used human cell lines and originates from the cancer patient Henrietta Lacks [26]. The line was extracted from a cervical cancer and is used in scientific research for its immortality and durability. Fully grown floating HeLa cells have a diameter of 17.1 ± 0.14 μm [27] and can survive for multiple days without interventions from the researcher. The cells are cultured from a frozen sample in Dulbecco's Modified Eagle's Medium (DMEM) with 10 % fetal bovine serum (FBS) and antibiotics (penicillin-streptomycin). The detailed culturing protocol can be found in Appendix A.

3.2.2. DYE LOADING AND EXPOSURE

Before the cells can be imaged for their ROS-concentration, the culture has to be loaded with a fluorescent dye. The Life Technologies Corporation CellROX Green fluorescent dye is used for these experiments because of its ease of use and compatibility with the lasers available at the microscope lab at Suzhou Institute of Biomedical Engineering and Technology (SIBET). When the HeLa cell culture reaches the required density (a minimum of 40 % is advised) the culture is stopped. The DMEM medium is replaced by 1mL of fresh 90 % DMEM 10 % FBS per 35mm Petri dish. The CellROX Green reagent has a molar concentration of 2.5 mM and a 5 μM concentration is required according to the CellROX data sheet [13]. The amount of CellROX Green reagent that has to be added to the cell suspension in each Petri dish is therefore

$$V_{CellROX} = \frac{c_{end}}{c_{CellROX}} * V_{suspension} = \frac{5\mu M}{2.5mM} * 1mL = 2\mu L. \tag{3.1}$$

When the 2 μL CellROX Green reagent is added to the cell suspension, the Petri dishes are placed back into the culturing cabinet. After 30 minutes the fluorescent dye is loaded with the cells and the 5 μM CellROX DMEM solution has to be washed with clean DMEM. Optionally the cells can be released from the Petri dish bottom with Phosphate buffered saline (PBS) or trypsin when required. Adding 1 mL of 90 % DMEM 10 % FBS finishes the process. With a fluorescent dye loaded, exposure to high intensity lights has to be avoided to reduce the photobleaching effect and influence on the exposure-experiments.

As a first trial to check the effect of light exposure on cellular ROS-concentrations, two Petri dishes with HeLa cells are prepared with CellROX Green. One of the two Petri dishes is exposed to a 810 nm LED light source for 10 minutes. The light irradiance at the cells during this exposure was 50 mW/cm^2. The other cell culture serves as a control and is kept in a dark box.

3.2.3. DIFFERENCE IN ROS-CONCENTRATION AFTER LIGHT EXPOSURE

Directly after or during the exposure, the confocal microscope has to be set up. A Leica TCS SP5 system is used for this procedure with an air objective with a 20x magnification. After turning on all systems a light source has to be chosen. At SIBET a selection of lasers is available, but for these experiments an argon UV-laser is used as it matches the requirements for the used fluorescent dye (CellROX Green). Appendix B shows the entire microscope setup procedure. With a 200 Hz acquisition speed and 1024x1024 resolution, the images from Figure 3.2 are taken.

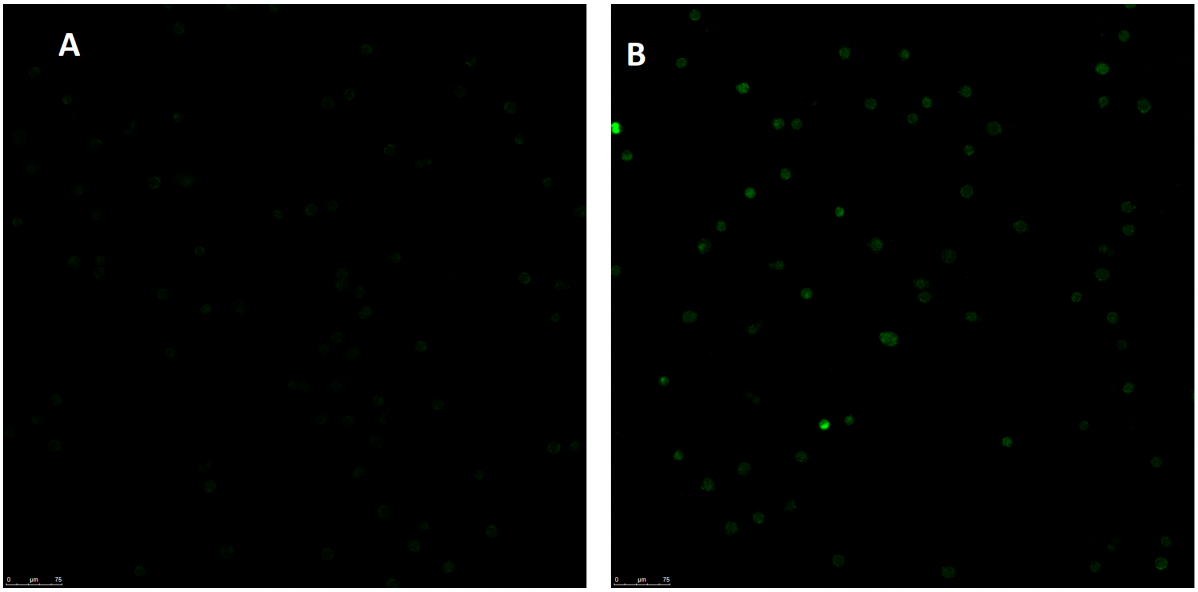

Figure 3.2: Two confocal microscopy images of HeLa cells with the CellROX Green fluorescent dye. The images are made with the Leica TCS SP5 system using an argon laser. **A:** HeLa cells without prior optical stimulation. **B:** HeLa cells with prior high intensity 810 nm light stimulation at 50 mW/cm^2 for 10 minutes. **Note:** fluorescent response at **A** might not be visible on all monitors.

From Figure 3.2 it becomes clear that HeLa cells produce and/or collect more reactive oxygen species after stimulation with high intensity 810 nm light. The difference in ROS concentration according to these images is twenty-fold, but it should be noted that during acquisition of the exposed cells some brightness is lost due to clipping at the maximum intensity. The actual difference might therefore be higher.

During this experiment the cells in the culture were able to communicate with each other using any of their signaling methods. With this experiment it is unclear if the increase in ROS concentration was influenced by the signaling of surrounding cells resulting in an increased or decreased ROS production and/or collection. Being able to separate cells and stimulate them individually would make it possible to research cell communication more in-depth.

4

EE: CELL RESEARCH AND MEMS

When it comes to cell research in any field, microstructures and microelectromechanical systems (MEMS) have played a large role in many different ways. The continuously evolving processes behind micro-machining have provided us with microneedles, microfluidic cell cultures, implantable electrodes, biosensors and many other important innovations. Current technologies allow for structures as small as several tens of nanometers, far below the size of human cells. This chapter describes the background for the design of a lab-on-a-chip which enables cell-separation and build-in optical stimulation of cells on a transparent platform.

4.1. EXISTING DEVICES

4.1.1. CELL SEPARATION AND TRAPPING

As was mentioned in the previous chapters, in order to fully understand cellular signaling without external disturbances from other cells, it is of our interest to fully separate a cell from its culture. This means that individual cells have to be taken from a suspension with large amount of cells and moved to a location where the other cells will no longer have a significant effect. The individual cells are to be kept stable and alive long enough for experiments involving optical stimulation. Previous research on the topic of cell trapping is abundant, showing a variety of methods for different applications and with mixed success rates.

MICROWELLS

One of the most simplistic methods is the use of microwells for single-cell trapping [28]. Microwells are arrays of small wells made to size for a single cell of a particular size. The processing of such device is relatively simple and based on well defined machining techniques. First a negative of the structures is made through standard micromachining processes. In [28] a silicon wafer is used on which a thin layer of MicroChem SU-8 2015 is spincoated for 30 seconds at 1300, 1700 and 2500 rpm. This yields layer heights of 15 to 25 μm. The wafers are then baked at 65^{o}C and 95^{o}C. After exposure with UV light through a mask defining the microstructures, the wafers are baked again and developed to form the master molds. After pouring a liquid PDMS on top of the wafers and another baking step, the PDMS can be peeled from the SU-8 structures to reveal the microwells.

When the microwells are fabricated, a cell suspension is poured over the wells and the cells are allowed to settle in the wells by means of gravity. After flushing the top layer, removing any excess cells, one is left with dozens of wells filled with single cells. With varying well depth and diameter, the researchers were able to achieve a single-cell occupancy of the wells of up to 92 percent [28]. Figure 4.1 shows the fabrication procedure and capture efficiencies [28].

Unfortunately, due to the single-use nature of these microwells, integrating optical stimulation is costly and time consuming.

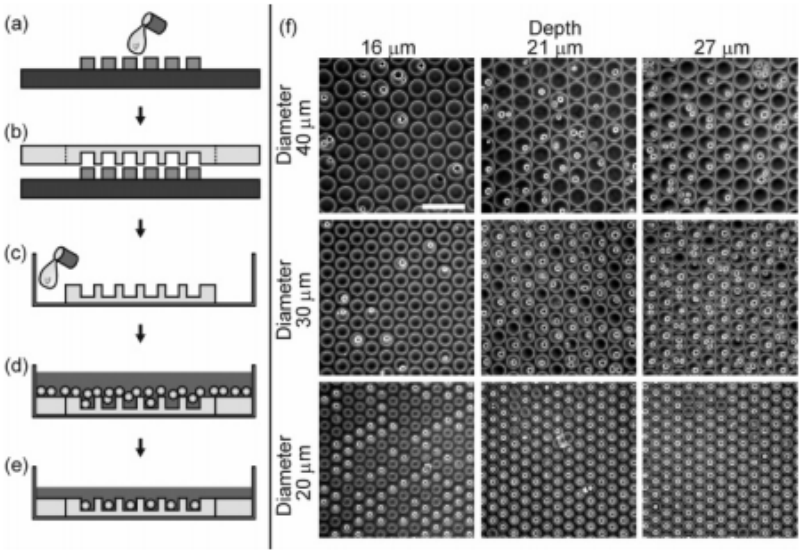

Figure 4.1: Single-cell trapping in PDMS microwells. **a-e:** The processing required for producing the PDMS microwells. **f:** Pictures of the microwells in different sizes after the procedures described in a to e. Image reproduced from Analytical Chemistry (2005) *77*, 5628-5634. Copyright 2005 American Chemical Society [28].

DIELECTROPHERESIS

Another more complex method discussed in literature is the use of dielectropheresis (DEP) – a force on induced polarization or charged dipoles in a nonuniform electric field. In the case of cells in a conductive medium, this dipole is formed in the cell by the electric field itself. A dipole in a nonuniform electric field will create a mechanical force due to the differences in Coulombic forces at each pole. This means that the location of a cell in a medium could be manipulated by nonuniform electric fields.

J. Voldman et al. designed a device that traps single cells with the use of DEP in arrays with fluid flows present [29]. Four gold electrodes arranged in a trapezoid operate with a 3 V and 20 MHz signal, which maximizes the trapping forces and minimize the effects on cellular function. The main advantage is that the cells can be selectively trapped and released. However, it requires complex machining and high frequency control. Moreover, the temperature increase caused by Joule heating can be cytotoxic [30].

LIGHT TRAPPING

As cells are relatively small and lightweight, they require very little force to be spatially manipulated. Photons, although they posses very little kinetic energy, can transfer enough momentum to a microscopic particle or cell to move it. T. N. Buican et al. designed a laser-based system capable of moving cells over 1 cm in three dimensions [31]. This was made possible by using a 488 nm argon-ion laser that, after beam-splitting, contributed to 300 mW of power to each the propulsion and deflection lasers. A beam diameters of under 100 μm results in an accuracy of 10 μm.

Unfortunately, the use of relatively high power lasers means that there will be an optical effect to the cells like described in Chapter 2. Any measurements on the cells would therefore be strongly influenced by the stimulating effect of the lasers used for displacement.

MICROFLUIDICS

Lastly, cells can be transported and separated by controlling the flow in the cell medium. In most cases the cells are trapped by having a current flow into channels smaller than the cells themselves. This causes cells to get trapped at the entrance of those channels, blocking the fluid flow which automatically prevents other cells to get trapped a the same location. S. Kobel et al. designed such microfluidic single-cell trapping chip with a trapping efficiency of 97.2 percent [32]. The cell traps and small gaps are fabricated by pattering two layers of MicroChem SU-8 into a long curving channel with small gaps between the inlet and the return channel. Figure 4.2 shows a schematic overview of the microfluidic channels.

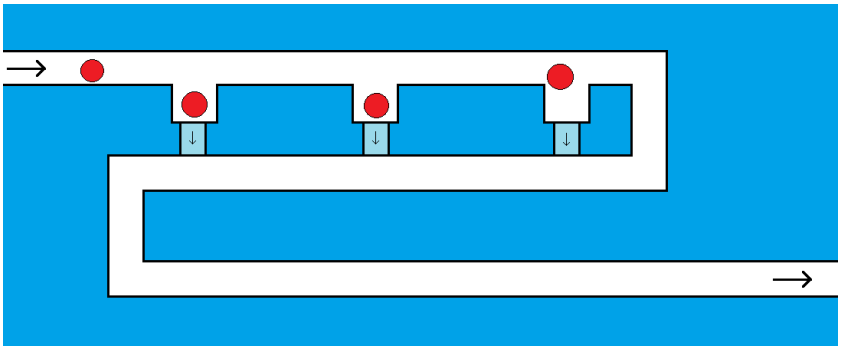

Figure 4.2: A schematic drawing of a microfluidic trapping mechanism based on a publication from S. Kobel et al. [32]. From the left side a cell suspension is pumped into the channels. Part of the flow goes through the main channel, but another part goes through small gaps between the traps and the return channel. This pulls cells into the traps, blocking the flow and taking up space in the traps. The cells can be released from the traps by reversing the flow.

Z. Zhu et al. proposed a similar trapping mechanism, but improved the release mechanism [33]. Instead of a single channel, Z. Zhu et al. make use of a separated cell channel and suction channel. The cells are still trapped at the entrance of small gaps because of the difference in pressure between the main channel and the suction channel, but are no longer housed in their own 'chambers'. To release the cells from their trap, electrodes in front of and behind the trap are charged causing the cells to be pushed away from the trap by the previously described dielectropheresis. This adds the functionality of releasing one cell at the time and not having to flush all the cells at once. Of course, this method does add to the complexity of the design and control.

4.1.2. A STABLE MICRO-ENVIRONMENT

Just like the humans they form by means of their large quantities, cells require a certain environment to live and survive. From this environment they take nutrients and, after processing those nutrients, the cells deposit their waste back into the environment. When this environment is not kept stable, the nutrients will deplete and the cytotoxic effect of the waste will start to have an effect. Under normal cell culturing circumstances the medium is therefor often replaced to remove the cytotoxic chemicals and replace them with fresh nutrients. However, during experiments in lab-on-a-chip devices like the ones discussed in the previous section, it is not that straightforward to refresh the medium. P.J. Hung et al. designed a structure for on-chip cell culturing with a continues flow of cell medium [34]. A large inlet is used to transport cells into a chamber after which the flow through the inlet is stopped. In order to maintain a constant flow of nutrients a culturing medium is allowed to flow through a large amount of perfusion channels of a much smaller diameter than the cells. The flow of the medium is small enough to not disturb the culturing of the cells, but is sufficiently large to keep the micro-environment stable. Figure 4.3 shows the end result of a single chamber from P.J. Hung et al. [34].

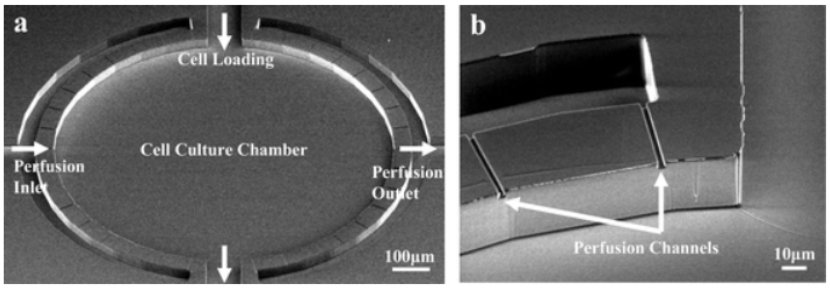

Figure 4.3: A stable micro-environment for cell culturing. **a:** SEM image of single culturing chamber. **b:** A SEM image showing details of the culturing chamber. Image reproduced from Lab Chip (2005) *5*, 44-48. Copyright 2005 The Royal Society of Chemistry [34].

4.1.3. OPTICAL STIMULATION

As was explained in the previous chapters, research on cellular response to optical stimulation is abundant. However, in those scenarios the light source is an external device, such as a laser or high-power LED system.

Research on cellular signals with the cells near or on the light source in the form of a lab-on-a-chip is scarce. LEDs are researched and used in situations where cells make physical contact to the light source though. Especially for optogenetics, LEDs are a popular choice for stimulating probes for both in-vivo and in-vitro applications.

An in-vivo device by N. McAlinden et al. uses commercial gallium nitride (GaN) microLEDs (SuperNovaOpto) with a diameter of 40 μm on a microprobe for high spectral resolution deep brain stimulation [35][36]. With the light source this close to the to be stimulated tissue, typical operating irradiance values of 1 to 10 mW/mm^2 are easily reached and surpassed. One should note that brain tissue is very sensitive to thermal changes, with 0.5 degrees C as an often used threshold approximation. Although LEDs are considered an efficient light source, a large portion of the consumed power is still converted to thermal energy, which heats the surrounding materials. However, since the LEDs in question sit on a sapphire substrate with a much larger thermal conductivity compared to brain tissue, a 200 ms light pulse of 600 mW/mm^2 does not exceed the thermal limit.

An in-vitro example of the use of μLEDs for optical stimulation of neurons comes from P. Degenaar et al. [37]. They designed a matrix of 256 μLEDs with a diameter of 25 μm and a center-to-center pitch of 150 μm. The device was fabricated in a similar manner as the previous device by etching a GaN-sapphire wafer to the n-GaN layer. The matrix is then used as a light source with the individual LEDs focused by a microscope onto a sample of neurons. While not mentioned by the authors, their device makes it possible to do individual light stimulation for cells in, for example, microwells. However, the system requires custom parts for a microscope and the cell-pitch needs to match the pitch of the μLEDs in the matrix.

Instead of separating the light sources from the samples with a microscope, the two parts could be combined into a single package. This would simplify the testing setup compared to using a microscope between the two devices while still being able to individually stimulate cells. The design of such device will be the focus of this thesis.

5

BME: BIO-COMPATIBILITY

A device coming into direct contact with live cells or their medium has to be biocompatible. Cytotoxic effects of any of the materials will have an effect on the experiments and have to be avoided at all costs. Copper is an example of a material often used in MEMS and other chips, but has well-known high toxicity [38]. In this chapter popular MEMS and research materials are investigated for their biocompatibility. Surface modifications including thin film depositions are also discussed as method to make cytotoxic materials biocompatible.

5.1. MEMS MATERIALS

5.1.1. SILICON

The currently most commonly used material as a basis for all micromachining is silicon with its excellent mechanical and electrical properties. Besides the usefulness of the material in MEMS devices, silicon is biocompatible and can be used for long term implantable device [39].

5.1.2. PDMS AND OTHER POLYMERS

Polydimethylsiloxane, better known as PDMS, is a flexible and transparent silicone elastomer with a variety of applications. It is often used in medical devices or research structures like the microwells described in chapter 4.1. PDMS is an elastic material with excellent chemical resistance giving it a high biocompatibility rating [40]. While PDMS is not used in micromachining directly, micro-scale structures can be made using a mold.

With the help of standard processing methods like photolithography and etching, a mold can be created from a silicon wafer. A flat polished wafer with structures formed using a positive or negative photoresist are often used in literature [41] [42]. To create different shapes of the vertical walls, the silicon wafer can be etched or multiple layers of photoresist can be used. The wafer with a negative of the design structures is then placed in a dish and submerged in a liquid PDMS. After curing at 70 degrees Celcius for 2 hours the PDMS can be peeled from the wafer to reveal the microstructures.

Other polymers like polycarbonate (PC), polystyrene (PS), and methyl-methacrylate (PMMA) are also suited for biomedical applications but require more involving processing [43][44][45]. All three of the materials can be patterned through laser ablation or electron beam lithography. They are less suited for the molding process of PDMS due to their stiff and brittle characteristics.

5.1.3. SU-8

While the photoresist SU-8 is sometimes used with PDMS as a mold, it is also a very chemically inert material itself. It is a light-sensitive polymer which polymerises, the material changes from a monomer to a polymer, when hit by UV light. Without any further material enhancements, the developed polymer is biocompatible and can be used both in-vivo and in-vitro. The hemolytic acitivity is comparable to that of FDA-approved materials like the previously discussed PDMS and medical steel [46].

Besides the biocompatibility SU-8 also has structural advantages over PDMS. While SU-8 does not have the same elastic properties, aspect ratio's of over 20 can be reached with standard photolithography [47]. This makes it an ideal candidate for low volume production of cell separation systems that do not require material flexibility. SU-8 is also transparent for light wavelengths from 360 nm and up as follows from Figure 5.1 [48].

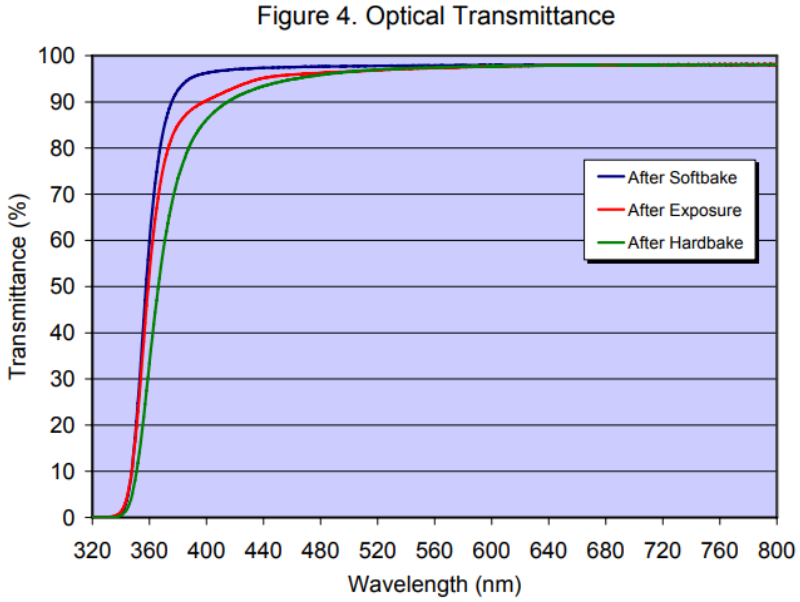

Figure 5.1: The optical transmittance of SU-8 for different wavelengths. Image reproduced from MicroChem [48].

5.2. SURFACE MODIFICATIONS

While some materials might be cytotoxic, material enhancements or thin film depositions can prevent the cells from coming into contact with those cytotoxic materials. Plasma deposition, graft polymerization, and chemical vapor deposition are some examples of coating and material enhancements for improved biocompatibility.

5.2.1. POLYMER PLASMA DEPOSITION

Poly-N-isopropylacrylamide (PNIPAAm) has been widely utilized as surface coating for biomaterials and tissue engineering applications. PNIPAAm has a temperature dependent hydrophobicity with boundary temperatures around cell culture conditions [49]. When the material is kept above the lower critical solution temperature (LCST) of 32 degrees Celsius, the surface of the material is hydrophobic. If PNIPAAm is cooled to below the LCST, the material surface turns hydrophilic. Together with the biocompatibility this is a useful property for controlled cell adhesion and cell release without mechanical or chemical interference [50].

The PNIPAAm is deposited onto a substrate material with a plasma glow discharge of NIPAM vapor [51].

5.2.2. GRAFT POLYMERIZATION

Like plasma deposition, cell adhesion can also be enhanced by surface coating PNIPAAm on PDMS by UV mediated graft polymerization. Graft polymerization uses a base material, a polymer, as a backbone for another polymer to grow on the surface [52]. The large polymer atomic string of the base material will receive branches of the copolymer. This changes the mechanical and chemical properties of the surface with different results for different polymers. Other polymers, such as acrylic acid (AA), acrylamide (AM), dimethylacrylamide (DMA), 2-hydroxyethylacrylate (HEA), and poly-ethylene glycol-monomethoxylacrylate (PEG) can also be grafted on PDMS using UV radiation and exhibit biocompatible properties with varying cell adhesion and hydrophilicity [53].

5.2.3. CHEMICAL VAPOR DEPOSITION

Through chemical vapor deposition (CVD), several materials of interest can be deposited. Plasma enhanced chemical vapor deposition (PECVD) or low pressure chemical vapor deposition (LPCVD) of silicon nitride (Si_3N_4) results in a surface material with high cell attachment properties [54]. The low temperature of involved in PECVD makes it ideal for temperature sensitive devices or devices with, for example, polymers that might burn during other deposition processes. Other materials that could be deposited through CVD and lead to biocompatible materials are silicon carbide and silicon dioxide, though with limited cell adhesion properties [39][55].

6

DEVICE DESIGN AND PROCESSING

Based on the theory described in the previous chapters, a device has to be designed which is able to separate single cells from a suspension and illuminate them individually using multiple wavelengths. The reaction to this illumination should be visible with a unmodified (confocal) microscope. Ideally the device consists of a matrix with many cell-LED pairs to increase the sample size of the cell experiments. The device has to be able to maintain a stable micro-environment in order to limit any cytotoxic effects.

In this chapter the design process of such a device will be described. First several conceptual versions will be discussed, after which the final design and its process flow will be described in detail. As the process flow involved several steps new to the Else Kooi Laboratory cleanroom, such as SU-8 coating on glass, wafer bonding using SU-8, and dicing of a silicon-glass stack, these steps will be described separately.

6.1. FIRST CONCEPTS

In Chapter 4.1 four different methods of trapping cells were described. While all of them do offer mechanisms of immobilizing individual cells and/or moving them to different locations, some of them are not suitable for a lab-on-a-chip involving optical simulations. As the name already implies, light trapping involves relatively high power lasers to manipulate the cells. This would result in optical stimulations not part of the experiment and possibly influencing the results of any light therapy or optogenetic studies. Furthermore, the Joule heating caused by dielectropheresis (DEP) and the delicate machining and control make this technique unsuitable for this device. That is why the first three concepts are based on the microwells of [28], the culturing chamber of [34], and the microfluidic system of [32].

6.1.1. MICROWELLS

As mentioned before, microwells are relatively simple to design and manufacture, however, integrating a light source does form challenges. Instead of using a master mold from SU-8 and polydimethylsiloxane (PDMS) for the final device, SU-8 is used as part of the finished chip. The high compatibility and transparency make SU-8 an excellent material for this purpose.

After a silicon oxide (SiO_2) layer is grown on a silicon wafer, aluminium interconnects are patterned on top of the oxide. MicroLEDs are then glued to the chips and wirebonded to the interconnects. A first coating of MicroChem SU-8 covers the LEDs and creates a smooth surface. A second layer of SU-8 is then patterned with the microwells and developed using MicroChem SU-8 Developer. A schematic drawing of the structure is shown in Figure 6.1.

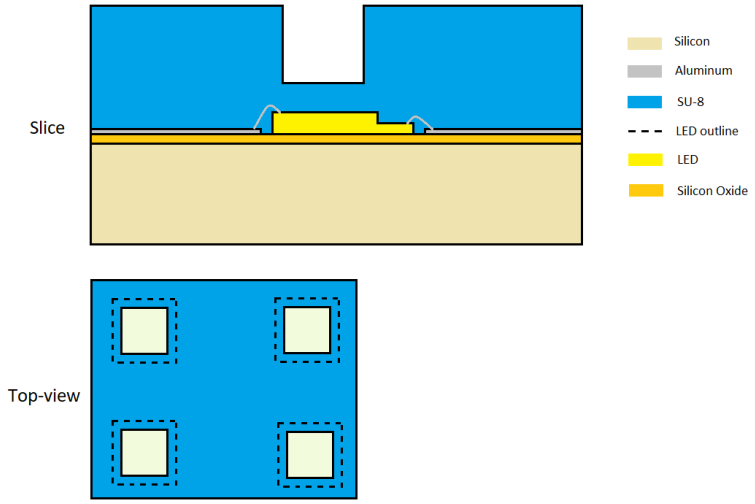

Figure 6.1: A schematic drawing of a microwell-based design for a lab-on-a-chip for optical stimulation of single cells. In the slice-view only one well is shown, while the top-view shows four microwells. The actual device will have more wells. Sizes are not to scale.

For the cell experiments a liquid containing the cells is poured over the matrix of wells and the cells are allowed to settle into those wells. After settling of a sufficient amount of cells the top of device is flushed leaving the captured cells in their wells. The LEDs can then be powered individually to start the optical exposure. However, because of the glass-like transparency of SU-8 there might be light diffusion through the SU-8 which could optically stimulate not only the intended cells, but also cells in nearby wells. Furthermore this platform would require the operator to refresh the medium regularly.

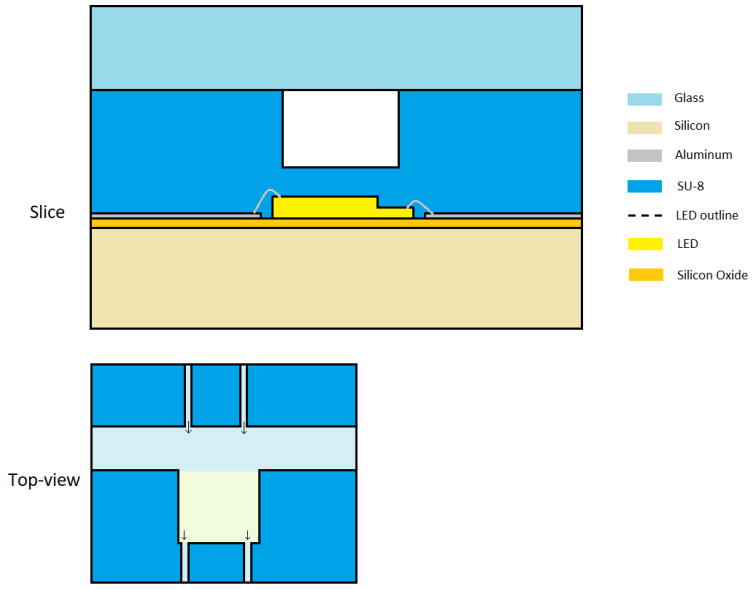

Figure 6.2: A schematic drawing of a culturing chamber-based design for a lab-on-a-chip for optical stimulation of single cells. In both views, only one chamber is shown. The actual device will have more chambers. Sizes are not to scale.

6.1.2. CULTURING CHAMBER

As microwells do not provide a fully self-sustaining environment for the cells, a culturing chamber could form a solution. SU-8 is again used as the structural material, but is now patterned to form microfluidic channels consisting of a main flow channel and small perfusion channels. Furthermore, an additional (glass) wafer is

required to seal the microfluidic channels. This glass wafer could be bonded to the SU-8 structures through pressure and heat bonding as described by S.G. Serra et al. [56]. A bonding pressure of 1.24 MPa to 2.48 MPa is required with a temperature above the glass transition temperature of 175 degrees Celsius. A schematic drawing is available in Figure 6.2.

When cells are fed through the main channel (from left to right in Figure 6.2), they will encounter a small flow of medium trapping them in the chamber. After the main flow is stopped, the flow through the perfusion channels is kept running, supplying the cells with fresh medium continuously. The width and/or height of the perfusion channels has to be significantly smaller than the diameter of a single cell. Of course the flow and pressure differences have to be kept at an appropriate level to avoid rupture of the cells.

6.1.3. MICROFLUIDIC TRAPPING

As an improvement over the previously described design, the amount of perfusion channels can be reduced to a single one by allowing medium to freely flow through the main supply channel after the settling of cells. If one replaces the cell suspension that flows through the main channel with a medium without cells after settling of the cells, the perfusion channel in the chamber can be used as a drain. Figure 6.3 gives an overview of the concept. The device is again structured using SU-8 and microLEDs are used for optical stimulation.

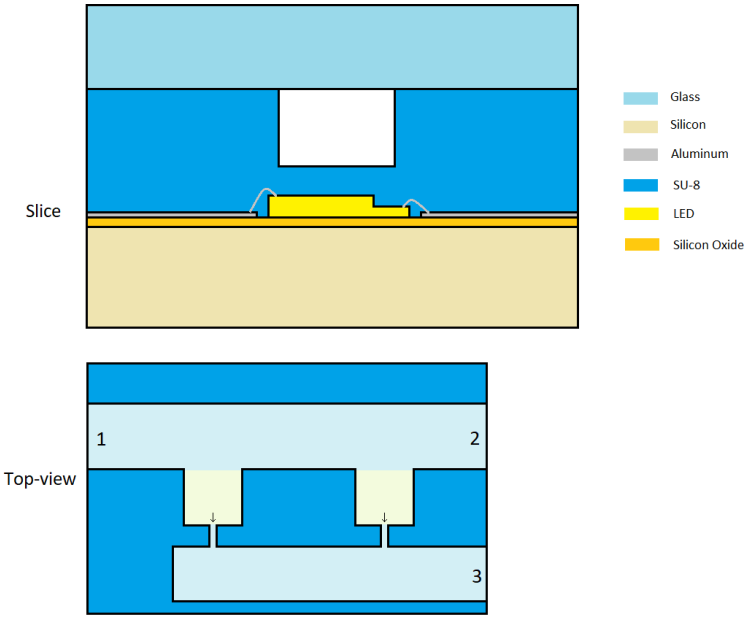

Figure 6.3: A schematic drawing of a microfluidics-based design for a lab-on-a-chip for optical stimulation of single cells. In the slice-view, only one chamber is shown, while the top-down-view shows two chambers in parallel. In the top-down-view **1** is the filling port from where first a cell suspension is loaded followed by a pure medium. **2** is used to flush any excess cells and is closed after flushing. **3** is kept at a lower pressure than **1** to maintain a flow through the perfusion channels. The actual device will have more chambers. Sizes are not to scale.

While slightly increasing the operational difficulties of the device, using the structure from Figure 6.3 the logistics of the fluids inside the chip are simplified compared to the culturing chamber-based concept. Cells are separated from the suspension using a similar flow-based method as described in section 4.1. Using chambers with different sizes and shapes, the ideal trapping conditions for HeLa cells can be determined experimentally.

6.2. FINAL DESIGN

As the project is limited by time, costs, and technology, none of the proposed concepts are directly implementable. While microLEDs are available, it is still a fairly new technology and suppliers are scarce. Low volume orders, like one for this device, are extremely costly and outside the budget of this thesis. This section explains the final design based on the microfluidic trapping concept in detail with solutions for the microLEDs, tube connections, and wirebonding.

6.2.1. MICROLED ALTERNATIVE

As aforementioned, microLEDs in the scale of several tens of micrometers are already available and the technology is evolving on a daily basis. However, unfortunately microLEDs are still extremely valuable, especially in low volume orders. To give an example; Samsung's commercial microLED-based television called 'The Wall' is only available upon request and costs tens of thousands of euros [57]. A solution has thus to be found to still allow for single-cell optical stimulation without the use of expensive microLEDs. Larger LEDs are available at a much lower price, but illuminate a much larger area, making it impossible to have a dense group of separated cells with each their own individually addressable LED. Besides that, an LED with a large area will consume more power and will therefore also increase the temperature of the cell.

To overcome these issues, the cells and LEDs are separated from one another with an additional wafer containing apertures or 'windows' to transfer the light to a single or multiple cells. These apertures are formed using the selective etching of potassium hydroxide (KOH) in silicon. KOH etches silicon preferably in the <100> plane and stops at the <111> plane (etch rate 80:1). If one uses a hard mask with square holes, the resulting etch would form pyramid-like structures with a surfaces at a 54.7 degree angle from the <100> plane. As a hard mask, silicon nitride (Si_3N_4) can be used. This material is highly resistant to KOH with negligible etch rate compared to silicon. Another advantage of silicon nitride is the ability to form a strong membrane over relatively large area. If a double-side polished silicon <100> wafer is covered with silicon nitride on both sides, one side can be used as masking layer while the other side can be used as stop layer and transparent membrane. In Figure 6.4 one can see the structure of this stack of three wafers.

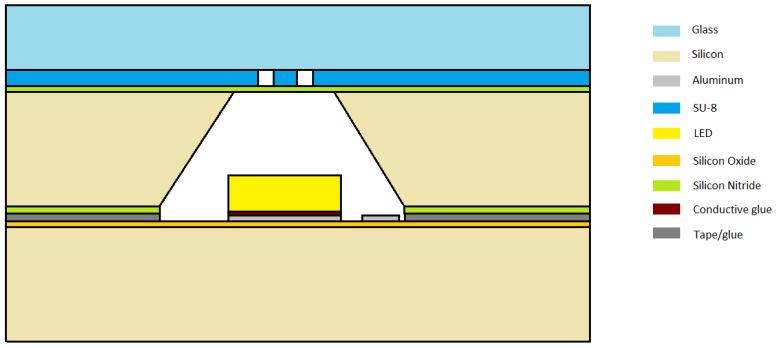

Figure 6.4: A schematic drawing of the device structure with the use of apertures to separate the relatively large LEDs from the cell chambers. Sizes are not to scale.

With the new structure, larger LEDs can be used with a thickness up to 500 μm (wafer thickness). However, LED width will be limited by the maximum stable size of the silicon nitride membrane. With a membrane thickness of 500 nm, the diameter of the membrane cannot exceed 500 μm to limit the risk of mechanical failure, such as cracks or complete shattering. Furthermore, the LED size will be limited by the 54.7 degree wall angle and additional room required for wirebonding. This will be discussed in more detail in Section 6.2.3.

6.2.2. TUBE CONNECTIONS

The SU-8 microfluidic channels are sandwiched between a silicon wafer and a glass wafer (Figure 6.4 shows this clearly), making fluidic connections not that obvious. One of the options is to use an additional thick SU-8 layer of the type 2075 patterned with square tube connections at the end of the microfluidic channels. This additional layer of 200 μm thick would provide enough room for capillary tubes to be inserted to the side of the chip and requires little additional processing steps. The method has been described in detail in literature for the use in a silicon-pyrex sandwich [58]. However, bio-compatible capillary tubes with an outer diameter of below 250 μm are very costly and do not fit the budget of this thesis.

Instead of an SU-8 2075 layer, additional holes will be etched in the bottom wafer (LED) and middle wafer (aperture) to reach the microfluidic channels from the bottom of the chip with more cost-efficient larger tubes. The tube holes in the aperture wafer can be etched using the same KOH-etching steps as with the LED apertures. The only changes that have to be made to this wafer are additional features on the back side mask, and an additional etching step on the front side silicon nitrite. The silicon nitrite membrane that is used as a window above the LEDs has to be removed from the locations where the tube meets the microfluidic channels. Similar to the back side hardmask, the front side silicon nitrite membrane can be patterned using a photoresist mask followed by an etching step in a plasma etcher.

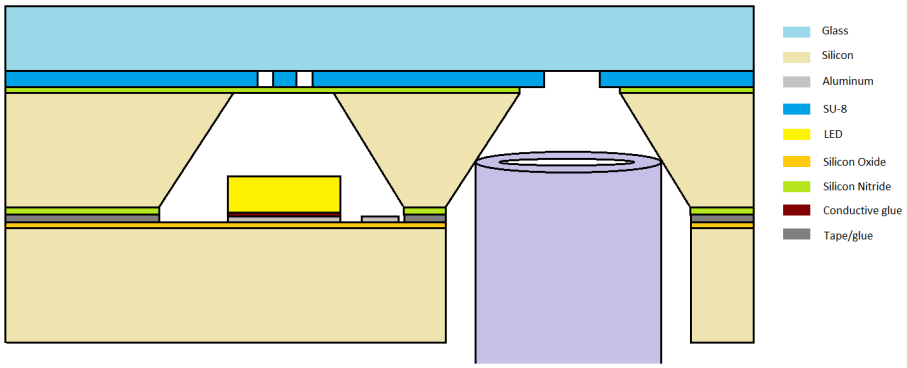

Figure 6.5: A schematic drawing of the device structure with holes in the aperture and LED wafers for tube connections. Sizes are not to scale.

The holes in the LED wafer will require a few additional processing steps. Deep reactive ion etching (DRIE) is used to create holes with vertical sidewalls, but as silicon oxide is an excellent stop-layer for DRIE and the wafer is covered with silicon oxide for improved resistivity between the interconnects and substrate, this oxide first has to be patterned on the back side. After patterning the holes for the tubes in the back side silicon oxide and the front side has been covered in photoresist to protect the chuck, the DRIE process is started and lands on the front side oxide. Leaving the photoresist on the front side, a wet etch removes the silicon oxide on the back side and the membranes on the front side as the etchent penetrates from the back through the holes. After stripping the photoresist, the through holes are ready. Figure 6.5 shows a schematic drawing of the finished design with tube holes.

6.2.3. WIREBONDING

Similar to the microfluidic channels, the interconnects on the LED wafer is sandwiched between two wafers: the LED wafer and the aperture wafer. This makes it impossible to directly wirebond the chip to a PCB and also limits the room for the wirebonding of the LEDs to the LED wafer - the room above and around the LEDs is limited by the aperture holes. Although the 500 μm thick wafers allow for LEDs up to 500 μm thick, a lot of LEDs have a connection on the top side and thus require additional room for wirebonding. To maximize the density of the LEDs while still keeping the costs reasonable, the LEDs from Table 6.1 are used. Each chip has two LEDs of every type to allow for cell experiments with different wavelengths while keeping other factors as similar as possible. These LEDs all have an n-contact on the top and a p-contact on the bottom, meaning that the LEDs have to be glued to the positive interconnect with conductive glue and wirebonded to the negative

interconnect.

Product	Wavelength	Brightness	Meas. current	Size	Polarity
C450EZ500	450 nm	110 mW	150 mA	480x480x170 μm	n-side up
LA HR20WP3	660 nm	12 mW	20 mA	500x500x190 μm	n-side up
LA EI20WP3	780 nm	8 mW	20 mA	500x500x190 μm	n-side up
LA NI20WP3	850 nm	8 mW	20 mA	500x500x190 μm	n-side up

Table 6.1: LEDs used in the lab-on-a-chip. All LEDs have the n-side connector on the top and the p-side connector on the bottom [59][60][61][62].

In order to leave sufficient room for wirebonding in each aperture, the sizes of the apertures have to be adjusted for LED size and wirebond clearance. With a minimal working clearance of 100 μm and a maximum LED size of 500x500x190 μm, the hole in the silicon nitride mask needs to be at least 1010x1010 μm, as becomes obvious from Figure 6.6. This image also shows that, with a standard wafer thickness of 500 μm, the silicon nitride membrane window will be a 309x309 μm square.

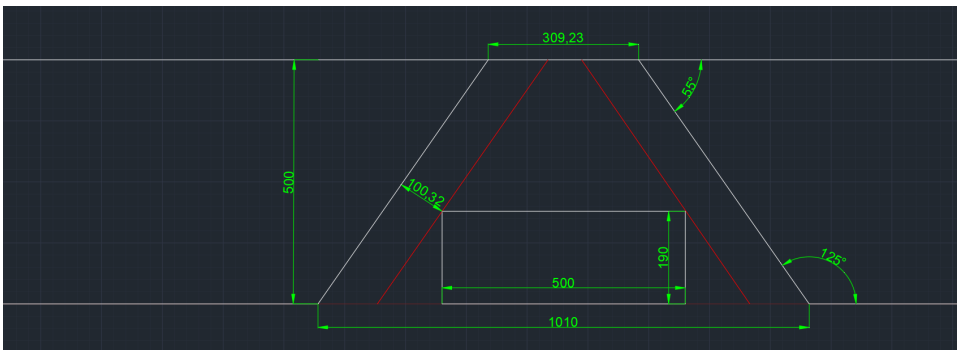

Figure 6.6: Technical drawing of the LEDs and aperture showing the dimensions of the silicon nitrite membrane (top), LED (middle), hole size (bottom), and wirebond clearance (middle). Dimensions are in micrometer. The red lines show the LED size limits based on a minimum wirebond clearance of 100 μm. Dimensions of the LED are taken from Table 6.1. Additional LED thickness from bonding glue is neglected in this image, but is non-zero.

6.3. MICROFLUIDIC SIMULATIONS

6.3.1. FLOW AND PRESSURE SIMULATIONS

While previous research showed promising results with similar microfluidic-based cell trapping devices, flow and pressure simulations were carried out to confirm the working of this particular variant. While the entire fluidic system will be composed of more than just the cell separation (reservoir, pump, tubing, connections to the chip, etc) the assumption is made that no major disruptions are present in those parts. This assumption is made to reduce the simulation difficulty and thus the simulation time. COMSOL's Laminar Flow physics are used for these simulations with water as the flow material. Water is suitable as a fluidic estimation of cell medium (DMEM). Figure 6.7 shows the flow velocity of water in the microfluidic channels; and Figure 6.8 shows the pressure lines of the same system. As there are multiple chamber designs and perfusion channel widths, these figures form an example, but the flow and pressure are similar for all variants.

Figure 6.7 shows that the flow speeds in each channel is nearly identical, meaning there should not be a significant difference in capture effectiveness of the different chambers. In order to avoid rupture of the HeLa cells, the pressure on the cell in a chamber has to be limited. Figure 6.8 shows that the change in pressure in each chamber varies slightly with the highest pressure change in the left-most chamber and the least pressure change in the right-most chamber. While this might have an effect on cell survival with high flow speeds, the difference will most likely be too small to play a significant role in the actual device due to process variations.

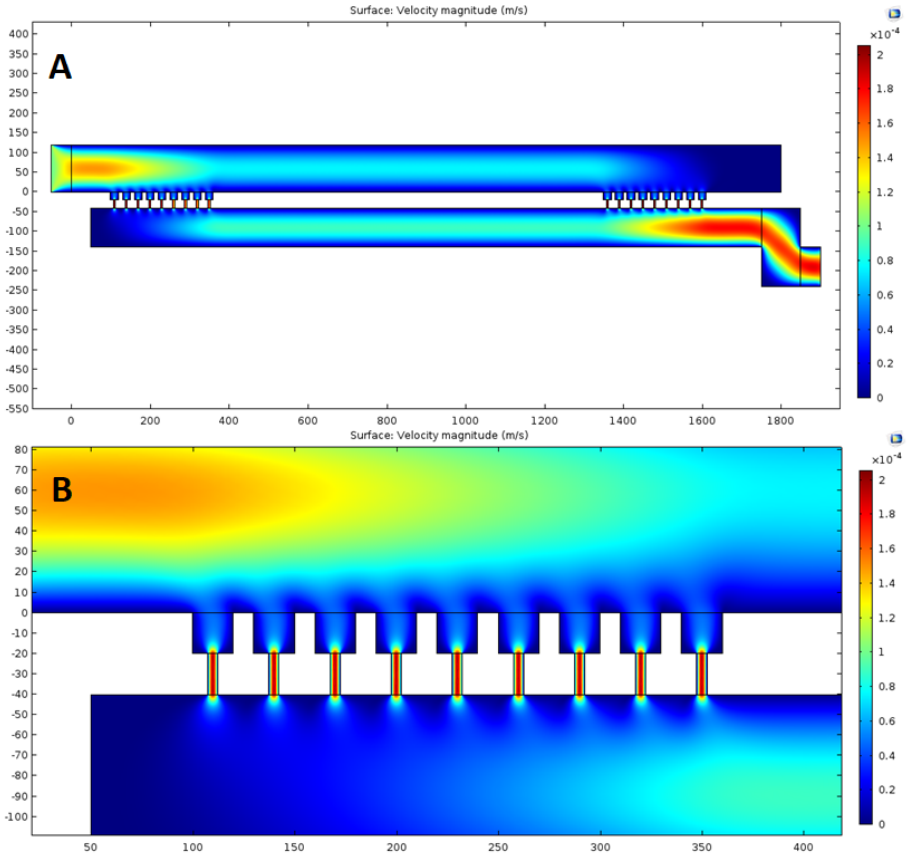

Figure 6.7: COMSOL Multiphysics flow simulations of one of the chamber designs. The inlet flow on the left hand side is 100 μm/s, which equals to roughly 100 μL/h. Changing the value of the inlet flow speed has a mostly linear proportional effect on the flow speeds elsewhere in the system. **A:** An overview of one microfluidic system. Five of those channels will be present in one chip. **B:** A zoomed-in view of the cell chambers.

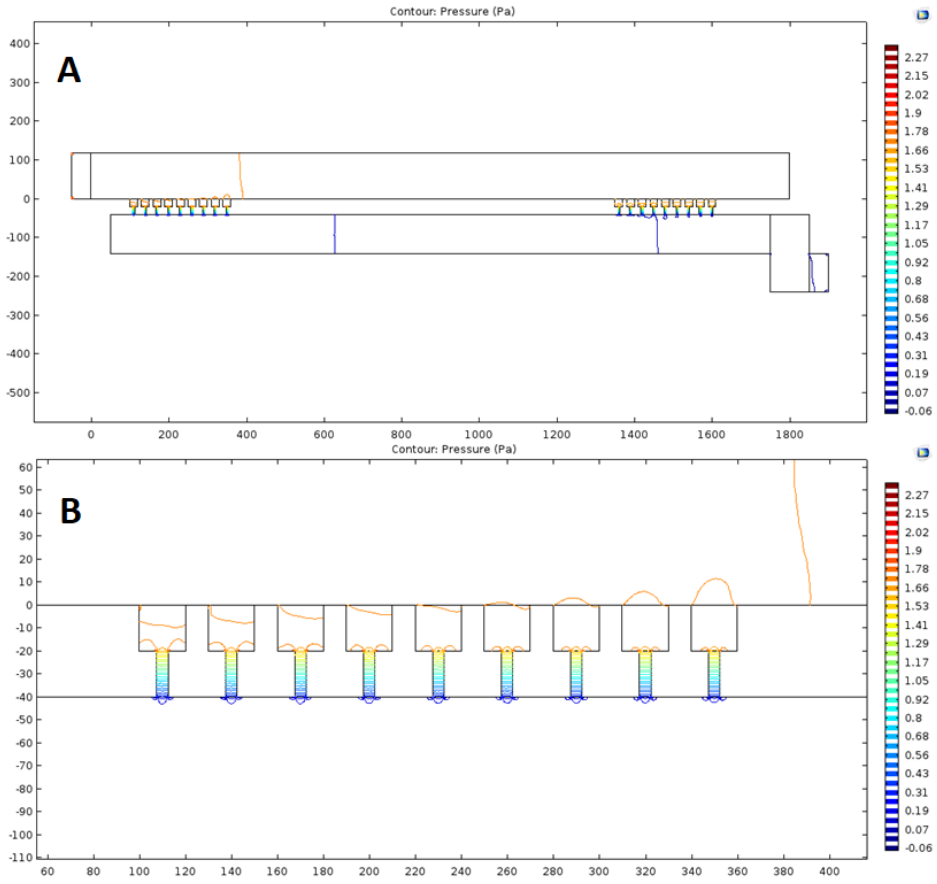

Figure 6.8: COMSOL Multiphysics pressure simulations of one of the chamber designs. **A:** An overview of one microfluidic system. Five of those channels will be present in one chip. **B:** A zoomed-in view of the cell chambers.

6.3.2. PARTICLE SIMULATION

While the fluid flow is quite evenly spread over every channel, it is still possible for particles (cells) to collect at just a few of the chambers. To verify the distribution of the particles in the microfluidic channels, the previously generated flow and pressure results are used in COMSOL's Particle Tracing for Fluid Flow physics. The particles are given the density of the to be used HeLa cells, which is approximately 1.06 g/ml and a diameter of 15 μm [63]. Unfortunately, due to limitations in COMSOL's software, the particle diameter will have no effect on the collisions with the walls. A particle with a diameter of 10 μm will therefore be able to pass through a channel with a width of 1 μm. To prevent the particles from passing through the channels, a filter is placed in each chamber which blocks all particles and freezes them in their position. Additionally, the software does not account for the influence of the particle on the laminar flow, meaning that once a particle enters a chamber, the flow is not blocked. The third and final limitation concerns particle-particle interaction. The particles do not interact with one another; and a chamber could therefore hold any amount of overlapping particles.

Figure 6.9 shows the result after running the simulation for 50 seconds. Two particles can still be seen floating in the main channel, while the others have taken a spot in one of the chambers. The very first chamber holds two particles as can be explained by the lack of particle to particle interaction. Moreover, in other locations one can see the particles passing boundaries as only their center point is used as a physical point. Even though the limitations are clear, the distribution of the particles is relatively even as a result of the even distribution of the flow through each channel.

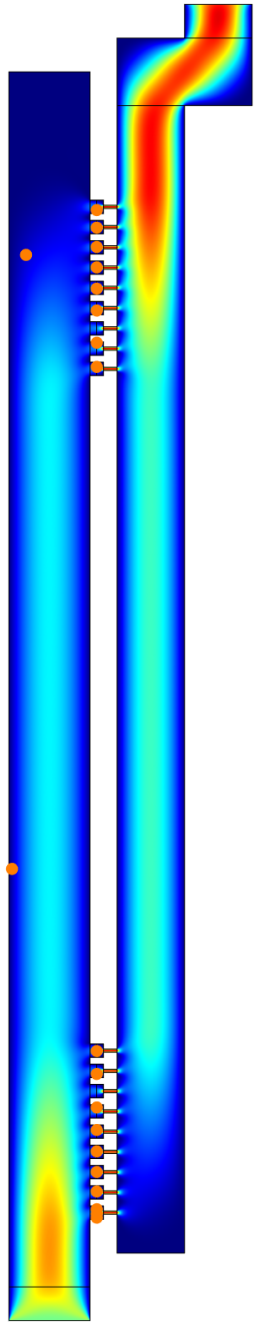

Figure 6.9: COMSOL Particle Tracing for Fluid Flow simulation of the microfluidic system with 20 particles with a diameter of 15 μm (orange dots). The blue-red gradient shows the flow speed relative to the inlet speed.

6.4. PROCESS FLOW

The three layers of the device are processed from three different wafers. Wafer 1 forms the LED interconnect layer (the bottom layer in Figure 6.5), wafer 2 forms the aperture layer (the middle layer in Figure 6.5), and wafer 3 is the glass layer with microfluidic structures (the top layer in Figure 6.5). The complete Else Kooi Laboratory (EKL) flow charts can be found in Appendix C. Pictures of all masks discussed in this section can be found in Appendix D.

6.4.1. WAFER 1

Wafer 1 is a double-sided polished silicon wafer with a thickness of 500 μm. The wafer is coated on the front side with photoresist in the EVG120 automated coating station. After exposure with the full wafer alignment markers (FWAM) in the ASML PAS5500/80 waferstepper and developing in the EVG120, the markers are etched using the Trikon Omega 201 plasma etcher.

The wafer is stripped and cleaned before deposition of 3000 nm (front side) and 4000 nm (back side) silicon oxide using Plasma Enhanced Chemical Vapor Deposition (PECVD). A manual back side photolithography step using the mask **Wafer_1_Back_Side_Tube_Hole** forms the openings for the oxide etch in the Drytek Triode 384T plasma etcher.

Another stripping and cleaning step prepares the wafer for a metallization step in the Trikon Sigma 204 sputter coater for a 675 nm Al (1 % Si) layer. Photolithography with the mask **Wafer_1_Front_Side_LED_IC** and plasma etching of the aluminium forms the interconnects for the LEDs.

After aluminium fence removal and alloying the entire front side is coated in photoresist to form a support layer for the deep reactive ion etching (DRIE). The through-wafer etch is performed in the SPTS Rapier at -10 degrees Celsius with the front side oxide as a stop layer. The photoresist at the front side supports the oxide film to prevent any cracks that could result in damage to the chuck. After removing the oxide, as well as stripping and cleaning the wafer, the wafer is ready for dicing and placing of the LEDs.

6.4.2. WAFER 2

Similar to wafer 1, wafer 2 is a double sided polished silicon wafer with a thickness of 500 μm and prepared with FWAM. The 500 nm silicon nitride membrane is deposited using low pressure chemical vapor deposition (LPCVD), after which a back side photolithography step is performed with the mask **Wafer_2_Back_Side_Apertures**. The starting holes for the apertures are etched into the nitride using the Drytek Triode 384T plasma etcher. After stripping and cleaning the front side is covered in resist with the **Wafer_2_Front_Side_Tube_Hole** mask. Another etching step in the plasma etcher forms the exit holes in some of the cavities for the tubes.

After stripping the resist and cleaning, the wafer is soaked in a KOH bath for 800 minutes to create the typical pyramid-shaped apertures in the silicon.

6.4.3. WAFER 3

Wafer 3 is a 500 μm thick glass wafer which is cleaned using RCA cleaning which consists of a heated bath of a 5:1:1 mixture of H_2O, NH_4OH, and H_2O_2. This is done to improve the bonding strength between the SU-8 and the glass.

SU-8 2025 is then coated using the Brewer Science manual spinners at 2000 rpm to create a film thickness of 20 μm. Due to regulations at the EKL cleanroom, the wafers containing polymers (SU-8) are considered contaminated and are no longer allowed to be processed in a large part of the facilities. After edge bead removal and a soft bake the SU-8 can be patterned through the mask **Wafer_3_Front_Side_Microfluidics** in the manual contact aligner. After developing in MicroChem SU-8 developer the wafer is ready for assembly with wafer 2.

6.4.4. ASSEMBLY

The assembly of the stack is done partly with wafer bonding and partly with chip-to-chip bonding. The glass wafer (wafer 3) and aperture wafer (wafer 2) are bonded together in the AML wafer bonder using SU-8 as the bonding material. Literature has shown that a bonding pressure of about 2 MPa and a temperature of 180

degrees Celsius results in the largest bonding area [56]. The wafers are then diced together in a wafer dicer.

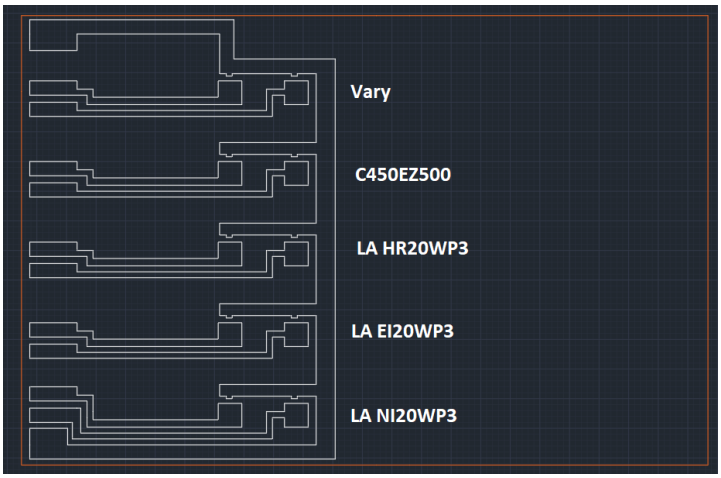

Figure 6.10: An image showing where each type of LED has to be placed. There are two LEDs of each type on every chip.

The LED interconnect wafer is diced separately and each chip receives ten LEDs using pick and place techniques and conductive glue at the bottom side. Figure 6.10 shows the positioning of each type of LED. The LEDs are wirebonded to the interconnects with the clearance from Figure 6.6 in mind. The end result is depicted in Figure 6.11 where eight of the ten LEDs are visible. Also visible in this picture are the DRIE holes meant for the microfluidic tubes. The visible dirt particles are present on the lenses of the microscope and therefore have no influence on the functioning of the device.

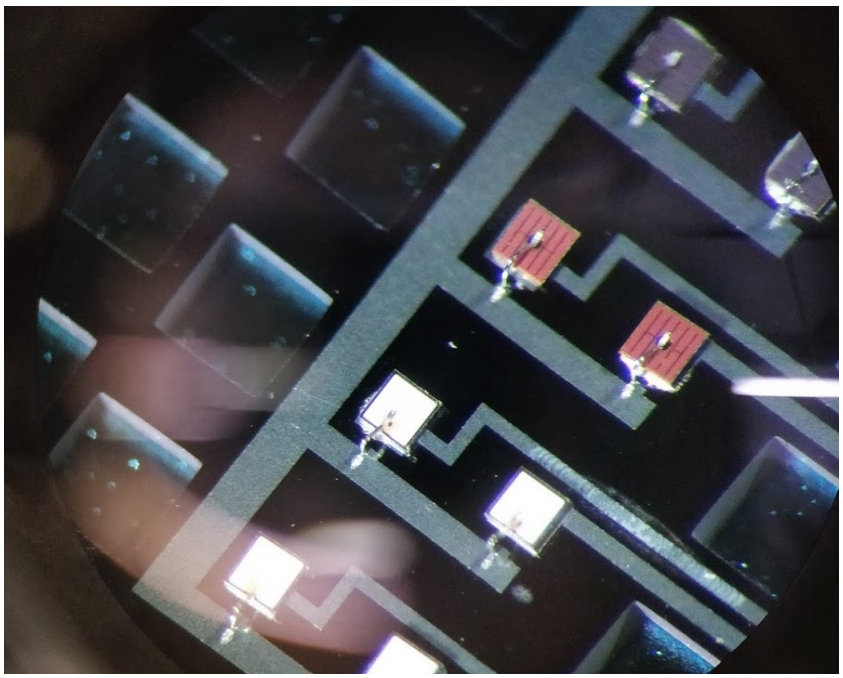

Figure 6.11: An image of a LED IC chip with the LEDs and their wirebonds visible. The holes on the left and right side are DRIE holes for the tubes.

After wirebonding the two parts are glued together and the entire stack is bonded to a PCB. Microfluidic tubes are then connected to the holes in the interconnect and aperture wafers with the use of glue making sure there is a watertight seal.

6.4.5. MASK DESIGN

The masks required for processing are all designed in AutoCAD 2017 and are based on the design from Section 6.2. The LED interconnect wafer (wafer 1) requires two masks. The first mask, used in step 13 of Wafer1 in Appendix C, defines the locations of the through-wafer deep reactive ion etching. These holes are used to guide the tubing to their respective microfluidic inlet or outlet as shown in Figure 6.5. Each square measures 1010x1010 μm and matches the size of the apertures in the aperture wafer (wafer 2). Figure 6.12A shows a single chip on the mask in detail. The entire mask can be found in Appendix D.

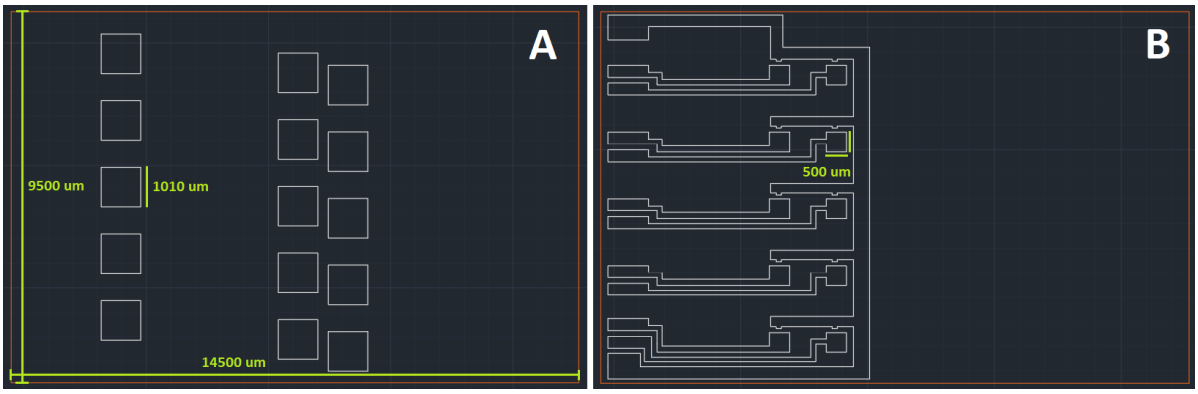

Figure 6.12: Details of the masks used for the LED interconnect wafer (wafer1). The orange lines are not part of the actual masks and only show the borders of each chip. **A:** A single chip of the mask **Wafer_1_Back_Side_Tube_hole** used in step 13 of Wafer1 in Appendix C. **B:** A single chip of the mask **Wafer_1_Front_Side_LED_IC** used in step 23 of Wafer1 in Appendix C.

The second mask for the LED interconnect wafer is used in step 23 of Wafer1 in Appendix C. This mask defines the interconnects for the LEDs. The LEDs are glued to the 500 μm squares with their p-side (anode) down and the n-side (cathode) is wirebonded to the traces next to the pads. Figure 6.12B shows a single chip on the mask in detail. The entire mask can be found in Appendix D. Because these masks have a very large critical feature size (over 100 μm for both), both masks for the LED interconnect wafer are produced on foil to reduce the costs.

Just like the LED interconnect wafer, the aperture wafer (wafer 2) requires two different masks. The first mask is used in step 5 of Wafer2 in Appendix C and defines the starting point for the KOH-etch. As was explained earlier in this chapter, the actual size of the square hole reduces the further the etch proceeds, so the mask is used to etch silicon nitride on the back of the wafer. Figure 6.13A shows a single chip on the mask in detail. The entire mask can be found in Appendix D.

Figure 6.13: Details of the masks used for the aperture wafer (wafer2). The orange lines are not part of the actual masks and only show the borders of each chip. **A:** a single chip of the mask **Wafer_2_Back_Side_Apertures** used in step 5 of Wafer2 in Appendix C. **B:** a single chip of the mask **Wafer_2_Front_Side_Tube_hole** used in step 12 of Wafer2 in Appendix C.

As the KOH-etch ends on a silicon nitride membrane, this membrane has to be removed at the locations

where the tube is attached and the liquid has to pass through. Mask **Wafer_2_Front_Side_Tube_hole** is used for this and shows the holes where the KOH-etch from the other mask will end. Figure 6.13B shows a single chip on the mask in detail. The entire mask can be found in Appendix D. Both masks for the aperture wafer are again produced on foil as a cost reduction.

The glass microfluidics wafer only requires a single photolithography with the mask **Wafer_3_Front_Side_Microfluidics**. The positive resist SU-8 is used with this mask resulting in the microfluidic structures described in Section 6.1.3. Figure 6.14 shows the mask in detail with two different zoom levels. Figure 6.14B shows an example of a trapping chamber shape, but many different shapes and sizes are used on a single wafer. The entire mask and all different chamber shapes can be found in Appendix D.

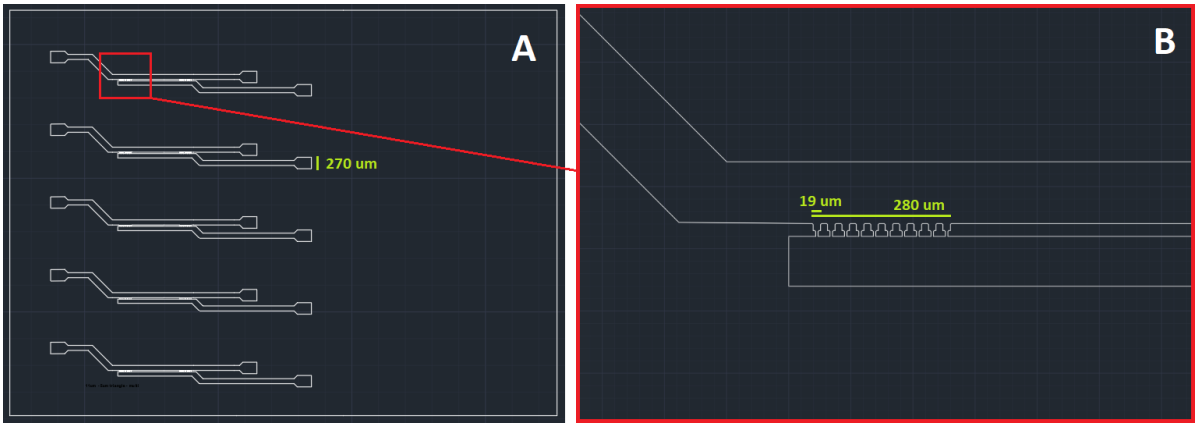

Figure 6.14: Details of the masks used for the microfluidic wafer (wafer3). **A:** a single chip of the mask **Wafer_3_Front_Side_Microfluidics** used in step 5 of Wafer3 in Appendix C. **B:** A detailed view of the mask showing the red square from **A**.

6.5. SU-8 PROCESSING ON GLASS

As the originally proposed MicroChem SU-8 2025 was not available in the cleanroom, an effort was made to dilute MicroChem's SU-8 2075 to the same viscosity as SU-8 2025 using cyclopentanone. Cyclopentanone is the solvent used in the SU-8 2000-series and can therefore be used to reduce the viscosity. The available SU-8 2075 has a viscosity of 22000 cSt (0.022 m^2/s) and consists of 73.45 % solids, while the required SU-8 2025 has a viscosity of 4500 cSt (0.0045 m^2/s) and consists of 68.55 % solids [48]. Using 50 mL of SU-8 2075,

$$50 * \frac{0.7345}{0.6855} - 50 = 3.57mL \tag{6.1}$$

of cyclopentanone has to be added to create a total of 53.57 mL of SU-8 2025. Unfortunately, mixing the chemicals proved to be very difficult due to the high viscosity of SU-8 2075 and the resulting mixture did not provide the required surface smoothness. Even after several days of resting, bubbles and ripples still formed after coating during the soft bake step. The irregularities were clearly visible to the naked eye, as can be seen in Figure 6.15. Besides that, the viscose chemical was hard to work with in the Brewer Science manual spinners. Instead of diluting SU-8 2075, it was therefore decided to use several layers of the much thinner MicroChem SU-8 3005 with a viscosity of 65 cSt [64]. A single layer of SU-8 3005 spinned at 1000 rpm should result in a layer thickness of 10 μm according to the datasheet.

A test cycle on a silicon test wafer with two layers of SU8-3005 spinned at 1000 rpm resulted in a layer-thickness of 14 μm, which is much lower than the expected 20 μm. 13 seconds (15 mW/cm^2) of exposure resulted in slight overexposure.

Another test cycle on a silicon wafer with three layers of SU-8 3005 spinned at 1000 rpm resulted in a layer thickness of 22 μm. It was exposed for 13 seconds and the structures were visible directly after placing the wafer on the hotplate for the post exposure bake. The baking steps included 1 minute at 65 degrees Celsius and 4 minutes at 95 degrees C. Development for 5 minutes in a glass beaker with propylene glycol methyl ether acetate (PGMEA) and a magnetic spinner at 100 rpm seemed enough to the naked eye (no white

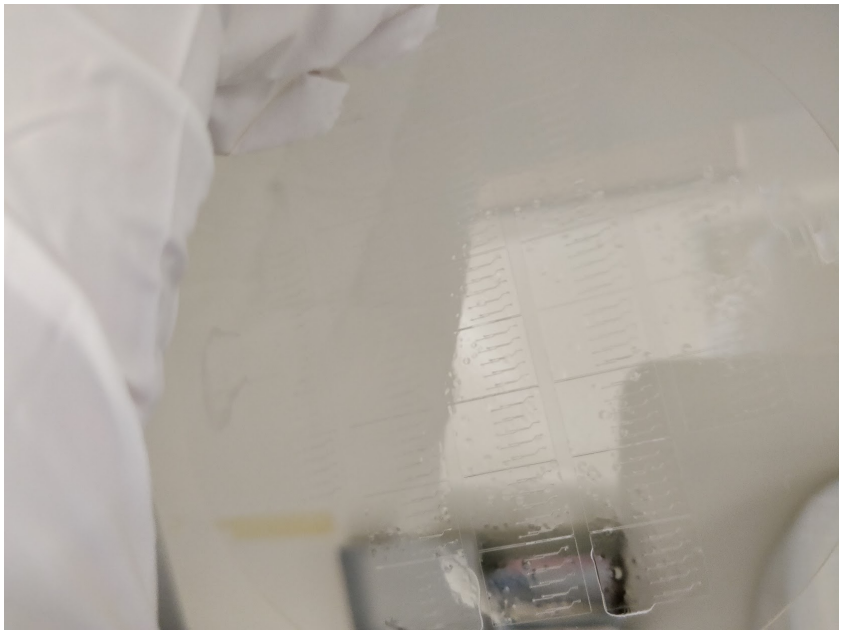

Figure 6.15: A glass wafer coated with diluted SU-8 2075. Irregularities in the SU-8 layer are clearly visible from this picture.

residues visible after rinsing with isopropyl alcohol), but after examination under a microscope it was concluded that the small cavities were underdeveloped. The SU-8 also seemed overexposed, but this could have been a result of underdevelopment in the bottom corners.

Three glass wafers were coated with SU-8 3005. Before coating, the wafers were cleaned in a solution of H_2O, NH_4OH, and H_2O_2 (5:1:1) at 75 degrees Celsius for ten minutes. This cleaning process is also known as RCA-I cleaning. Each wafer is then coated three times at 1000 rpm, resulting in an average layer-thickness of 24 μm ($\pm$4 μm).

The first glass wafer was exposed for 18 seconds (the SU-8 3000 datasheet describes an exposure factor of 1.5 for glass wafers compared to silicon wafers). Directly after exposure, the wafer was placed on a hotplate at 65 degrees Celsius for 1 minute followed by 95 degrees Celsius for 4 minutes. After about 40 seconds, the structures became visible to the naked eye. According to the SU-8 3000 datasheet, a proper exposure can be identified by seeing the structures appear after about one minute at the hotplate. 40 seconds seems about right. Again the development time was set at 5 minutes, but this time the spin speed of the magnetic stirrer was increased to 250 rpm. The increased spin speed resulted in better development, but the exposure time was too low, as some (exposed) SU-8 fragments were removed entirely during the development. As SU-8 absorbs part of the UV light for polymerization, the exposure dose was too low near the glass surface resulting in bad polymerization and thus bad adhesion.

The second glass wafer was processed in the same manner, but with a longer exposure time of 22 seconds. This resulted in a very slight underexposure with some small structures not adhering properly to the glass.

The third glass wafer was exposed for 28 seconds and developed for 6 minutes; all other parameters were the same as with the second glass wafer. This resulted in minor over-exposure, but the adhesion to the glass was much better.

6.6. SU-8 WAFER BONDING

To bond the glass microfluidics wafer with the silicon aperture wafer, initially the two wafers are first aligned under a microscope and temporarily taped together using kapton tape. For the actual SU-8 bonding, the wafer stack is placed in the AML-AWB-04 aligner wafer bonder.

A clean silicon wafer is used as a dummy wafer on top of the stack. This is necessary because normally

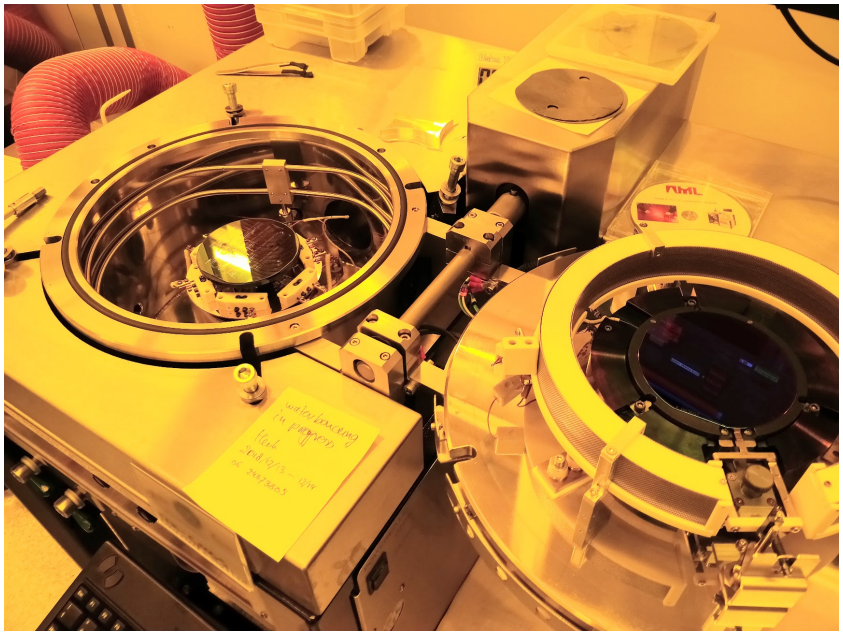

Figure 6.16: The AML wafer bonder. On the left the stack of the silicon and glass wafer is placed on the bottom chuck, on the right a dummy wafer is placed on the top chuck.

the wafers are still separated when placed in the AML wafer bonder. One of the two wafers should be placed on the top chuck and clamped between three pins of a slightly lower height than the wafer itself. Because in our case the wafers are already lightly bonded before using the AML wafer bonder, the top chuck would be empty and the clamping pins would be exposed. This would mean that during bonding, the pins from the top chuck would apply a very local pressure to the wafers leading to an almost certain destruction of the wafers. By placing a dummy wafer on the the top chuck, the clamping pins are not able to touch the other wafers and the dummy wafer will transfer the heat and pressure from the chuck to the to be bonded wafers. The two wafers in the AML wafer bonder together with the dummy wafer can be seen in Figure 6.16. Under vacuum, the wafer stack is heated to a temperature of 200 degrees Celsius and is bonded under a pressure of 5000 N for two hours. Unfortunately, the wafers still cracked near the edges where kapton tape was present, most likely due to the nonuniform pressure because of the thickness the kapton tape adds. Figure 6.17 shows one of the cracked wafer stacks as a result of the kapton tape.

To avoid the use of kapton tape during bonding, the wafers are placed on a hotplate after aligning and temporarily taping them together with tape. The wafers are first heated to a temperature of 65 degrees Celsius after which the temperature is increased to 120 degrees C. A little bit of pressure is applied by hand to the wafer using tweezers, which makes an irregular bond of the SU-8 to the aperture wafer. After cooling the bond is strong enough to remove the tape, but too weak and too irregular for the finished device. The wafers are therefore again placed in the AML wafer bonder together with the aforementioned dummy wafer. With the temperature at 200 degrees Celsius and a pressure of 5000 N for two hours, the wafers did not crack. However, the bonding was too inconsistent as became clear from the Newton's rings — one of the few advantages of using a glass wafer. Figure 6.18 gives an example of the nonuniformly bonded wafers. The temperature is set to 200 degrees C, but the pressure is increased to 8000 N for two hours. This resulted in a much better bond of 70 percent.

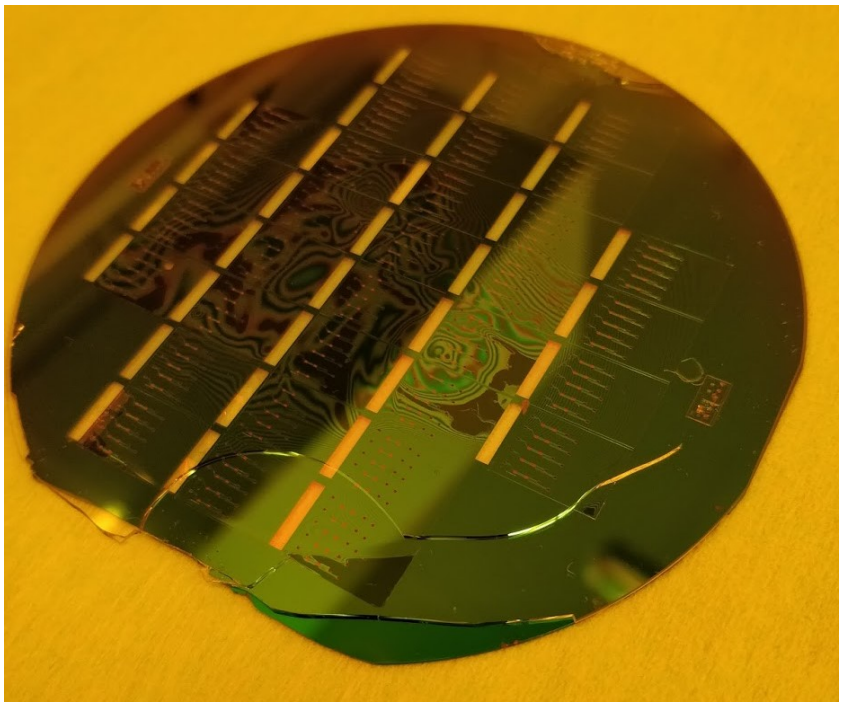

Figure 6.17: A cracked wafer stack. The crack is caused by a nonuniform pressure which is the result of the use of kapton tape on the top and bottom sides in this picture.

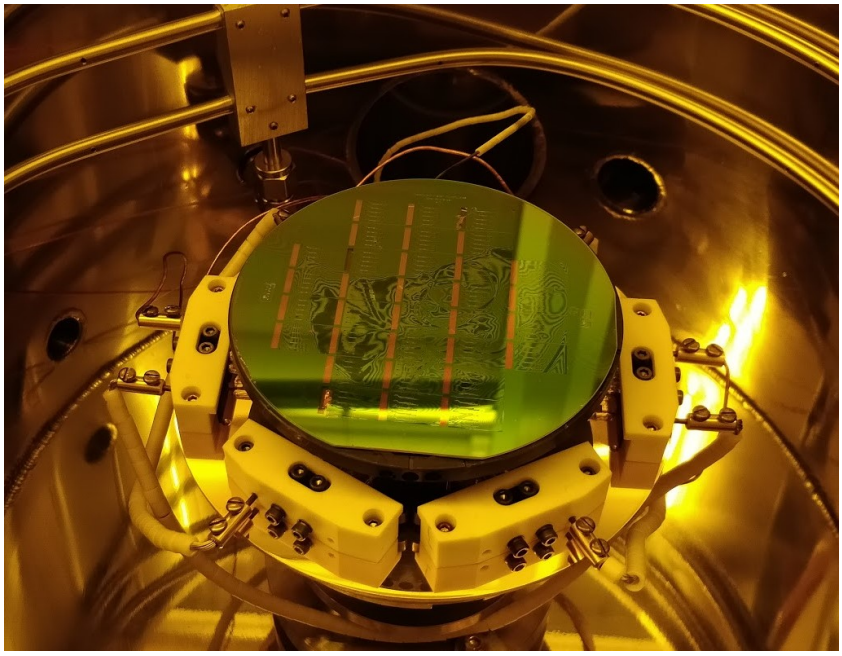

Figure 6.18: An irregular bond due to low bonding pressure. Newton rings are visible around the bonded (dark) areas showing different air layer thicknesses.

6.7. DICING

To section the wafer into individual chips, a sawing wafer dicer was used. The LED interconnect wafer showed no problems during dicing. However, due to the increased thickness and different materials of the wafer stack from the aperture wafer and microfluidic wafer, dicing of those wafers was not possible in a single go. The wear on the saw blades was so high, multiple blades would be required for a single cut. As a solution, the wafers were cut in two steps. First 500 μm deep cuts were made into the silicon wafer, followed by another run of 500 μm deep cuts into the glass wafer. This resulted in much less wear on the saw blades.

6.8. LED CONTROL

For individual control of each of the LEDs, an Arduino MEGA 2560 is used, which is controlled through a Matlab graphical user interface (GUI). The GUI allows for control of each of the ten LEDs with on/off and PWM functionality. The software also allows the user to connect to the Arduino through a specified COM-port and start or disable all LEDs at once. An image of the Matlab GUI can be found in Appendix E.

Each of the digital I/O connections of the Arduino MEGA 2560 is able to supply 20mA at 3.3V, but this is not always sufficient for driving the LEDs. An amplifier board has therefore been designed which amplifies the signal to a resistor-controlled current. The resistors can be tuned to the desired values and let each LED operate at its own forward current. The forward current from the amplifier circuit is equal to $I = (5 - V_f)/R$, where V_f is the forward voltage of the LED. Figure 6.19 shows the schematic for the amplifier circuit, while Figure 6.20 shows the matching PCB. The input consists of five LED control connections, a 3.3V connection, and a ground connection from the Arduino. The power for the operational amplifiers is supplied by a 5V power adapter which connects to the board through a barrel connector. The amplifier board only allows for the control of five LEDs, but each channel has two output connections to be able drive all ten LEDs with one amplifier board. If required, two amplifier boards can be used in parallel for individual control of ten LEDs.

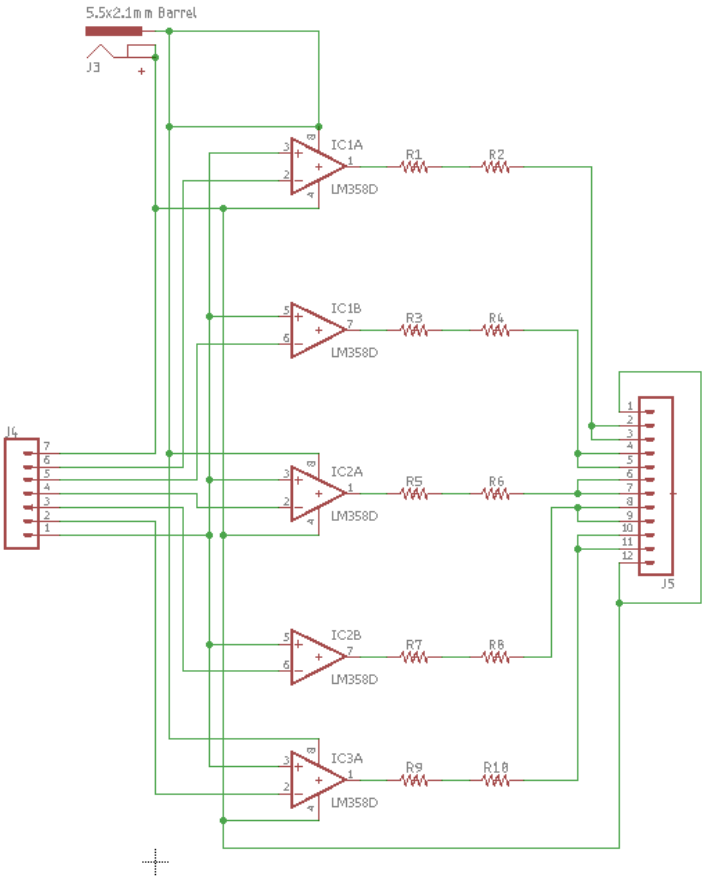

Figure 6.19: Schematic of the amplifier circuit for LED control.

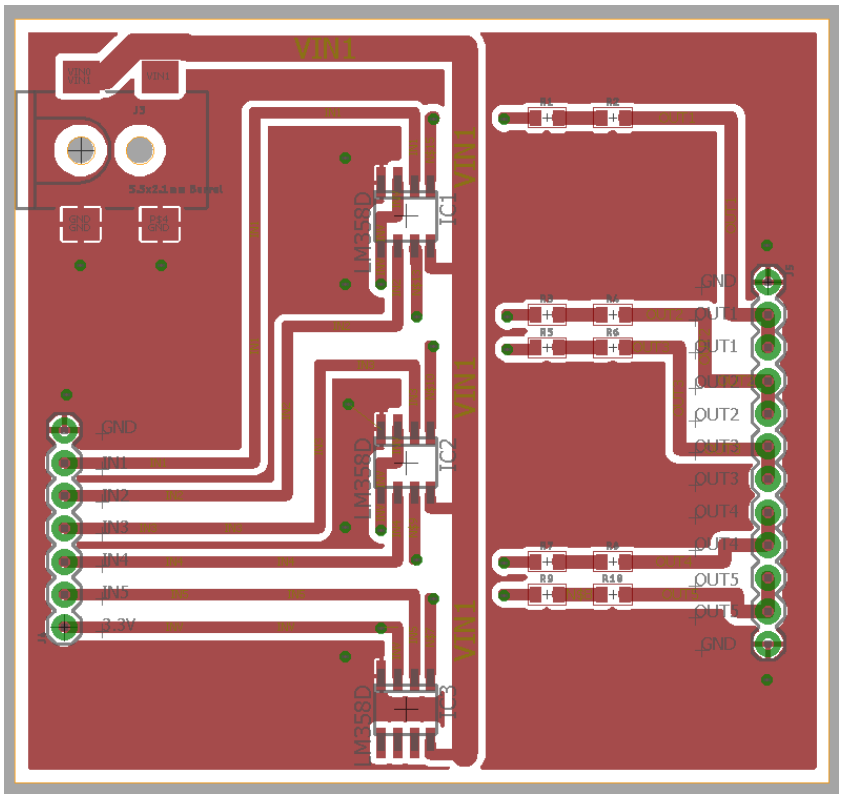

Figure 6.20: The PCB matching the circuit from Figure 6.19. The back side connections are left out for image clarity. An image of the PCB with back side conductive layer enabled can be found in Appendix F

.

7

RESULTS

While a total of eight devices are finished and in (partly) working order, in processing, a large amount of wafers was lost. Most of those wafer were destroyed due to the previously described problems during SU-8 photolithography and wafer bonding, but the use of foil masks also were the cause of some defects. The plastic foil is easily scratched and, although it is taped onto a flat glass plate, the foil was not perfectly smooth with the glass. This caused scraping marks on the photoresist invisible to the naked eye during contact alignment, which ruined some of the subsequent processing steps. Of the five aperture wafers, five IC wafers and five microfluidic wafers (not counting dummy wafers for experiments), only one wafer stack of the aperture wafers and microfluidic wafers was left after bonding. Three of the five IC wafers made it to the end as one wafer had scraping marks, and the other got contaminated in the plasma etcher with particles from a previous user. After dicing, eight devices did not show any defects and had a good bond between the SU-8 microfluidics and the aperture wafer.

Because the manufacturing process received a lot of unexpected delays, the functioning of the microfluidics could not be tested. Although the literature and simulations are promising, real experiments will have to be done to confirm the principle.

7.1. LIGHT OUTPUT

The light output from the LEDs is, of course, current and wavelength dependent. Using a 9 mm^2 light sensor, the light output is measured from the top of the chip. While the SU-8, glass, and silicon nitride membrane are transparent to all used wavelengths [48], some of the light from the LEDs might be lost due to diffusion and reflection in the SU-8 and glass. Table 7.1 shows the measurement results and the converted brightness at the cells in $mW/\mu m^2$. The conversion uses the area of the aperture hole, approximately 900 μm^2, the area of the light sensor, 9 mm^2, and the assumption that all light originating from the aperture reaches the sensor.

LED	Wavelength	Test current	Measured brightness	Brightness at cells
C450EZ500	450 nm	30 mA	19.1 mW	2.12 $mW/\mu m^2$
LA HR20WP3	660 nm	30 mA	14.6 mW	1.62 $mW/\mu m^2$
LA EI20WP3	780 nm	30 mA	8.5 mW	0.94 $mW/\mu m^2$
LA NI20WP3	850 nm	30 mA	8.2 mW	0.91 $mW/\mu m^2$

Table 7.1: Brightness of the LEDs as measured with a 9 mm^2 sensor and converted to $mW/\mu m^2$ at the cells. This conversion assumes that all light passing through the aperture reaches the sensor. Actual values might be higher.

Although Table 7.1 only shows the results for a single test current, LED brightness is relatively linear in its operating region with respect to the forward current. Unfortunately, due to delays in processing and time constraints, measurements on a range of test currents could not be included in this thesis work.

8

Conclusion

The main goal of this project was to fabricate a device which facilitates the Suzhou Institute of Biomedical Engineering and Technology in their research on the reaction of cells to light stimulation. More specifically, a device was required to simplify the stimulation of individual cells while maintaining a stable environment and being able to view the signaling reaction through a confocal microscope. The knowledge gained with such device can help researchers understand cell signaling and potentially aid in the search for cures. The resulting device functions as a proof of concept for more large scale production with a larger budget.

The end result is a chip build up from three different wafers. The top part is a glass wafer with microfluidic channels formed by a layer of SU-8. Although the functioning of the device has yet to be proven, according to simulations the microfluidic channels separate cells into different chambers with one cell in each chamber. The middle wafer, a silicon wafer with pyramid-shaped holes and silicon nitride windows, separates the cells from LEDs on the bottom wafer. This bottom wafer not only functions as a heat sink for the LEDs, but also houses the interconnects which transport the signals from an Arduino and amplifier board to the LEDs.

During processing, a wide variety of unexpected obstacles appeared, causing delays in the project. The processing of the aperture and interconnect wafers went smoothly as they mostly involved process steps often used in EKL. Coating, exposing, and developing SU-8 on a glass wafer, however, proved to be more challenging than initially expected. As the originally proposed MicroChem SU-8 2025 was not available at the time, other versions of the SU-8 material had to be used. A first try was made by diluting SU-8 2075 to the same viscosity as SU-8 2025 by adding more of the solvent cyclopentanone. This lowered the viscosity enough to be able to spincoat layers with a thickness near the expected 25 μm, but irregularities in the layer thickness and other deformations rendered the chemical unusable. Even resting the diluted SU-8 2075 for multiple days did not remove unwanted irregularities. Instead, coating the glass wafer with multiple layers of the much less viscose SU-8 3005 resulted in a consistent layer thickness of 22 μm. However, it should be noted that this did not correspond to the layer thickness mentioned in the SU-8 3000 datasheet.

The next big challenge was the wafer bonding of the aperture wafer and microfluidic wafer. Wafer bonding using SU-8 was also a new process in the EKL cleanroom and resulted in multiple cracked wafers. The high bonding pressure and use of kapton tape did not fare well with the glass and silicon wafers. Pre-bonding the two wafers by hand on a hotplate did help, but the resulting bond was not perfect as Newton rings were clearly visible indicating a small air gap between the two wafers on the areas where the SU-8 did not bond with the aperture wafer.

The stack of the silicon and glass wafer then continued to cause problems at the wafer dicer, causing the saw blades to wear too quickly. To overcome this issue, the wafer stack was diced in two parts, minimising the abrasion of the saw.

To conclude, a total of eight devices are now ready to be used in biomedical cell experiments. These lab-on-a-chip devices are designed to separate and expose individual cells with four different wavelengths ranging from 450 nm to 850 nm. The glass top allows for the operator to view the cell response through a

(confocal) microscope, which makes the device suitable for a large range of different cell signaling experiments. While the device is designed to work with the HeLa cell line, other cells similar in shape and size can also be used. The devices will be used at SIBET for ROS-measurements and, in a later stage, other cell signaling experiments. With this device, research into light stimulation of cells is simplified without the need for large specialized tools. It could help provide researchers with new knowledge on light sensitivity, which could lead to the development of new cures.

9

Discussion

Although the work on this thesis project ended in May 2019, future work will still be required to further analyze the functioning of the device in cell experiments and improve the processing. The project will be continued at SIBET in China where it will be used to collect a variety of signaling data. Although the devices are finished, there are some recommendations for future work.

In order to improve the wafer bonding with SU-8, the coating of the glass wafer has to be optimized. The irregular bonding is most likely caused by small fluctuations in the layer thickness, which could possibly be improved by using a more suitable version of SU-8 like SU-8 2025. Another option could be to coat the aperture wafer with a very thin layer of SU-8 as a bonding glue. This layer could fill the gaps between the SU-8 microfluidic structures and the aperture wafer. The SU-8 glue can be exposed after bonding through the glass wafer to finish the polymerisation, but the silicon nitride membranes do not allow for the use of vacuum chucks during spincoating.

Allowing for more spacing between the LED pads and wirebonding pads will simplify the placing of the LEDs. The LEDs are glued to their respective pads, but due to the small size of the LEDs and viscosity of the glue, the conductive glue sometimes shorts the positive and negative pads. By increasing the distance between the two pads, there is more room for error which could increase the yield.

In future work, the mini-LEDs could also be exchanged for the originally proposed micro-LEDs. This could greatly improve the density of the individual cells on the chip while lowering the difficulty of the manufacturing process by removing the need for an aperture wafer. This will, however, increase the complexity of the interconnects and increase the price of a single device.

Other improvements could be made to the functionality of the devices. The cell chambers are sufficiently large enough to add a diverse set of sensors. For example, optoacoustic imaging, an imaging technique where the acoustic reaction of cells to optical stimulation is measured, is developed for medical diagnosis. This imaging method relies on results from groups of cells. By adding an acoustic sensor to each chamber, the mechanical response of the cell could be measured. Other sensors that could be added in future work are chemical sensors which measure the outflow of each chamber, or temperature sensors next to the cells.

Despite the limitations the design shows great potential for cell research and with future work the device could be expanded with more specialized functionality.

BIBLIOGRAPHY

[1] E. Mester, B. Szende, and P. Gärtner, *The effect of laser beams on the growth of hair in mice,* Radiobiologia, radiotherapia **9**, 621 (1968).

[2] E. N. Marieb and K. Hoehn, *Human anatomy & physiology*, 10th ed. (Pearson, 2016).

[3] M. S. Almén, K. J. Nordström, R. Fredriksson, and H. B. Schiöth, *Mapping the human membrane proteome: a majority of the human membrane proteins can be classified according to function and evolutionary origin,* BMC biology **7**, 50 (2009).

[4] M. Yáñez, J. Gil-Longo, and M. Campos-Toimil, *Calcium binding proteins,* in *Calcium signaling* (Springer, 2012) pp. 461–482.

[5] D. E. Clapham, *Calcium signaling,* Cell **131**, 1047 (2007).

[6] M. J. Berridge, P. Lipp, and M. D. Bootman, *The versatility and universality of calcium signalling,* Nature reviews Molecular cell biology **1**, 11 (2000).

[7] J. A. McCubrey, L. S. Steelman, W. H. Chappell, S. L. Abrams, E. W. Wong, F. Chang, B. Lehmann, D. M. Terrian, M. Milella, A. Tafuri, *et al., Roles of the raf/mek/erk pathway in cell growth, malignant transformation and drug resistance,* Biochimica et Biophysica Acta (BBA)-Molecular Cell Research **1773**, 1263 (2007).

[8] C. Peyssonnaux and A. Eychène, *The raf/mek/erk pathway: new concepts of activation,* Biology of the Cell **93**, 53 (2001).

[9] H. Davies, G. R. Bignell, C. Cox, P. Stephens, S. Edkins, S. Clegg, J. Teague, H. Woffendin, M. J. Garnett, W. Bottomley, *et al., Mutations of the braf gene in human cancer,* Nature **417**, 949 (2002).

[10] R. Mittler, S. Vanderauwera, N. Suzuki, G. Miller, V. B. Tognetti, K. Vandepoele, M. Gollery, V. Shulaev, and F. Van Breusegem, *Ros signaling: the new wave?* Trends in plant science **16**, 300 (2011).

[11] J. F. Turrens, *Mitochondrial formation of reactive oxygen species,* The Journal of physiology **552**, 335 (2003).

[12] F. Muller, *The nature and mechanism of superoxide production by the electron transport chain: its relevance to aging,* Journal of the American Aging Association **23**, 227 (2000).

[13] *mp 10422 CellROX Oxidative Stress Reagents*, Life Technologies Corporation (2012).

[14] C. Vrijman, A. Van Drooge, J. Limpens, J. Bos, J. Van Der Veen, P. Spuls, and A. Wolkerstorfer, *Laser and intense pulsed light therapy for the treatment of hypertrophic scars: a systematic review,* British Journal of Dermatology **165**, 934 (2011).

[15] P. Avci, T. T. Nyame, G. K. Gupta, M. Sadasivam, and M. R. Hamblin, *Low-level laser therapy for fat layer reduction: A comprehensive review,* Lasers in surgery and medicine **45**, 349 (2013).

[16] J. M. Bjordal, C. Couppé, R. T. Chow, J. Tunér, and E. A. Ljunggren, *A systematic review of low level laser therapy with location-specific doses for pain from chronic joint disorders,* Australian Journal of Physiotherapy **49**, 107 (2003).

[17] M. Elman and J. Lebzelter, *Light therapy in the treatment of acne vulgaris,* Dermatologic surgery **30**, 139 (2004).

[18] P. Avci, G. K. Gupta, J. Clark, N. Wikonkal, and M. R. Hamblin, *Low-level laser (light) therapy (lllt) for treatment of hair loss,* Lasers in surgery and medicine **46**, 144 (2014).

[19] J. G. M. e Lima, M. F. C. de Andrade, A. Bergmann, *et al.*, *Low-level laser therapy in secondary lymphedema after breast cancer: systematic review,* Lasers in medical science **29**, 1289 (2014).

[20] A. Guru, R. J. Post, Y.-Y. Ho, and M. R. Warden, *Making sense of optogenetics,* International Journal of Neuropsychopharmacology **18**, pyv079 (2015).

[21] A. V. Kravitz, B. S. Freeze, P. R. Parker, K. Kay, M. T. Thwin, K. Deisseroth, and A. C. Kreitzer, *Regulation of parkinsonian motor behaviours by optogenetic control of basal ganglia circuitry,* Nature **466**, 622 (2010).

[22] B. C. Knollmann, *Pacing lightly: optogenetics gets to the heart,* Nature methods **7**, 889 (2010).

[23] U. Nussinovitch and L. Gepstein, *Optogenetics for in vivo cardiac pacing and resynchronization therapies,* Nature biotechnology **33**, 750 (2015).

[24] Institute for Molecular Bioscience - The Univeristy of Queensland, *Confocal microscopes,* (2019), accessed: 12-04-2019.

[25] G. A. Callaghan, C. Riordan, W. S. Gilmore, I. A. McIntyre, J. M. Allen, and B. M. Hannigan, *Reactive oxygen species inducible by low-intensity laser irradiation alter dna synthesis in the haemopoietic cell line u937,* Lasers in Surgery and Medicine: The Official Journal of the American Society for Laser Medicine and Surgery **19**, 201 (1996).

[26] W. F. Scherer, J. T. Syverton, and G. O. Gey, *Studies on the propagation in vitro of poliomyelitis viruses: Iv. viral multiplication in a stable strain of human malignant epithelial cells (strain hela) derived from an epidermoid carcinoma of the cervix,* Journal of Experimental Medicine **97**, 695 (1953).

[27] A. B. Borle, *Kinetic analyses of calcium movements in hela cell cultures: I. calcium influx,* The Journal of general physiology **53**, 43 (1969).

[28] J. R. Rettig and A. Folch, *Large-scale single-cell trapping and imaging using microwell arrays,* Analytical chemistry **77**, 5628 (2005).

[29] J. Voldman, M. L. Gray, M. Toner, and M. A. Schmidt, *A microfabrication-based dynamic array cytometer,* Analytical chemistry **74**, 3984 (2002).

[30] U. Seger-Sauli, M. Panayiotou, S. Schnydrig, M. Jordan, and P. Renaud, *Temperature measurements in microfluidic systems: Heat dissipation of negative dielectrophoresis barriers,* Electrophoresis **26**, 2239 (2005).

[31] T. N. Buican, M. J. Smyth, H. A. Crissman, G. C. Salzman, C. C. Stewart, and J. C. Martin, *Automated single-cell manipulation and sorting by light trapping,* Applied optics **26**, 5311 (1987).

[32] S. Kobel, A. Valero, J. Latt, P. Renaud, and M. Lutolf, *Optimization of microfluidic single cell trapping for long-term on-chip culture,* Lab on a Chip **10**, 857 (2010).

[33] Z. Zhu, O. Frey, D. S. Ottoz, F. Rudolf, and A. Hierlemann, *Microfluidic single-cell cultivation chip with controllable immobilization and selective release of yeast cells,* Lab on a Chip **12**, 906 (2012).

[34] P. J. Hung, P. J. Lee, P. Sabounchi, N. Aghdam, R. Lin, and L. P. Lee, *A novel high aspect ratio microfluidic design to provide a stable and uniform microenvironment for cell growth in a high throughput mammalian cell culture array,* Lab on a Chip **5**, 44 (2005).

[35] N. McAlinden, D. Massoubre, E. Richardson, E. Gu, S. Sakata, M. D. Dawson, and K. Mathieson, *Thermal and optical characterization of micro-led probes for in vivo optogenetic neural stimulation,* Optics letters **38**, 992 (2013).

[36] N. McAlinden, E. Gu, M. D. Dawson, S. Sakata, and K. Mathieson, *Optogenetic activation of neocortical neurons in vivo with a sapphire-based micro-scale led probe,* Frontiers in neural circuits **9**, 25 (2015).

[37] P. Degenaar, B. McGovern, R. Berlinguer-Palmini, N. Vysokov, N. Grossman, V. Pohrer, E. Drakakis, and M. Neil, *Individually addressable optoelectronic arrays for optogenetic neural stimulation,* in *2010 Biomedical Circuits and Systems Conference (BioCAS)* (IEEE, 2010) pp. 170–173.

[38] J. C. Wataha, C. Hanks, and R. G. Craig, *In vitro synergistic, antagonistic, and duration of exposure effects of metal cations on eukaryotic cells,* Journal of biomedical materials research **26**, 1297 (1992).

[39] G. Kotzar, M. Freas, P. Abel, A. Fleischman, S. Roy, C. Zorman, J. M. Moran, and J. Melzak, *Evaluation of mems materials of construction for implantable medical devices,* Biomaterials **23**, 2737 (2002).

[40] A. Mata, A. J. Fleischman, and S. Roy, *Characterization of polydimethylsiloxane (pdms) properties for biomedical micro/nanosystems,* Biomedical microdevices **7**, 281 (2005).

[41] E. Leclerc, A. Corlu, L. Griscom, R. Baudoin, and C. Legallais, *Guidance of liver and kidney organotypic cultures inside rectangular silicone microchannels,* Biomaterials **27**, 4109 (2006).

[42] T. Fujii, *Pdms-based microfluidic devices for biomedical applications,* Microelectronic Engineering **61**, 907 (2002).

[43] S. Ibrahim, D. A. Higgins, and T. Ito, *Direct-write multiphoton photolithography: a systematic study of the etching behaviors in various commercial polymers,* Langmuir **23**, 12406 (2007).

[44] M. Ni, W. H. Tong, D. Choudhury, N. A. A. Rahim, C. Iliescu, and H. Yu, *Cell culture on mems platforms: a review,* International journal of molecular sciences **10**, 5411 (2009).

[45] H. Duan, J. Zhao, Y. Zhang, E. Xie, and L. Han, *Preparing patterned carbonaceous nanostructures directly by overexposure of pmma using electron-beam lithography,* Nanotechnology **20**, 135306 (2009).

[46] K. V. Nemani, K. L. Moodie, J. B. Brennick, A. Su, and B. Gimi, *In vitro and in vivo evaluation of su-8 biocompatibility,* Materials Science and Engineering: C **33**, 4453 (2013).

[47] J. Liu, B. Cai, J. Zhu, G. Ding, X. Zhao, C. Yang, and D. Chen, *Process research of high aspect ratio microstructure using su-8 resist,* Microsystem Technologies **10**, 265 (2004).

[48] *SU-8 2000 Permanent Epoxy Negative Photoresist*, MicroChem (2015), version 4.

[49] A. Kushida, M. Yamato, C. Konno, A. Kikuchi, Y. Sakurai, and T. Okano, *Temperature-responsive culture dishes allow nonenzymatic harvest of differentiated madin-darby canine kidney (mdck) cell sheets,* Journal of Biomedical Materials Research: An Official Journal of The Society for Biomaterials, The Japanese Society for Biomaterials, and The Australian Society for Biomaterials and the Korean Society for Biomaterials **51**, 216 (2000).

[50] T. Okano, N. Yamada, H. Sakai, and Y. Sakurai, *A novel recovery system for cultured cells using plasma-treated polystyrene dishes grafted with poly (n-isopropylacrylamide),* Journal of biomedical materials research **27**, 1243 (1993).

[51] Y. V. Pan, R. A. Wesley, R. Luginbuhl, D. D. Denton, and B. D. Ratner, *Plasma polymerized n-isopropylacrylamide: synthesis and characterization of a smart thermally responsive coating,* Biomacromolecules **2**, 32 (2001).

[52] Z. Xu, L. Wan, and X. Huang, *Surface modification by graft polymerization,* Surface Engineering of Polymer Membranes , 80 (2009).

[53] S. Hu, X. Ren, M. Bachman, C. E. Sims, G. Li, and N. Allbritton, *Surface modification of poly (dimethylsiloxane) microfluidic devices by ultraviolet polymer grafting,* Analytical chemistry **74**, 4117 (2002).

[54] J. Wei, P. L. Ong, F. E. Tay, and C. Iliescu, *A new fabrication method of low stress pecvd sinx layers for biomedical applications,* Thin Solid Films **516**, 5181 (2008).

[55] C. Coletti, *Silicon carbide biocompatibility, surface control, and electronic cellular interaction for biosensing applications,* University of South Florida Scholar Commons (2007).

[56] S. Serra, A. Schneider, K. Malecki, S. Huq, and W. Brenner, *A simple bonding process of su-8 to glass to seal a microfluidic device,* in *Proceedings of 3rd International Conference on Multi-Material Micro Manufacture, Borovets, Bulgaria* (2007) pp. 3–5.

[57] Samsung, *The Wall - See the greatness,* Brochure (2019).

[58] J. Carlier, S. Arscott, V. Thomy, J. Fourrier, F. Caron, J. Camart, C. Druon, and P. Tabourier, *Integrated microfluidics based on multi-layered su-8 for mass spectrometry analysis,* Journal of micromechanics and Microengineering **14**, 619 (2004).

[59] *Cree EZ500-n Gen 2 LED*, Cree (2018).

[60] *LA HR20WP3 Premium Edition Hyper Red 20 mil*, Light Avenue (2015), version 1.1.

[61] *LA EI20WP3 Premium Edition Infrared (780 nm) 20 mil*, Light Avenue (2015), version 1.1.

[62] *LA EI20WP3 Premium Edition Near Infrared 20 mil*, Light Avenue (2015), version 1.1.

[63] R. P. Ron Milo, *Cell biology by the numbers* (Garland Science, 2015).

[64] *SU-8 3000 Permanent Epoxy Negative Photoresist*, MicroChem.

A

HeLa cell culture protocol

Required materials:

- Fetal bovine serum (FBS)
- DMEM medium (with Penicillin-Streptomycin antibiotics)
- Culture flask
- Pipette
- Trypsin

Maintain a sterile working environment:

- Sterilize the fume cabinet with UV light before the procedure for at least 30 minutes.
- Clean your hands (gloves) with alcohol repeatedly.
- Always clean the desk with alcohol before placing any culture-related items on it.
- Use a new pipette pipe for each step.

Culturing procedure

1. Remove the medium from the current culture.
2. Wash the cells with 5mL FBS-free DMEM gently.
3. Digest the cells with 5mL trypsin until the cells are peeled off.
4. Place the cells in the culturing cabinet for 5 minutes (37 degrees C).
5. Add 5mL DMEM with 10 % FBS to stop the digestion and put it in a flask for centrifuging. Make sure to flush the flask repeatedly so all cells are loosened from the surface.
6. Centrifuge the cells at 1000rpm for 5 minutes.
7. Remove the liquid and suspend the cells in 10 % PBS DMEM. Flush the flask repeatedly to suspend all cells. Divide the cells over two new culture flasks with 25mL 10 % PBS DMEM in each flask.
8. Put the cells in the culturing cabinet (37 degrees C). The culture should be fully grown after 48 hours, but check the cell density before any followup procedure.

B

LEICA TCS SP5 SYSTEM SETUP FOR CELLROX AND NUCBLUE

Start all systems according to the instructions from Figure B.1 and place the sample on the microscope platform. Use the mercury lamp to put the sample into focus.

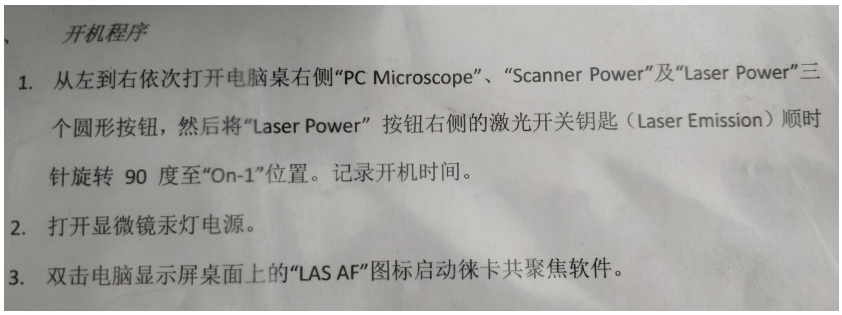

Figure B.1: Leica TCS SP5 system startup instructions. Translated: **1.** Start the systems with the switches from left to right: "PC Microscope", "Scanner Power", and "Laser Power". Then turn the "Laser Power" and turn the Laser Emission key 90 degrees clockwise to the "On-1" position. **2.** Turn on the microscope mercury lamp power supply. **3.** Double click on the "LAS AF" icon on the computer desktop to launch the Leica Software.

Software settings

- In the Leica Confocal software, turn on the appropriate light sources. For CellROX Green enable the Argon laser with an intensity of 20 %. For NUCBlue enable the 405 diode.
- In the Beam Path settings:
  - Set the objective to 20x (AIR). For CellROX Green enable UV to 100 %. For NUCBlue enable visible with 488nm at 50 %, all others should be set to 0 %.
  - PMT1 should be set to a green color with spectral detection at 509 nm to 530 nm (CellROX Green).
  - PMT2 should be set to a blue color with spectral detection at 450 nm to 480 nm (NUCBlue).
  - PMT3 should be disabled.
  - PMT Trans should be set to Scan-DIC.
- In the Acquisition settings:
  - Format to a resolution of 1024x1024 pixels.
  - Speed to 200 Hz.

After readjusting the focus by using the confocal sweep, image acquisition can be started. The system will make multiple passes during which the microscope should not be touched.

C

Flow charts of device processing in EKL cleanroom 100

FLOW CHART MICROFLUIDIC DEVICE (wafer1 + wafer2)

V1.1

Name of owner: Roel Stortelder
Name of mentor: Henk van Zeijl

Run number: .....

Masks: COMURK; Wafer_1_Back_Side_Tube_hole; Wafer_1_Front_Side_LED_IC; Wafer_2_Back_Side_Apertures; Wafer_2_Front_Side_Tube_hole

Wafers: **2x** Dubbelsided polished silicon

PCC: NONE

Wafer1 + Wafer2 (Si, doublesided polished)

1. **Coating Front Side**

   Use the coating station of the EVG120 system with program **"Co – 3012 – 1.4um".**

2. **Alignment and exposure Front Side**

   Use the ASML PAS5500/80 waferstepper. Expose mask **COMURK** with job **FWAM** and use the correct exposure energy (check the energy table).

3. **Developing Front Side**

   Use the developer station of the EVG120 system with program **"Dev – SP"**.

4. **Wafers numbering Front Side**

   Use the glass pens next to the EVG120 system to label the **front side** of the wafers: "Run number – wafer number – BS".

5. **Plasma etching: Alignment markers on front side**

   Use the Trikon Omega 201 plasma etcher. Use sequence **URK_NPD** with a temperature of **20 degree C**. Afterwards inspect the wafers with a microscope. No residues or undercut are allowed.

6. **Layer stripping: photoresist**

   Use the Tepla Plasma 300 system to remove the photoresist. Use **"program 1"**: 1000W and automatic endpoint detection + 2 minutes overetching.

7. **Standard Si cleaning: HNO3 99% and 69.5%**
   a. Clean **10 minutes** in fuming nitric acid at ambient temperature. Use wet bench **"HNO3 99% (Si)"** and the carrier with the **red dot.**
   b. Rinse in the Quick Dump Rinser with the standard program.
   c. Clean **10 minutes** in concentrated nitric acid at 110C. Use wet bench **"HNO3 69% 110C (Si)"** and the carrier with the **red dot.**
   d. Rinse in the Quick Dump Rinser with the standard program.
   e. Use the Avenger Ultra-Pure 6 rinser/dryer with the standard program and the white carrier with a **red dot.**

----------!Only Wafer1 from here!----------

8. **SiO_2 PECVD deposition front side - 3µm**

   Use the Novellus Concept One PECVD reactor to deposit **3000nm** Silicon Oxide. Use recipe **".xxx-siostd"**. Use the logbook of the system to calculate the deposition time.

9. **Measurement: Oxide thickness front side**
   Use the Leitz MPV-SP measurement system for layer thickness measurements on the **front side**.
   Use program "**Th. SiO2 on Si, >50m auto5pts**"
   Expected layer thickness: 3000nm

10. **SiO_2 PECVD deposition back side - 4µm**
    Use the Novellus Concept One PECVD reactor to deposit **4000nm** Silicon Oxide. Use recipe **".xxx-siostd"**. Use the logbook of the system to calculate the deposition time.

11. **Measurement: Oxide thickness back side**
    Use the Leitz MPV-SP measurement system for layer thickness measurements on the **back side**.
    Use program "**Th. SiO2 on Si, >50m auto5pts**"
    Expected layer thickness: 4000nm

12. **Coating back side**
    Use the coating station of the EVG120 system with program **"Co – 3012 – 1.4um".**

13. **Alignment and exposure at back side**
    Use the manual aligner to do flat alignment use the correct exposure energy (check the energy table). Use mask **Wafer_1_Back_Side_Tube_hole.**

14. **Developing back side**
    Use the developer station of the EVG120 system with program **"Dev – SP"**.

15. **Inspection**
    Visually inspect the wafers through a microscope. No residues are allowed.

16. **Plasma etching: 4000nm at back side**
    Use the Drytek Triode 384T plasma etcher to etch **4000nm oxide** at the back side. Use a copy of program **STDOXIDE**. Set the etch time to 600 seconds. (etch rate: 7-10nm/s)

17. **Inspection**
    Visually inspect the wafers. No oxide residues are allowed.

18. **Layer stripping: photoresist**
    Use the Tepla Plasma 300 system to remove the photoresist. Use **"program 1"**: 1000W and automatic endpoint detection + 2 minutes overetching.

19. **Standard Si cleaning: HNO3 99% and 69.5%**
    a. Clean **10 minutes** in fuming nitric acid at ambient temperature. Use wet bench **"HNO3 99% (Si)"** and the carrier with the **red dot.**
    b. Rinse in the Quick Dump Rinser with the standard program.
    c. Clean **10 minutes** in concentrated nitric acid at 110C. Use wet bench **"HNO3 69% 110C (Si)"** and the carrier with the **red dot.**
    d. Rinse in the Quick Dump Rinser with the standard program.
    e. Use the Avenger Ultra-Pure 6 rinser/dryer with the standard program and the white carrier with a **red dot.**

20. **Wet etchinig: oxide dip etch**
    a. Use wet bench **"0.55% HF"** at ambient temperature for **4 minutes** and the carrier with the **black dot.**
    b. Rinse in the Quick Dump Rinser with the standard program
    c. Use the Avenger Ultra-Pure 6 rinser/dryer with the standard program and the white carrier with a **black dot.**

21. **Metallization: 675nm Al with 1% Si at the front side**
    Use the TRIKON SIGMA 204 sputter coater for the deposition of an aluminum metal layer on the wafers. Use recipe **675nm Al @ 350C.**

22. **Coating front side**
    Use the coating station of the EVG120 system with program **"Co – 3012 – 1.4um".**

23. **Alignment and exposure at front side**
    Use the manual aligner to do flat alignment use the correct exposure energy (check the energy table). Use mask **Wafer_1_Front_Side_LED_IC.**

24. **Developing front side**
    Use the developer station of the EVG120 system with program **"Dev – SP"**.

25. **Inspection**
    Visually inspect the wafers through a microscope. No residues are allowed.

26. **Plasma etching: 675nm Aluminum on front side**
    Use the Trikon Omega 201 plasma etcher. Use sequence **"AL06-350"** with a temperature of **25C**. Afterwards **inspect the wafers** with a microscope. No residues or undercut are allowed.

27. **Aluminum fence removal**
    a. Use the Tepla Plasma 300 system to remove the photoresist. Use **"program 1"**: 1000W and automatic endpoint detection + 2 minutes overetching.
    b. Rinse for 1 minute in wet bench **"H20/Triton X-100 tbv Al. Ets"**. Use the carrier with the **yellow dot**.
    c. Use wet bench **"Al. ets 35C"** for **30 seconds** and the carrier with the **yellow dot**.
    d. Rinse in the Quick Dump Rinser with the standard program
    e. Use the Avenger Ultra-Pure 6 rinser/dryer with the standard program and the white carrier with a **black dot.**

28. **Cleaning: HNO3 99% Metal**
    a. Clean **10 minutes** in fuming nitric acid at ambient temperature. Use wet bench **"HNO3 99% (metal)"** and the carrier with the **red and yellow dot.**
    b. Rinse in the Quick Dump Rinser with the standard program.
    c. Use the Avenger Ultra-Pure 6 rinser/dryer with the standard program and the white carrier with a **black dot.**

29. **Alloying**
    Heat the wafers to **400^{O}C** for **20 minutes**. Use furnace tube **C4** with program **"ALLOY1".** NOTE: Because of the cooling down of the boat and paddle, the loading time may **not exceed 10 minutes**!!!

30. **Coating front side**
    Use the coating station of the EVG120 system with program **"Co – 3012 – 3.2um".**

31. **Bake photoresist**
    Do an additional baking in the memmert oven at **130C** for **1 hour**.

32. **Through-wafer etch from back side**
    Use the SPTS Rapier with program **"EKL_flatbottom"** at **-10C** for **200 cycles**.

33. **Oxide wet etch**
    Use the wet etching bench to remove the residual oxide film from the cavities.

34. **Layer stripping: photoresist**
    Use the Tepla Plasma 300 system to remove the photoresist. Use **"program 1"**: 1000W and automatic endpoint detection + 2 minutes overetching.

35. **Standard Si cleaning: HNO3 99% and 69.5%**
    a. Clean **10 minutes** in fuming nitric acid at ambient temperature. Use wet bench **"HNO3 99% (Si)"** and the carrier with the **red dot.**
    b. Rinse in the Quick Dump Rinser with the standard program.
    c. Clean **10 minutes** in concentrated nitric acid at 110C. Use wet bench **"HNO3 69% 110C (Si)"** and the carrier with the **red dot.**
    d. Rinse in the Quick Dump Rinser with the standard program.
    e. Use the Avenger Ultra-Pure 6 rinser/dryer with the standard program and the white carrier with a **red dot.**

Wafer2 (Si, doublesided polished)

NOTE: FIRST STEPS ARE ALREADY DONE TOGETHER WITH WAFER1

1. **Standard Si cleaning: HNO3 99% and 69.5% (optional if directly after zero layer + cleaning)**
    f. Clean **10 minutes** in fuming nitric acid at ambient temperature. Use wet bench **"HNO3 99% (Si)"** and the carrier with the **red dot.**
    g. Rinse in the Quick Dump Rinser with the standard program.
    h. Clean **10 minutes** in concentrated nitric acid at 110C. Use wet bench **"HNO3 69% 110C (Si)"** and the carrier with the **red dot.**
    i. Rinse in the Quick Dump Rinser with the standard program.
    j. Use the Avenger Ultra-Pure 6 rinser/dryer with the standard program and the white carrier with a **red dot.**

2. **LPCVD Silicon Nitride deposition (500nm)**
    Use the oven **E2** for LPCVD silicon nitride deposition. Use recipe 1: **"4inchstd"** for about **1h5m** for the deposition of 500nm LPCVD SiN. Check the logbook for exact time.

3. **Measurement: Nitride thickness**
    Use the Leitz MPV-SP measurement system for layer thickness measurements on **both sides**.
    Use the correct program for SiN measurements
    Expected layer thickness: 500nm

4. **Coating back side**
    Use the coating station of the EVG120 system with program **"Co – 3012 – 1.4um".**

5. **Alignment and exposure at back side**
    Use the manual aligner to do flat alignment use the correct exposure energy (check the energy table). Use mask **Wafer_2_Back_Side_Apertures.**

6. **Developing back side**
    Use the developer station of the EVG120 system with program **"Dev – SP"**.

7. **Inspection**
    Visually inspect the wafers through a microscope. No residues are allowed.

8. **Plasma etching: 500nm SiN at back side**
    Use the Drytek Triode 384T plasma etcher to etch **500nm nitride** at the back side. Use a copy of program **STDNITRIDE**. Set the etch time to 100 seconds.

9. **Layer stripping: photoresist**

   Use the Tepla Plasma 300 system to remove the photoresist. Use **"program 1"**: 1000W and automatic endpoint detection + 2 minutes overetching.

10. **Standard Si cleaning: HNO3 99% and 69.5%**
    a. Clean **10 minutes** in fuming nitric acid at ambient temperature. Use wet bench **"HNO3 99% (Si)"** and the carrier with the **red dot.**
    b. Rinse in the Quick Dump Rinser with the standard program.
    c. Clean **10 minutes** in concentrated nitric acid at 110C. Use wet bench **"HNO3 69% 110C (Si)"** and the carrier with the **red dot.**
    d. Rinse in the Quick Dump Rinser with the standard program.
    e. Use the Avenger Ultra-Pure 6 rinser/dryer with the standard program and the white carrier with a **red dot.**

11. **Coating front side**

    Use the coating station of the EVG120 system with program **"Co – 3012 – 1.4um".**

12. **Alignment and exposure at front side**

    Use the manual aligner to do flat alignment use the correct exposure energy (check the energy table). Use mask **Wafer_2_Front_Side_Tube_hole.**

13. **Developing front side**

    Use the developer station of the EVG120 system with program **"Dev – SP"**.

14. **Inspection**

    Visually inspect the wafers through a microscope. No residues are allowed.

15. **Plasma etching: 500nm SiN at front side**

    Use the Drytek Triode 384T plasma etcher to etch **500nm nitride** at the back side. Use program **STDNITRIDE**. Set the etch time to 100 seconds.

16. **Layer stripping: photoresist**

    Use the Tepla Plasma 300 system to remove the photoresist. Use **"program 1"**: 1000W and automatic endpoint detection + 2 minutes overetching.

17. **Cleaning: HNO3 99% and 69.5%**
    f. Clean **10 minutes** in fuming nitric acid at ambient temperature. Use wet bench **"HNO3 99% (Si)"** and the carrier with the **red dot.**
    g. Rinse in the Quick Dump Rinser with the standard program.
    h. Clean **10 minutes** in concentrated nitric acid at 110C. Use wet bench **"HMO3 69% 110C (Si)"** and the carrier with the **red dot.**
    i. Rinse in the Quick Dump Rinser with the standard program.
    j. Use the Avenger Ultra-Pure 6 rinser/dryer with the standard program and the white carrier with a **red dot.**

18. **Wet etchinig: KOH etch**
    a. Use wet bench **"KOH etch"** at ambient temperature for **800 minutes** and the carrier with the **black dot.**
    b. Rinse in the Quick Dump Rinser with the standard program
    c. Use the Avenger Ultra-Pure 6 rinser/dryer with the standard program and the white carrier with a **black dot.**

    NOTE: Wafers contain delicate structures after the etching step (membranes)

19. **Cleaning: HNO3 99% and 69.5%**
    d. Clean **10 minutes** in fuming nitric acid at ambient temperature. Use wet bench **"HNO3 99% (Si)"** and the carrier with the **red dot.**
    e. Rinse in the Quick Dump Rinser with the standard program.
    f. Clean **10 minutes** in concentrated nitric acid at 110C. Use wet bench **"HNO3 69% 110C (Si)"** and the carrier with the **red dot.**
    g. Rinse in the Quick Dump Rinser with the standard program.
    h. Use the Avenger Ultra-Pure 6 rinser/dryer with the standard program and the white carrier with a **red dot.**

    NOTE: Wafers contain delicate structures (membranes)

FLOW CHART MICROFLUIDIC DEVICE (Wafer3 + assembly only)

V1.2

Name of owner: Roel Stortelder
Name of mentor: Henk van Zeijl

Run number: .....

Masks: Wafer_3_Front_Side_Microfluidics

Wafers: **1x** glass

PCC: **SU-8 (polymer) on wafer 3**

Wafer 3 (glass wafer) – Poly lab

1. **RCA cleaning**
   Perform an RCA cleaning step on the glass wafer (SAL)
2. 20um SU-8 2015 spin-coat (2000rpm)

   NOTE: WAFER CONTAINS POLYMER (SU-8)

3. Edge Bead Removal
4. Soft bake for 3-4 minutes @ 95^{o}C
5. Patterning through mask (**Wafer_3_Front_Side_Microfluidics**) @225mJ/cm^{2} (+40% with filter) with the contact aligner
6. Post Exposure Bake for 1 minute @ 65^{o}C and 4-5 minutes @ 95^{o}C
7. SU-8 developing in SU-8 developer or acetone for 4 minutes. Ultrasonic bath might be helpful.
8. Spray/wash with SU-8 developer for 10 seconds
9. Wash with Isopropyl Alcohol for 10 seconds **(Figure 8)**
10. If there is still a white film present after washing: just do another developing step.

Assembly – MEMS lab – NOTE: WAFERS CONTAIN POLYMER (SU-8)

1. Wafer 3 (Microfluidic wafer) is placed on top of wafer 2 (aperture wafer).
2. Bond with pressure of 2 MPa and at 180 degrees C.
3. Dice the assembly of the microfluidic wafer and aperture wafer.
4. Dice wafer 1 (LED IC).
5. Pick and place the LEDs with conductive glue on the pads of the LED IC chips.
6. Heat the LED IC chips in the oven at 120 degrees C to cure the glue.
7. Wirebond the LEDs to the traces on the LED IC chips.
8. Attach microfluidic-aperture chips to the LED chips with glue.
9. Heat the completed chips in the oven at 120 degrees C to cure the glue.
10. Glue the chips to the PCB (high thermal conductive glue).
11. Wirebond the chips to the traces on the PCB.
12. Attach the tubing using glue.

D

MASK DESIGNS

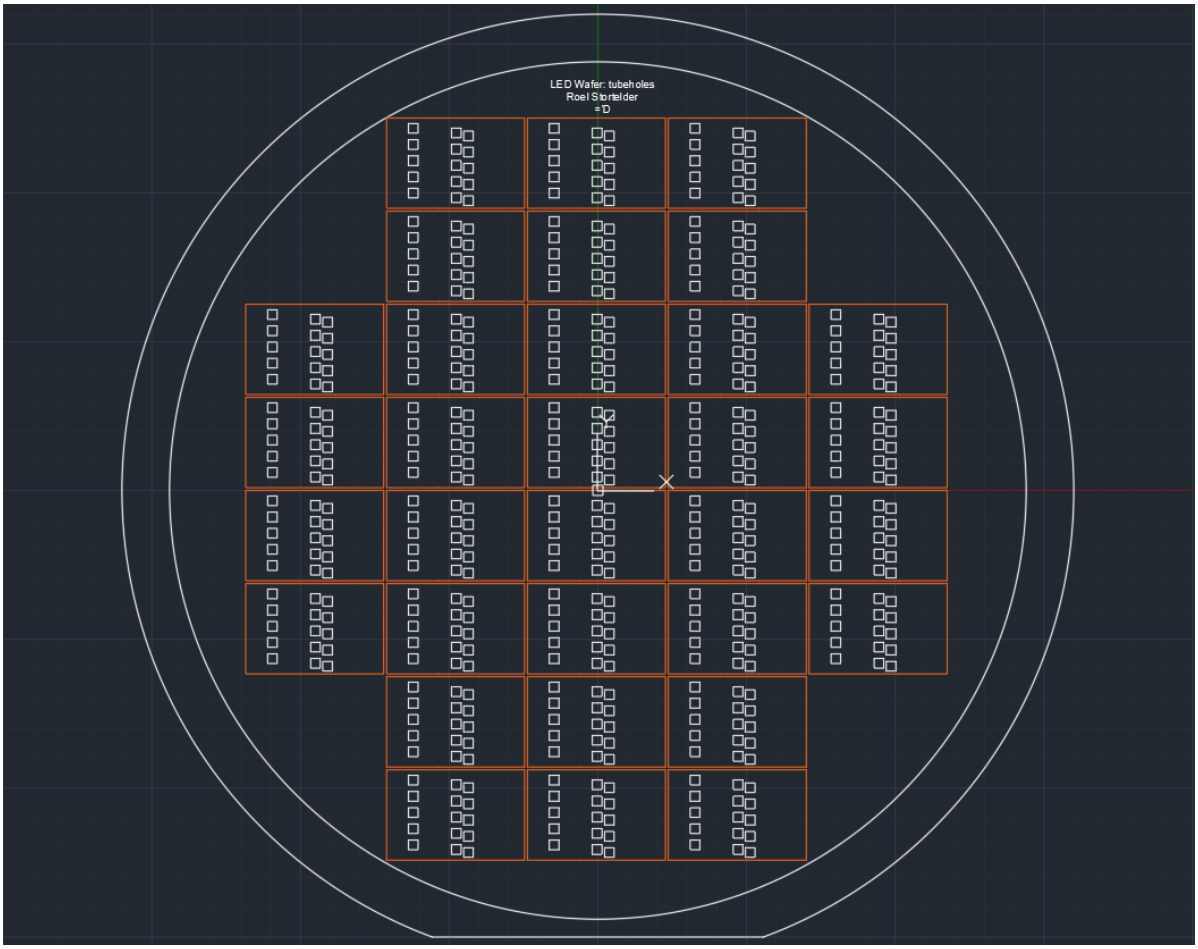

Figure D.1: Mask **Wafer_1_Back_Side_Tube_hole** used in step 13 of Wafer1 in Appendix C. The image shows the entire wafer without alignment markers. The orange lines are not part of the actual mask and only show the borders of each chip.

Figure D.2: Mask **Wafer_1_Back_Side_Tube_hole** used in step 13 of Wafer1 in Appendix C. The image shows a single chip. The squares show the through-wafer holes of the deep reactive ion etching. The orange lines are not part of the actual mask and only show the borders of the chip. The width of the orange box is 14500 μm.

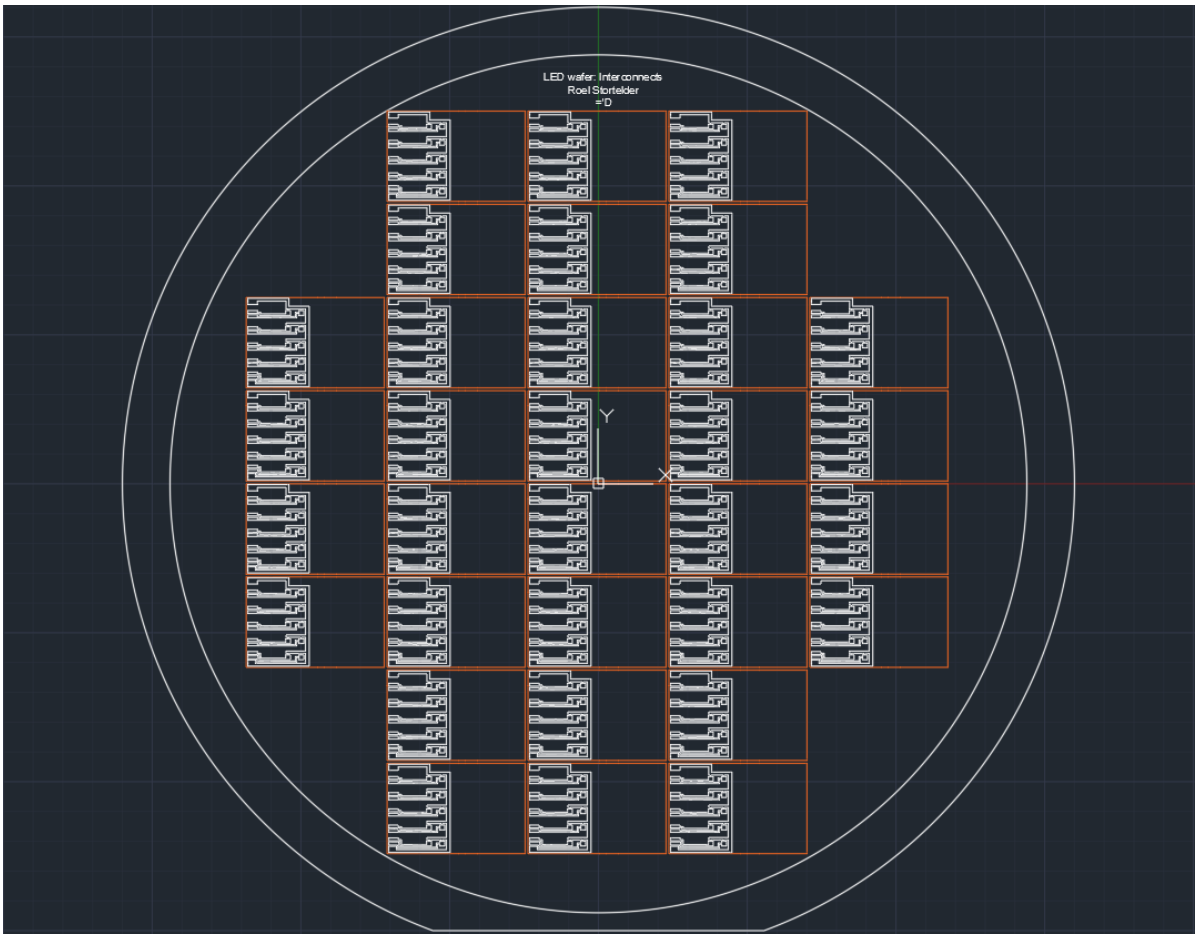

Figure D.3: Mask **Wafer_1_Front_Side_LED_IC** used in step 23 of Wafer1 in Appendix C. The image shows the entire wafer without alignment markers. The orange lines are not part of the actual mask and only show the borders of each chip.

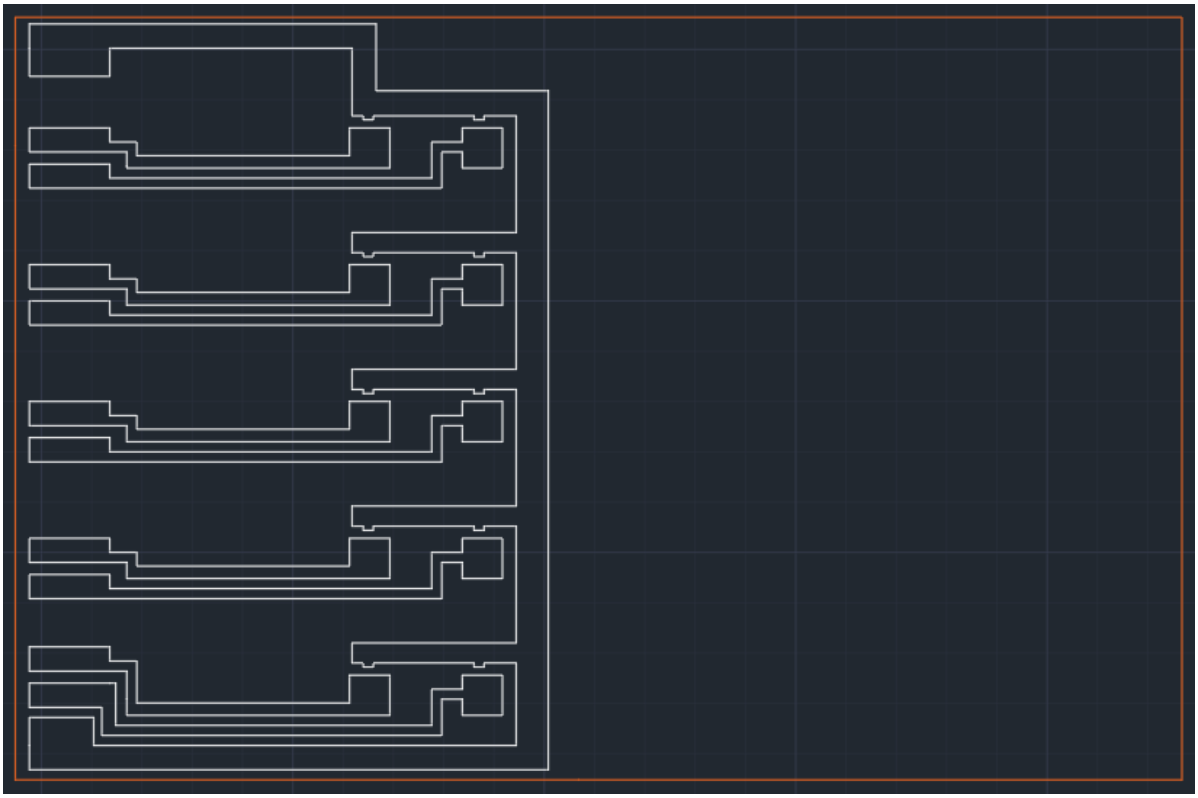

Figure D.4: Mask **Wafer_1_Front_Side_LED_IC** used in step 23 of Wafer1 in Appendix C. The image shows a single chip. This mask defines the aluminium interconnects for the LEDs. The orange lines are not part of the actual mask and only show the borders of the chip. The width of the orange box is 14500 μm.

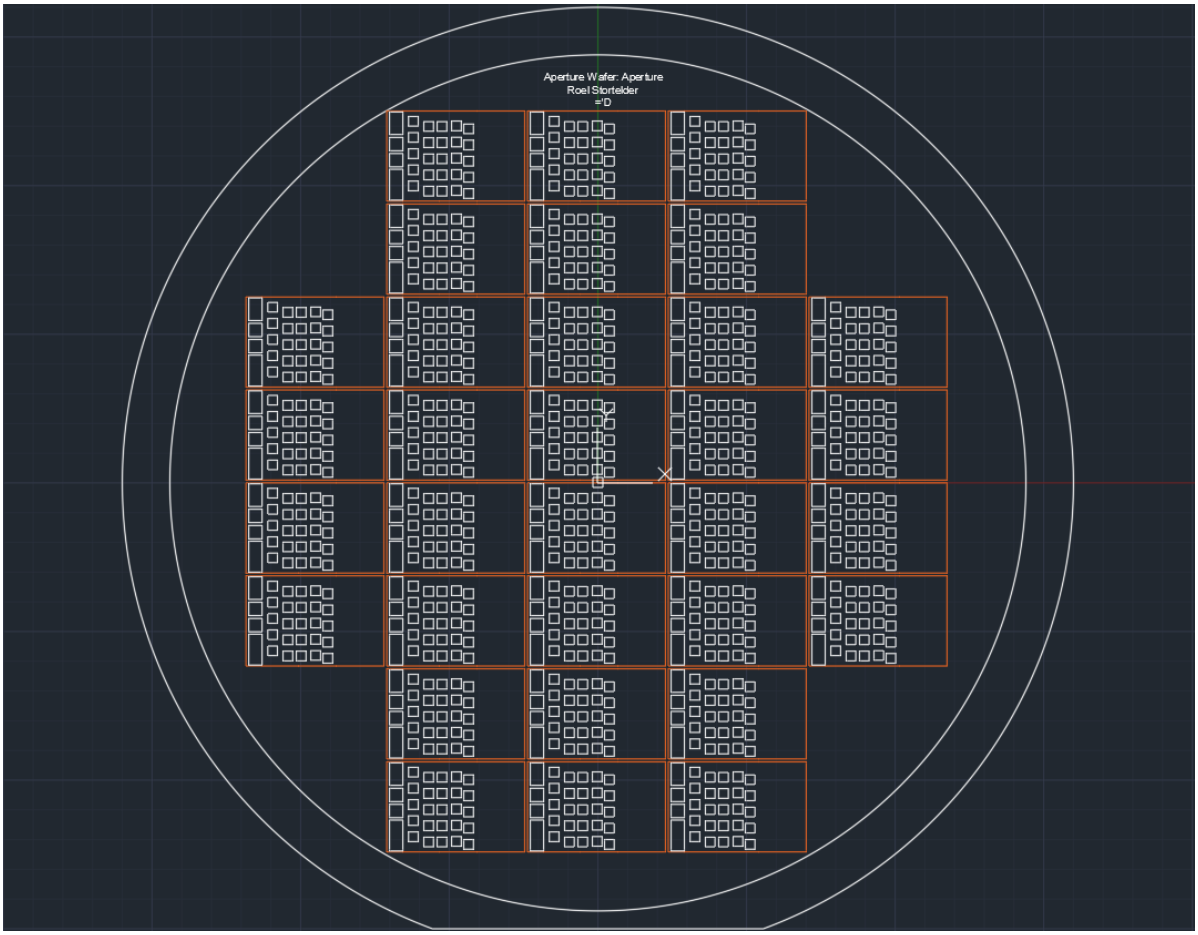

Figure D.5: Mask **Wafer_2_Back_Side_Apertures** used in step 5 of Wafer2 in Appendix C. The image shows the entire wafer without alignment markers. The orange lines are not part of the actual mask and only show the borders of each chip.

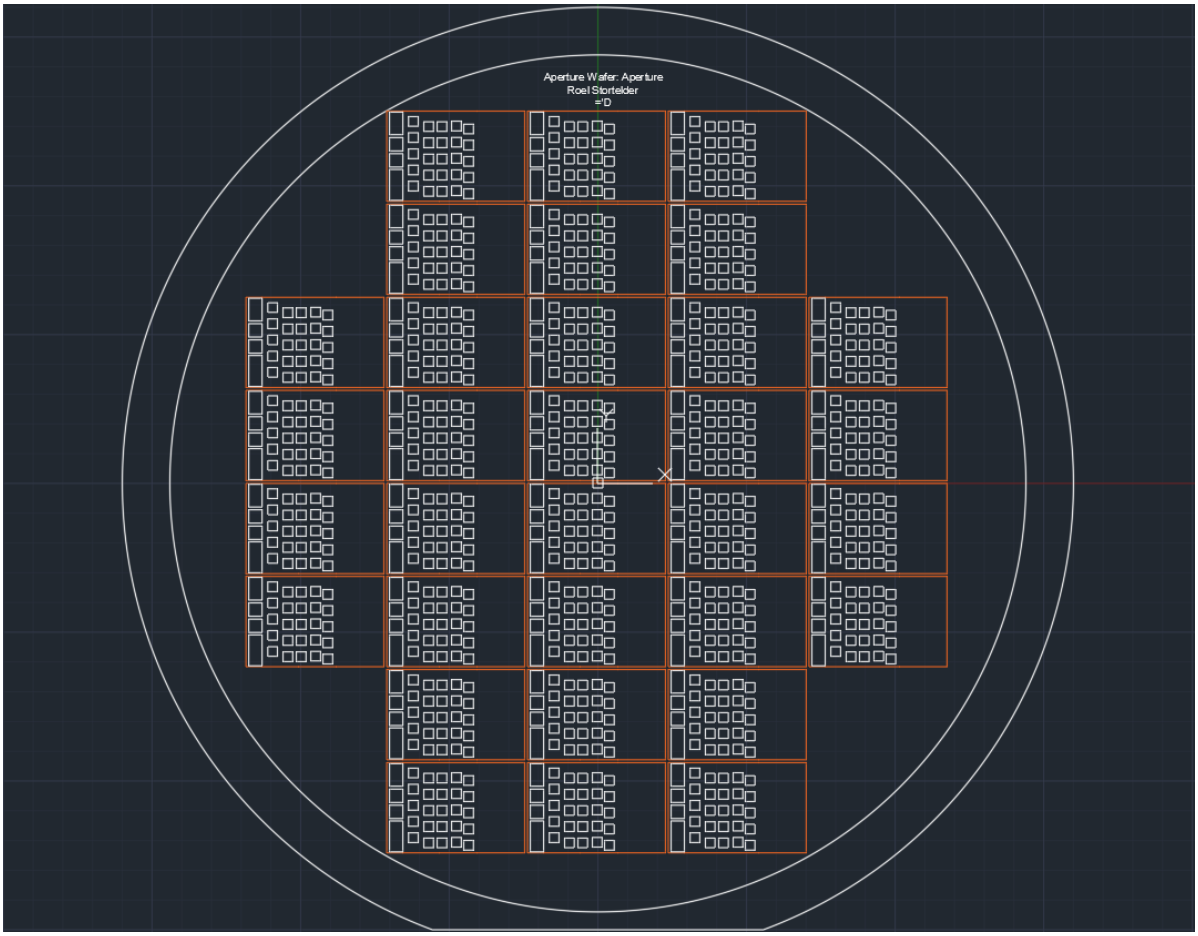

Figure D.6: Mask **Wafer_2_Back_Side_Apertures** used in step 5 of Wafer2 in Appendix C. The image shows a single chip. The masks defines the holes in the back side silicon nitride membrane for the KOH-etch. The orange lines are not part of the actual mask and only show the borders of the chip. The width of the orange box is 14500 μm.

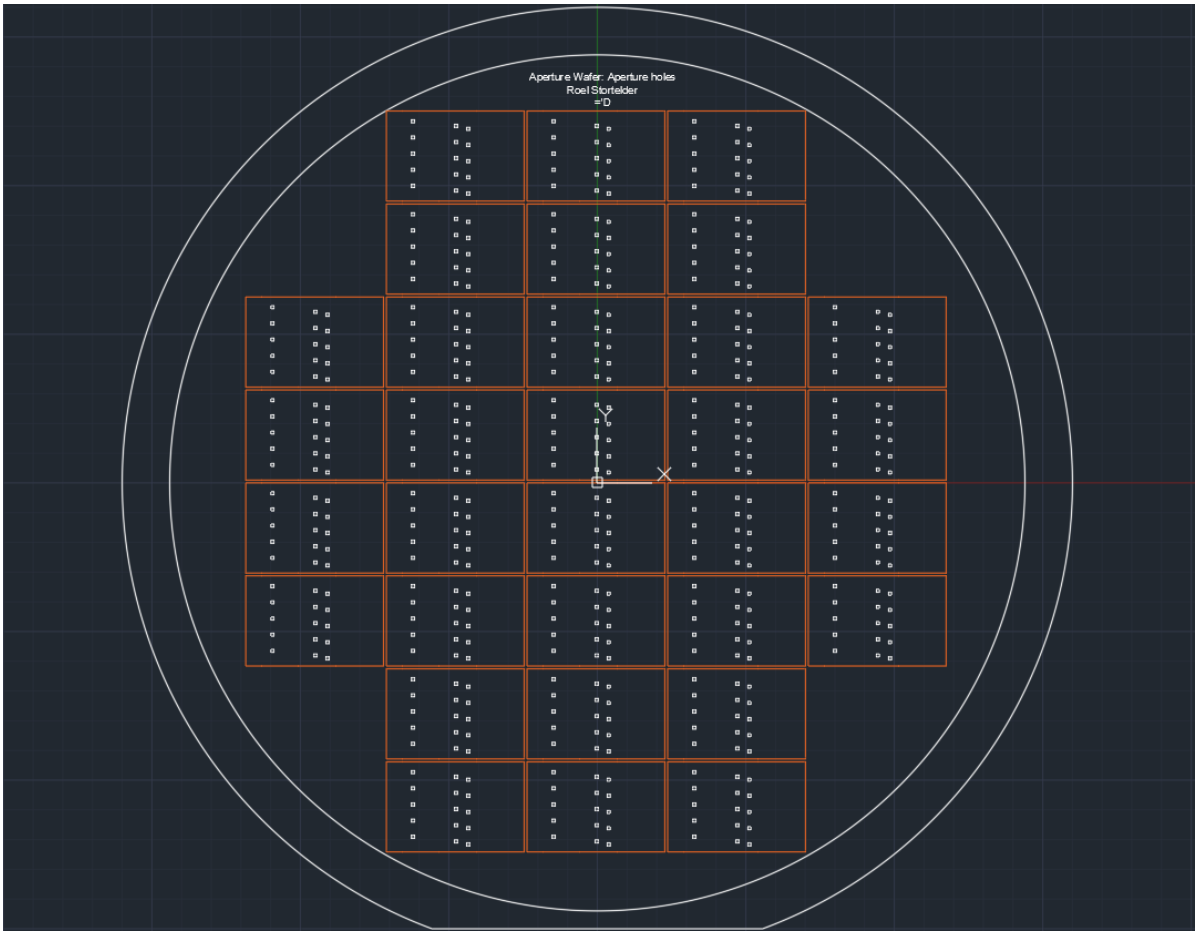

Figure D.7: Mask **Wafer_2_Front_Side_Tube_hole** used in step 12 of Wafer2 in Appendix C. The image shows the entire wafer without alignment markers. The orange lines are not part of the actual mask and only show the borders of each chip.

Figure D.8: Mask **Wafer_2_Front_Side_Tube_hole** used in step 12 of Wafer2 in Appendix C. The image shows a single chip. The masks defines the holes in the front side silicon nitride membrane where the microtubes will connect. The orange lines are not part of the actual mask and only show the borders of the chip. The width of the orange box is 14500 μm.

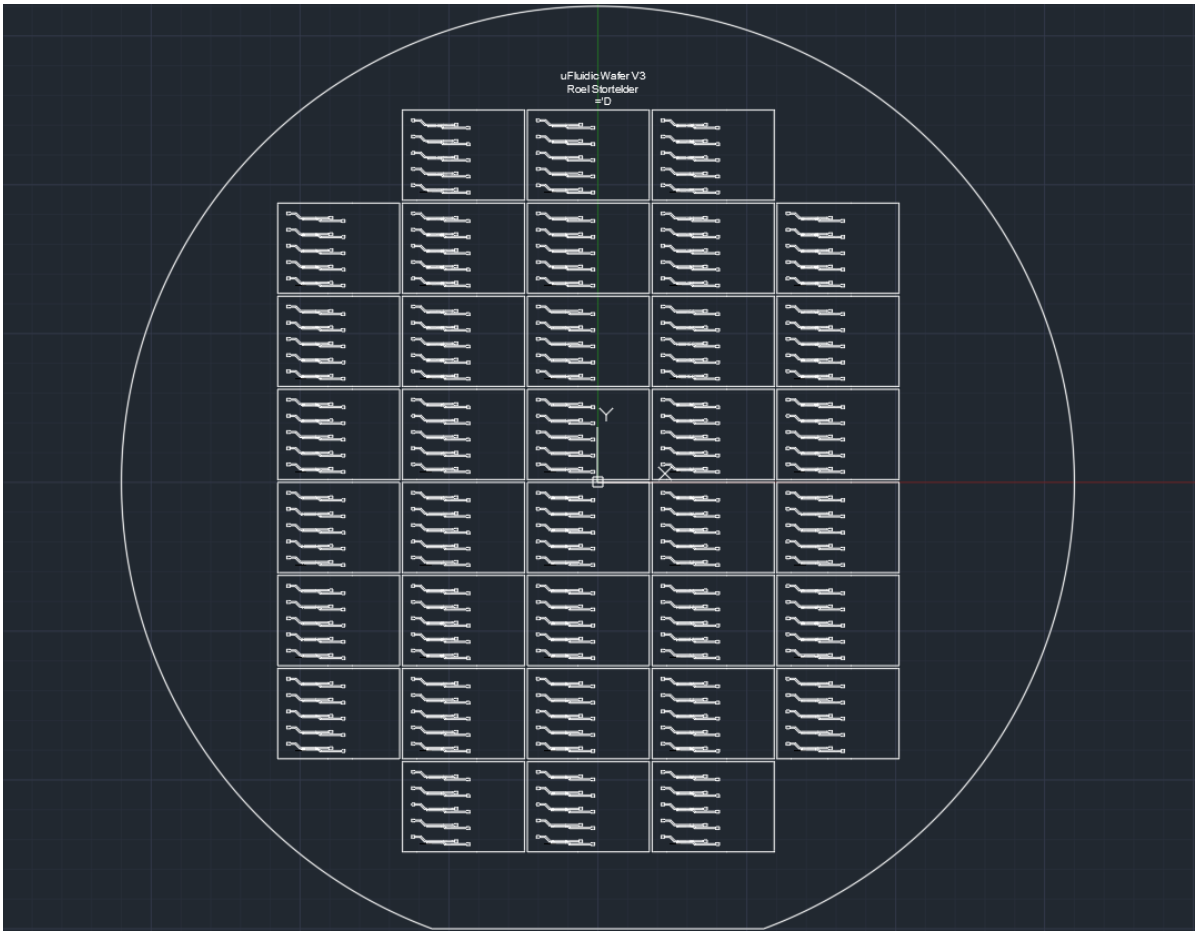

Figure D.9: Mask **Wafer_3_Front_Side_Microfluidics** used in step 5 of Wafer3 in Appendix C. The image shows the entire wafer without alignment markers.

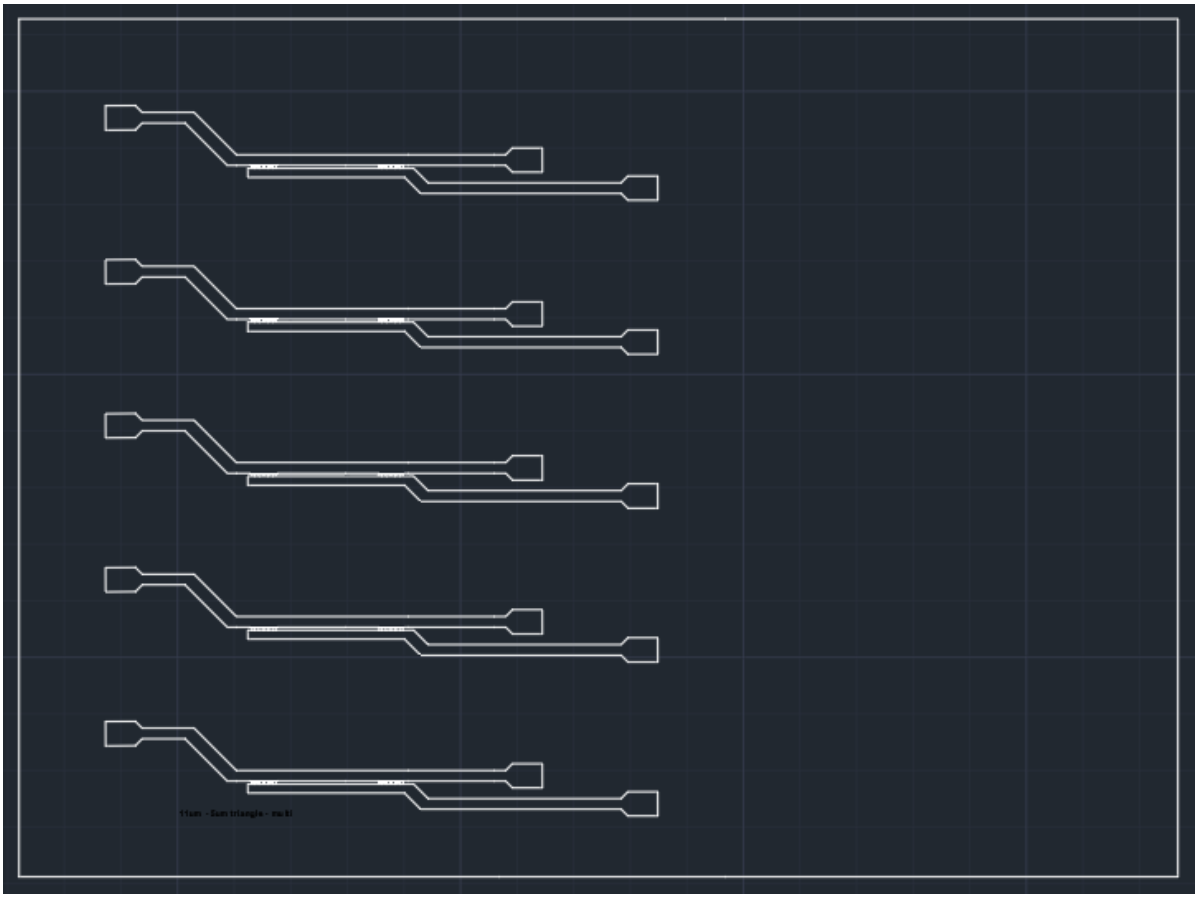

Figure D.10: Mask **Wafer_3_Front_Side_Microfluidics** used in step 5 of Wafer3 in Appendix C. The image shows a single chip. The microfluidic inlet ports (left side) and outlet ports (right side) are clearly visible.

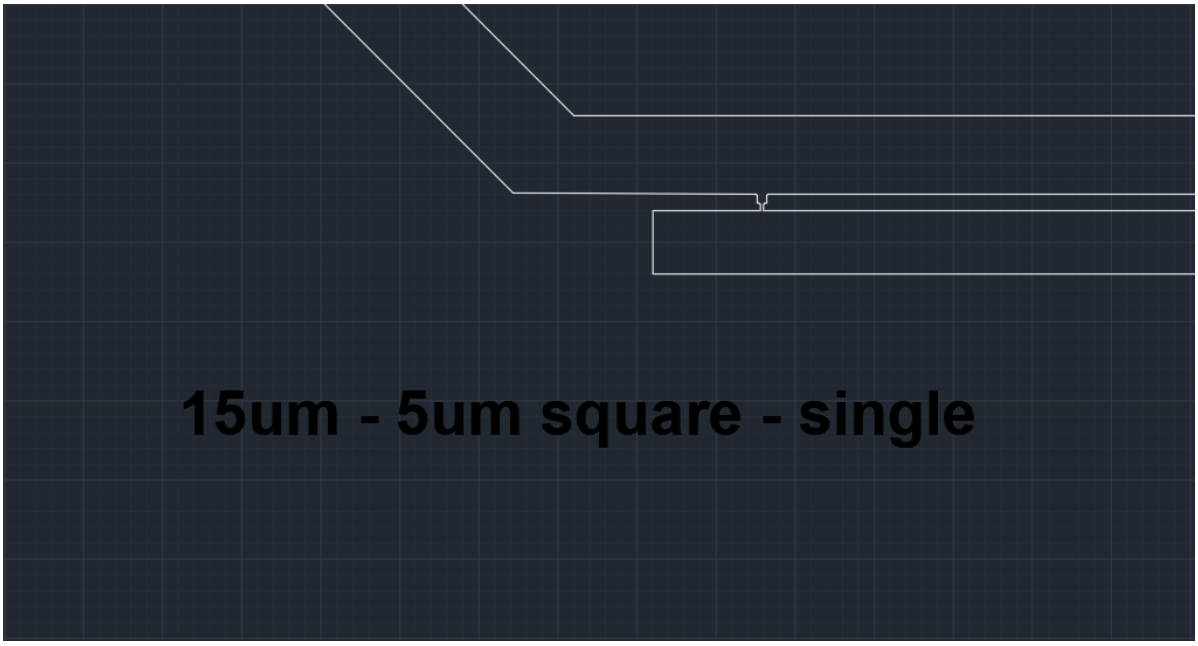

Figure D.11: Mask **Wafer_3_Front_Side_Microfluidics** used in step 5 of Wafer3 in Appendix C. The image shows the microfluidics in detail. In this example a single cell can be trapped above an LED in a square chamber with a width of 15 μm and a channel width of 5 μm.

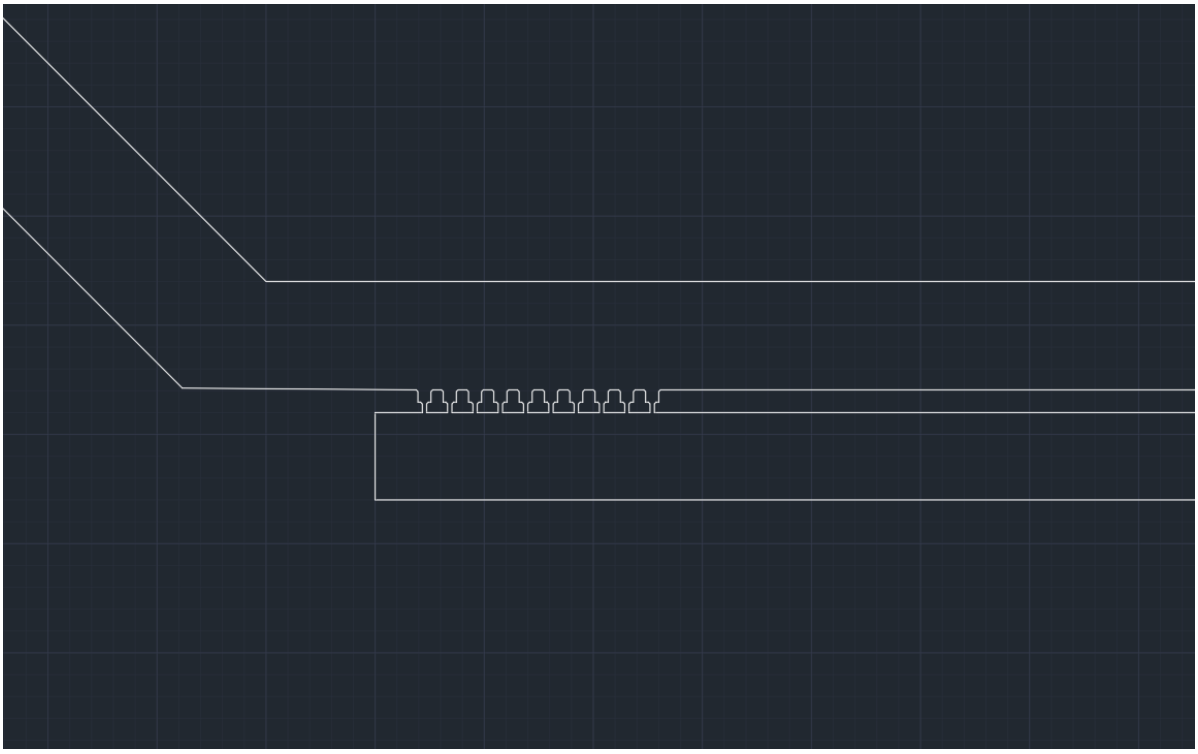

Figure D.12: Mask **Wafer_3_Front_Side_Microfluidics** used in step 5 of Wafer3 in Appendix C. The image is a zoomed-in version of Figure D.10. A total of ten cells can be trapped above a single LED in rounded square chambers.

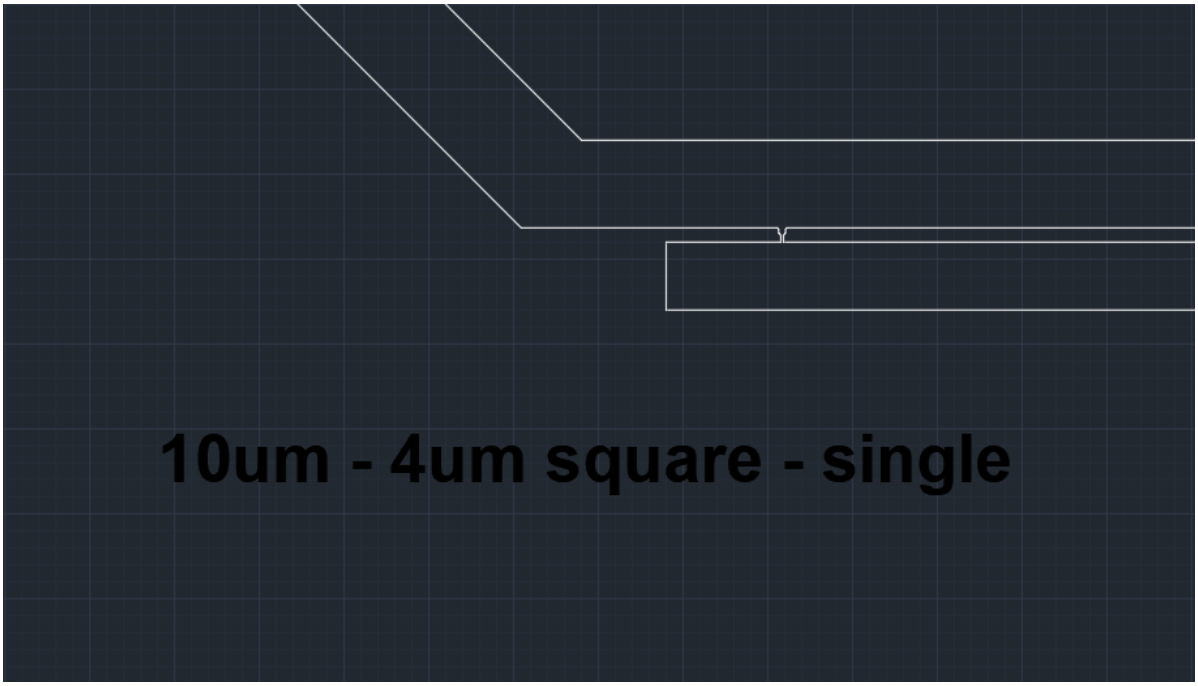

Figure D.13: Mask **Wafer_3_Front_Side_Microfluidics** used in step 5 of Wafer3 in Appendix C. The image shows the microfluidics in detail. In this example a single cell can be trapped above an LED in a square chamber with a width of 10 μm and a channel width of 4 μm.

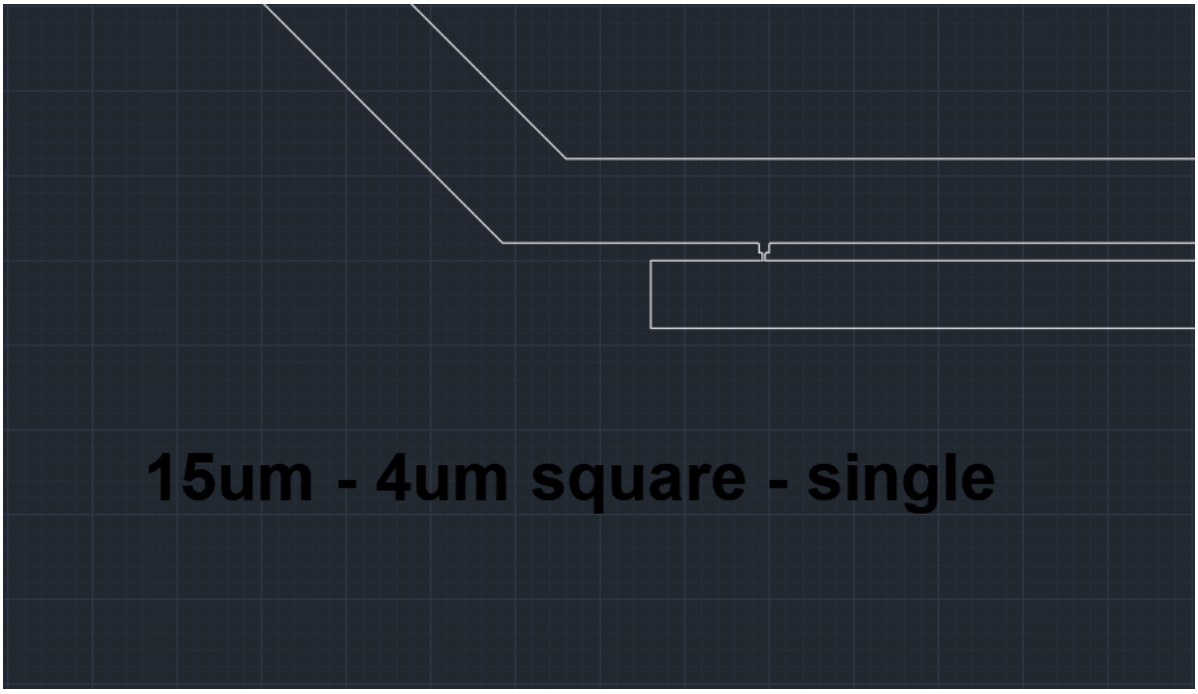

Figure D.14: Mask **Wafer_3_Front_Side_Microfluidics** used in step 5 of Wafer3 in Appendix C. The image shows the microfluidics in detail. In this example a single cell can be trapped above an LED in a square chamber with a width of 15 μm and a channel width of 4 μm.

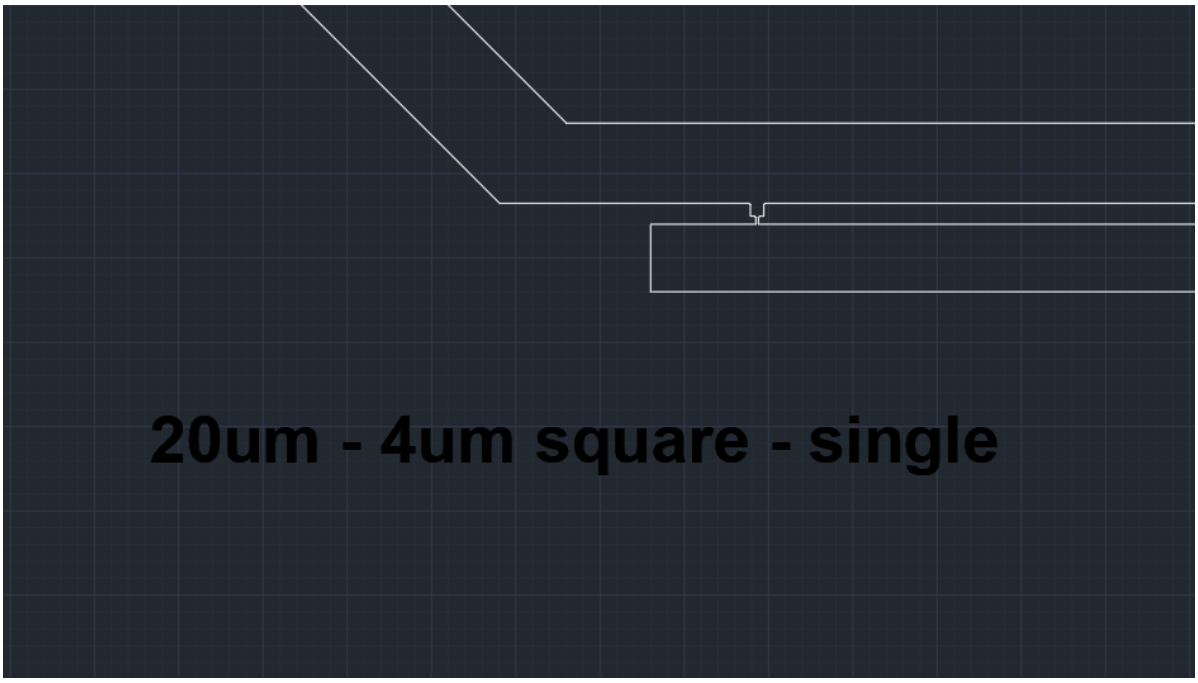

Figure D.15: Mask **Wafer_3_Front_Side_Microfluidics** used in step 5 of Wafer3 in Appendix C. The image shows the microfluidics in detail. In this example a single cell can be trapped above an LED in a square chamber with a width of 20 μm and a channel width of 4 μm.

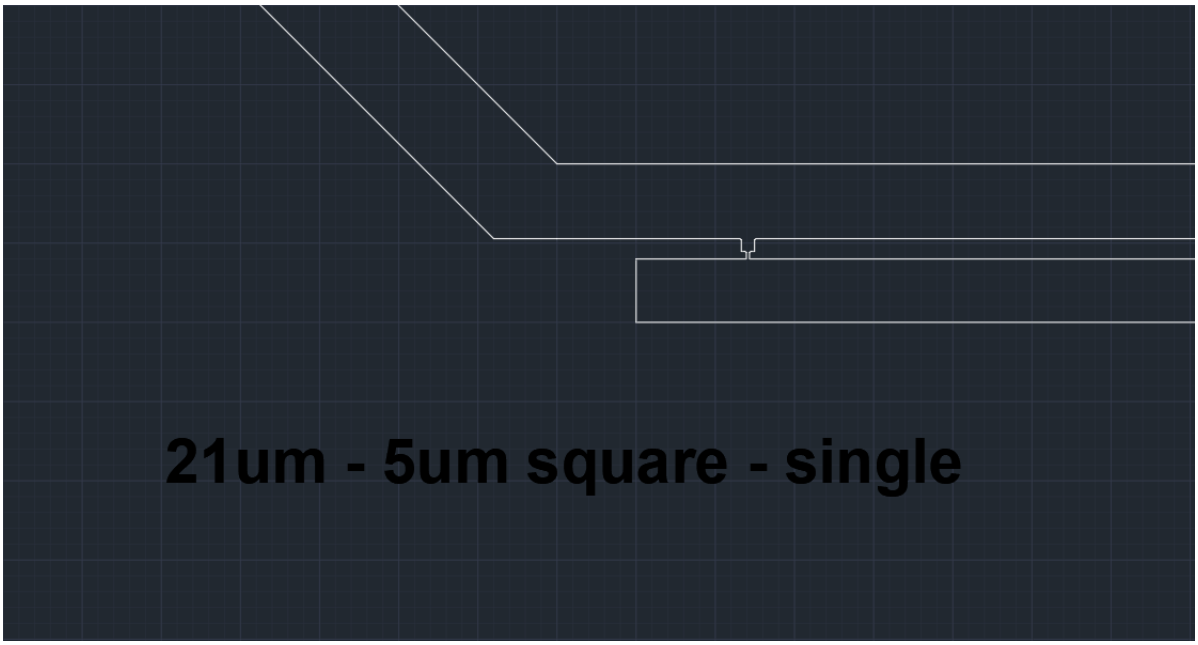

Figure D.16: Mask **Wafer_3_Front_Side_Microfluidics** used in step 5 of Wafer3 in Appendix C. The image shows the microfluidics in detail. In this example a single cell can be trapped above an LED in a square chamber with a width of 21 μm and a channel width of 5 μm.

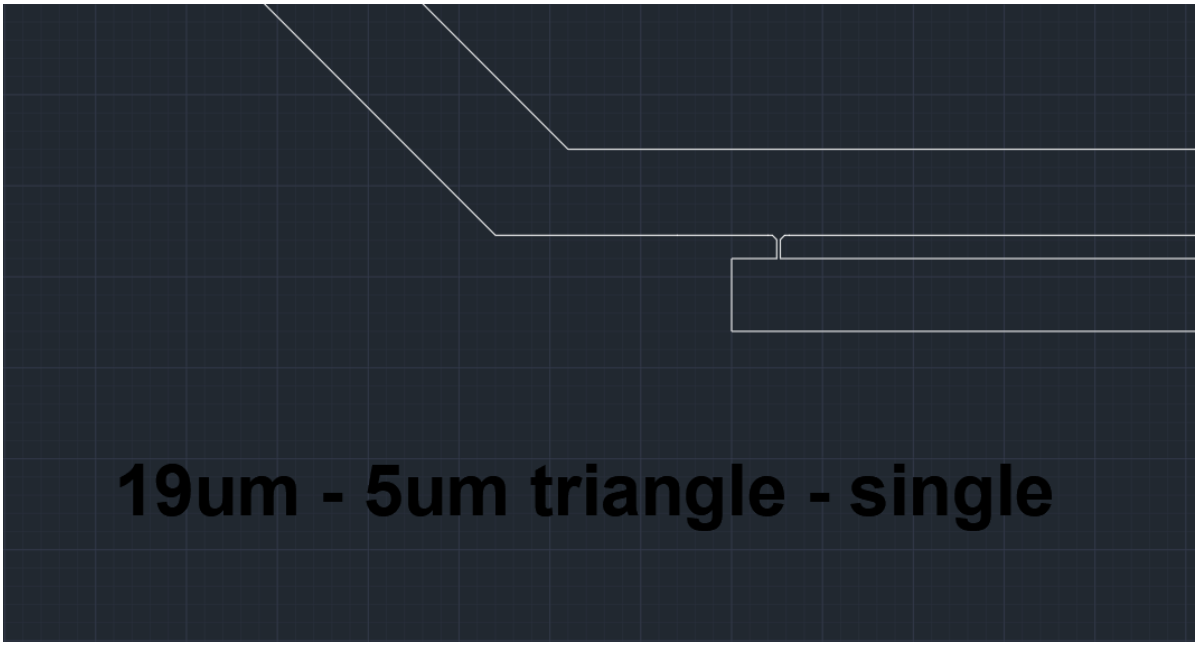

Figure D.17: Mask **Wafer_3_Front_Side_Microfluidics** used in step 5 of Wafer3 in Appendix C. The image shows the microfluidics in detail. In this example a single cell can be trapped above an LED in a triangle-shaped chamber with a width of 19 μm and a channel width of 5 μm.

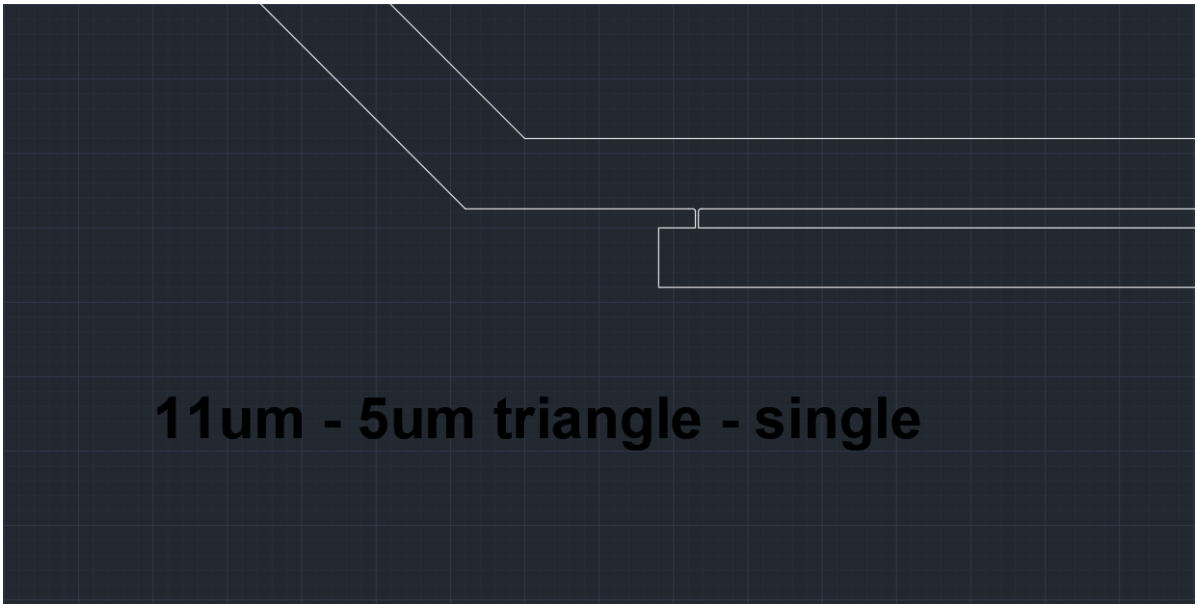

Figure D.18: Mask **Wafer_3_Front_Side_Microfluidics** used in step 5 of Wafer3 in Appendix C. The image shows the microfluidics in detail. In this example a single cell can be trapped above an LED in a triangle-shaped chamber with a width of 11 μm and a channel width of 5 μm.

E

MATLAB GUI FOR LED CONTROL

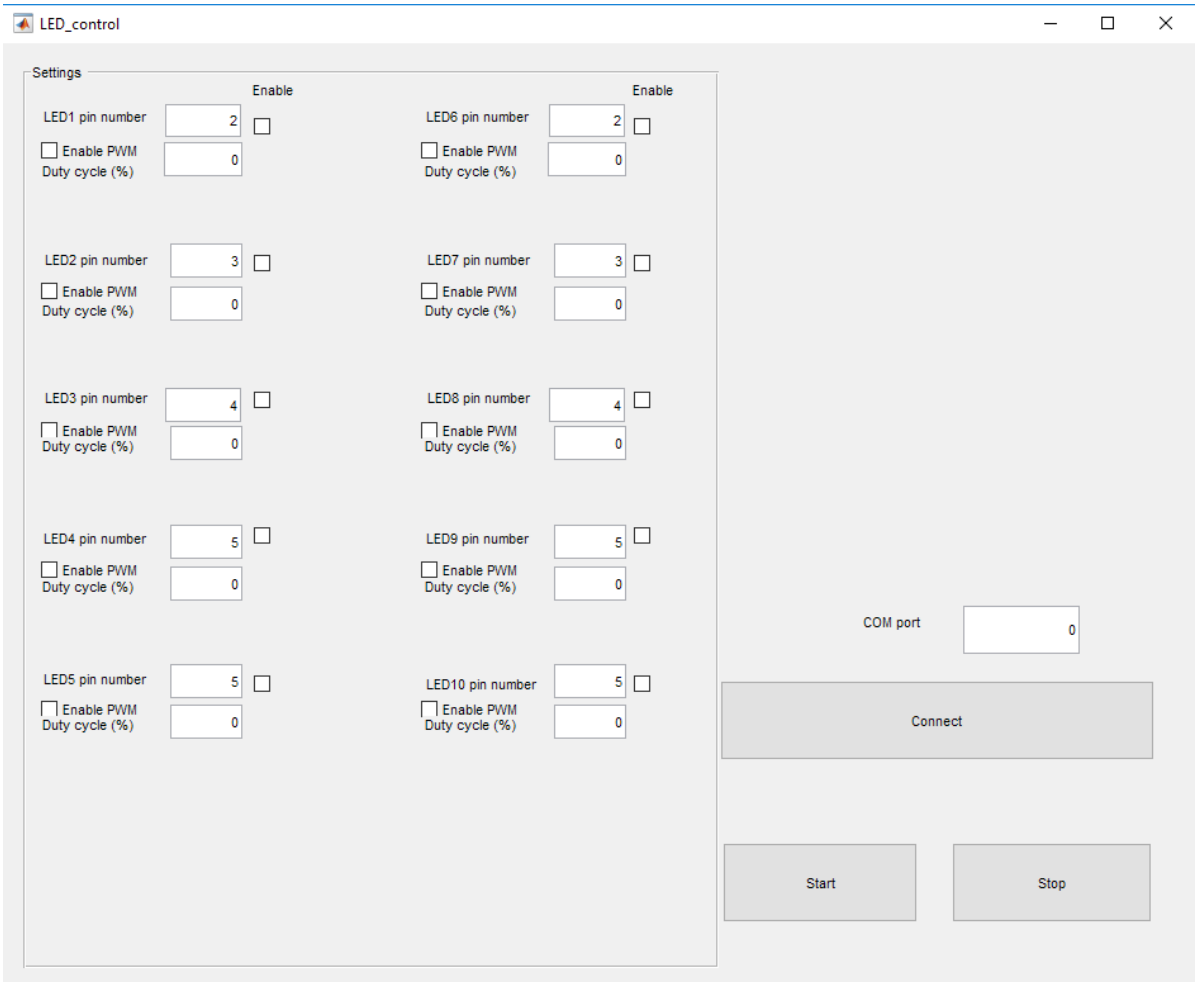

Figure E.1: A Matlab GUI for individual control of the ten LEDs through an Arduino.

F

Amplifier PCB for LED control

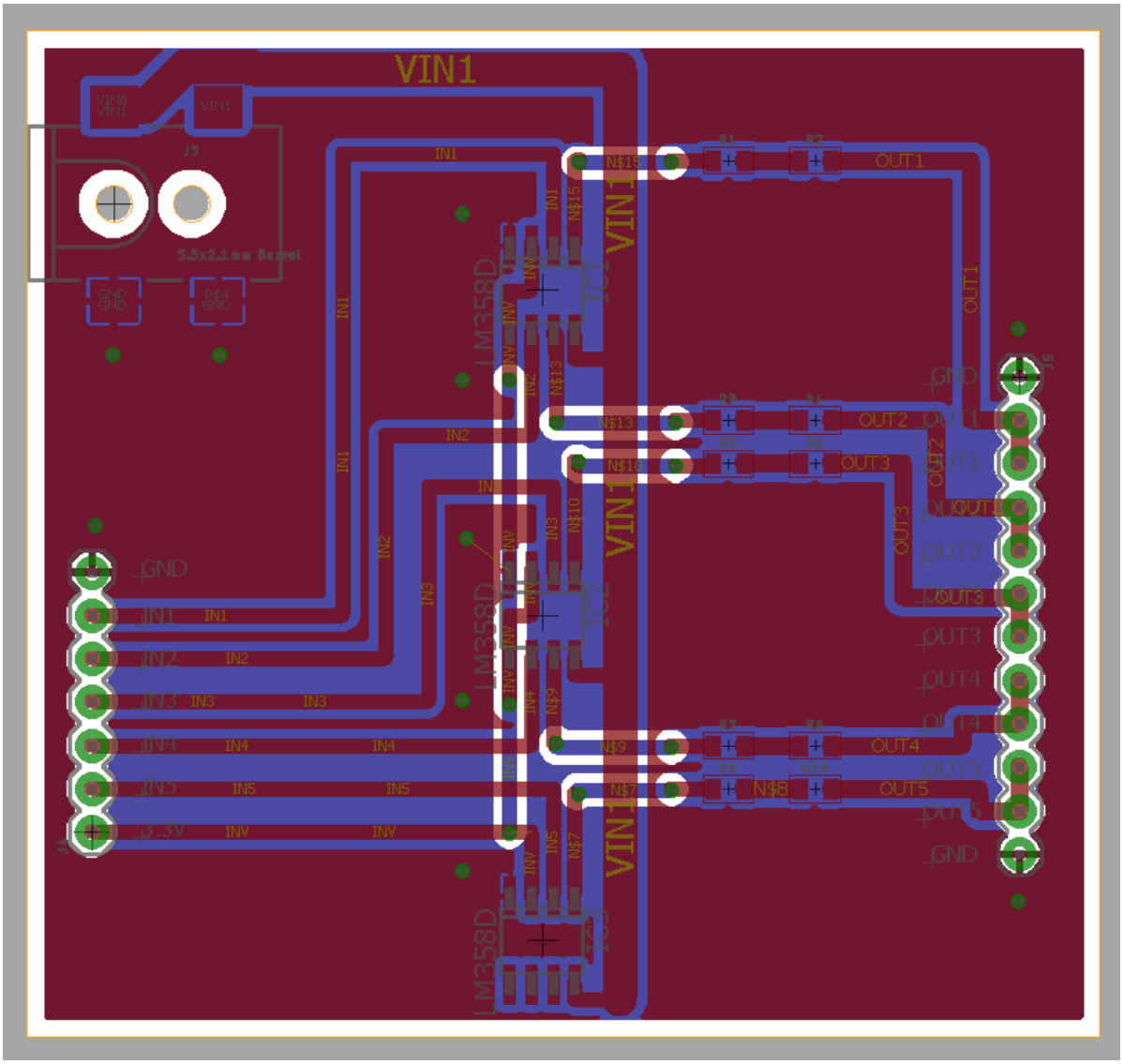

Figure F.1: The PCB matching the circuit from Figure 6.19 with all layers enabled.